Cell Systems

# Dissecting RAF inhibitor resistance by structure-based modeling reveals ways to overcome oncogenic RAS signaling

--Manuscript Draft--

| | |
|---|---|
| **Manuscript Number:** | CELL-SYSTEMS-D-17-00367R1 |
| **Full Title:** | Dissecting RAF inhibitor resistance by structure-based modeling reveals ways to overcome oncogenic RAS signaling |
| **Article Type:** | Research Article |
| **Keywords:** | RAF inhibitors; drug resistance; mathematical modeling; MAPK pathway; oncogenic RAS; drug synergy; RAF dimerization; conformational transitions of the DFG-motif and αC-helix |
| **Corresponding Author:** | Boris N Kholodenko, Ph.D.<br>University College Dublin<br>Dublin, IRELAND |
| **First Author:** | Oleksii S Rukhlenko |
| **Order of Authors:** | Oleksii S Rukhlenko |
| | Fahimeh Khorsand |
| | Aleksandar Krstic |
| | Jan Rozanc |
| | Leonidas G Alexopoulos |
| | Nora Rauch |
| | William S Hlavacek |
| | Richard G Posner |
| | Silvia Gómez-Coca |
| | Edina Rosta |
| | Cheree Fitzgibbon |
| | David Matallanas |
| | Jens Rauch |
| | Walter Kolch |
| | Boris N Kholodenko, Ph.D. |
| **Abstract:** | Clinically used RAF inhibitors are ineffective in RAS-mutant tumors, enhancing homo- and heterodimerization of RAF kinases, and leading to paradoxical activation of ERK signaling. Numerous mechanisms of RAF inhibitor resistance result in enhanced RAF dimerization and cannot be overcome by existing RAF inhibitors. A way to overcome resistance is the use of inhibitor combinations, but it is unclear how the best combinations can be chosen. Using a combined experimental and computational approach, we built a mechanistic dynamic model to analyze combinations of structurally different RAF inhibitors, which can efficiently suppress MEK/ERK signaling. This next-generation model of the RAS/ERK pathway integrates thermodynamics and kinetics of drug-protein interactions, structural elements, post-translational modifications and cell mutational status, predicting best RAF inhibitor combinations for cancer cells harboring oncogenic RAS and/or BRAFV600E. Synergistic inhibition of ERK signaling in mutant NRAS, HRAS and BRAFV600E cells was corroborated by experiments, demonstrating the power of structure-based dynamic modeling. |

# Dissecting RAF inhibitor resistance by structure-based modeling reveals ways to overcome oncogenic RAS signaling

Oleksii S. Rukhlenko[1], Fahimeh Khorsand[1], Aleksandar Krstic[1], Jan Rozanc[2,3], Leonidas G. Alexopoulos[3,4], Nora Rauch[1], William S. Hlavacek[5], Richard G. Posner[6], Silvia Gómez-Coca[7], Edina Rosta[7], Cheree Fitzgibbon[1], David Matallanas[1], Jens Rauch[1], Walter Kolch[1,8,9], Boris N. Kholodenko[1,8,9]*

1 – Systems Biology Ireland, University College Dublin, Ireland

2 – University of Luxembourg, Luxembourg

3 – ProtATonce Ltd, Athens, Greece

4 – National Technical University of Athens, Athens, Greece

5 – Theoretical Biology and Biophysics Group, Theoretical Division, Los Alamos National Laboratory, Los Alamos, NM, USA

6 – Department of Biological Sciences, Northern Arizona University, Flagstaff, AZ, USA

7 – Department of Chemistry, King's College London, London, UK

8 – Conway Institute of Biomolecular & Biomedical Research, University College Dublin, Ireland

9 – School of Medicine and Medical Science, University College Dublin, Belfield, Dublin 4, Ireland

*Corresponding author. Email: boris.kholodenko@ucd.ie

**Abstract.**

Clinically used RAF inhibitors are ineffective in RAS-mutant tumors, enhancing homo- and heterodimerization of RAF kinases, and leading to paradoxical activation of ERK signaling. Numerous mechanisms of RAF inhibitor resistance result in enhanced RAF dimerization and cannot be overcome by existing RAF inhibitors. A way to overcome resistance is the use of inhibitor combinations, but it is unclear how the best combinations can be chosen. Using a combined experimental and computational approach, we built a mechanistic dynamic model to analyze combinations of structurally different RAF inhibitors, which can efficiently suppress MEK/ERK signaling. This next-generation model of the RAS/ERK pathway integrates thermodynamics and kinetics of drug-protein interactions, structural elements, post-translational modifications and cell mutational status, predicting best RAF inhibitor combinations for cancer cells harboring oncogenic RAS and/or BRAFV600E. Synergistic inhibition of ERK signaling in mutant NRAS, HRAS and BRAFV600E cells was corroborated by experiments, demonstrating the power of structure-based dynamic modeling.

**Bullet points**

Next-generation model integrates kinetic, thermodynamic and cellular data

RAF dimers are effectively targeted by two structurally different RAF inhibitors

Best RAF inhibitor combinations are selected for diverse genetic backgrounds

Predicted RAF inhibitor combinations overcome oncogenic RAS signaling to ERK

# Introduction

The RAS/RAF/MEK/ERK pathway is pivotal for cell proliferation and survival and is frequently hyperactivated in tumors. Oncogenic mutations in the RAS genes (H-RAS, K-RAS, and N-RAS) occur in about 30% of cancers (Prior et al., 2012; Stephen et al.). Despite a three-decade long effort at developing RAS inhibitors, there is still no clinically available drug. As a result, the development of inhibitors of the kinases downstream of RAS has become a hot topic in drug development (Caunt et al., 2015; Rahman et al., 2014). Considerable efforts have focused on RAF kinases, owing to frequent BRAF mutations that drive cancer and developmental disorders (Rauch et al., 2016). The most common oncogenic BRAF mutation, BRAFV600E is found in ca 8% of human tumors and 60% of melanomas (Weinstein et al., 2013; Holderfield et al., 2014)). The ATP-competitive RAF inhibitors in clinical use, vemurafenib and dabrafenib, show high initial response rates in patients with mutant BRAFV600E malignant melanomas, but the effects are short-lived (Holderfield et al., 2014). Moreover, about 30% of patients develop secondary skin hypertrophy or malignances because of paradoxical ERK activation in wild-type (WT) BRAF cells (Yaktapour et al., 2014). Paradoxical ERK activation is particularly pronounced in mutant RAS tumors conveying intrinsic resistance to RAF inhibitors (Zhang et al., 2015), which can even accelerate tumor growth and invasion (Sanchez-Laorden et al., 2014).

Homo- and hetero-dimerization of the RAF kinases BRAF and CRAF (gene name RAF1) significantly increases their catalytic activities and represents a key event in the activation of normal and oncogenic RAF pathways (Freeman et al., 2013; Garnett et al., 2005; Rushworth et al., 2006). The binding of RAF molecules to active RAS drives RAF dimerization by inducing conformational changes, dephosphorylation of inhibitory residues and bringing RAF molecules into proximity of each other (Dhillon et al., 2002; Kholodenko et al., 2000; Weber et al., 2001). Enhanced RAF kinase dimerization driven by oncogenic RAS mutations or upregulation of upstream receptors leads to intrinsic or acquired resistance to RAF inhibitors (Lito et al., 2013; Nazarian et al., 2010). Other resistance mechanisms connected with increased RAF dimerization include CRAF overexpression (Holderfield et al., 2014; Lito et al., 2013), BRAF amplification (Shi et al., 2012), and BRAFV600E splice variants exhibiting enhanced dimerization potential (Poulikakos et al., 2011). All clinically used RAF inhibitors are ineffective against RAS mutant tumors (Hatzivassiliou et al., 2010; Poulikakos et al., 2010) and show poor performance in BRAF mutant colorectal cancers (Holderfield et al., 2014). Thus, more effective therapeutic strategies are currently needed to target mutant BRAF driven cancers.

Protein kinases toggle between inactive and active conformations that differ by the positions of the highly conserved DFG motif and αC-helix. ATP-competitive RAF inhibitors can be classified based on their preferential binding to different (IN or OUT) conformations of the DFG motif and αC-helix (IN and OUT positions correspond to active and inactive kinase conformations, respectively) (Fabbro, 2015; Karoulia et al., 2016; Roskoski, 2016). A broad classification includes three inhibitor types: αC-IN/DFG-IN (denoted CI/DI, Type I), αC-OUT/DFG-IN (CO/DI, Type I ½), and αC-IN/DFG-OUT (CI/DO, Type II), see table S1. The observation that ATP-competitive inhibitors bind with different affinities to active and inactive kinase conformations received much attention in the drug discovery effort, but mostly in terms of inhibitor structures. We have recently reported that fundamental thermodynamic principles governing allosteric inhibitor effects can explain both paradoxical RAF kinase activation and common resistance mechanisms to RAF inhibitors (Kholodenko, 2015). Our work suggested that a combination of two structurally different RAF inhibitors may offer a path to abolish resistance (Kholodenko, 2015). However, to understand which inhibitor types to combine and in which cellular contexts, we need to connect thermodynamic and structural analyses of inhibitor-RAF interactions with biochemical, mutational and pathway regulation data, including dynamics of posttranslational modifications (PTMs) and feedback loops.

Here, we present a mechanistic ERK pathway model that integrates the structural, thermodynamic and kinetic analyses of RAF kinases, inhibitors and their interactions with pathway biochemical data and cellular genetic profiles to faithfully predict RAF inhibitor responses at the network level. This comprehensive model is based on extended studies of RAF kinase regulation by multiple phosphosites and dimerization, and intensive RAF inhibitor research. Our model predicts a number of surprising, hidden properties of network responses to different types of RAF inhibitors and makes new strides in understanding resistance to these drugs. The model suggests that synergy can emerge between Type I and Type II, as well as between Type I ½ and Type II inhibitors and predicts new ways of overcoming RAF inhibitor resistance in RAS mutant cells. Our experimental results on responses of MEK/ERK signaling to different RAF inhibitor types and their combinations in melanoma cells bearing oncogenic RAS, BRAFV600E mutations, or both BRAFV600E and NRAS mutations support model predictions. Inhibition of oncogenic RAS signaling in MEL-JUSO cells ($NRAS^{Q61L/WT}$, $HRAS^{G13D/G13D}$) is associated with reduced cell proliferation and colony formation. The results suggest a new principle of targeting the same kinase with two structurally different inhibitors that bind to different kinase conformations.

# Results

## Exploiting RAF dimer asymmetry as drug target

Structural studies of the BRAF and CRAF kinase domains show that dimers are asymmetric, and that RAF inhibitors often only bind one protomer. This asymmetry allows allosteric activation of a RAF protomer by a drug-bound protomer and is a critical feature of the paradoxical ERK pathway activation induced by many RAF inhibitors (Hu et al., 2013; Jambrina et al., 2014; Jambrina et al., 2016; Kholodenko, 2015; Yao et al., 2015). This asymmetry is hallmarked by different (IN-OUT) orientations of the αC-helix together with distinct IN and OUT conformations of the DFG motif (Figs. 1 and S1). These conformations occur naturally (Fig. 1B), but can be stabilized by RAF inhibitors, as suggested by crystallographic structures of BRAF with different inhibitors (Figs. 1C, 1D and S1). These structural changes combined with the evidence from thermodynamic studies that dimerization can substantially change the affinity of protomers for a drug (Kholodenko, 2015), prompted us to hypothesize that combining RAF inhibitors that preferentially bind to alternative αC-helix and DFG motif conformations should be able to block RAF dimer activity. As RAF dimerization involves not only conformational changes but also is governed by dynamic PTMs, which are difficult to track by structural and biochemical studies, we developed an integrated computational model that allowed us to analyze both the phosphorylation and conformational dynamics in mechanistic detail.

## Structural, thermodynamic and kinetic mechanisms integrated in a model

Protein functions are regulated by (de)phosphorylation of specific residues on multiple interacting, regulatory and catalytic domains (Pawson and Nash, 2003; Romano et al., 2014; Rubinstein et al., 2016). The ensuing protein states determine the affinities and rates of numerous interactions, including homo- and hetero dimerization, other protein associations, binding of inhibitors, and catalysis. To precisely account for the complexity of these interactions that occur sequentially or in parallel, we implement a rule-based, domain-oriented approach, which explicitly monitors the conformational and phosphorylation states of pathway kinases, including inhibiting and activating phosphosites (Borisov et al., 2008; Chylek et al., 2014; Varga et al., 2017). Our model describes conformational states of RAF monomers and dimers in terms of IN and OUT positions of the DFG motif and the αC-helix. These positions depend on RAF binding to RAS-GTP, the phosphorylation states of key residues (see below), the dimerization status (e.g., allosteric transactivation of a free RAF protomer by inhibitor-bound protomer (Hu et al., 2013)), and binding of RAF inhibitors that can stabilize the αC-helix and the DFG motif in the IN or OUT position, depending on the inhibitor

structure. Each rule in our RAS/ERK pathway model determines a set of chemical reactions, whose rates depend on the conformational, phosphorylation and spatial localization states of RAS, BRAF, CRAF, MEK and ERK (see Methods and Supplemental Experimental Procedures, SI). Below we briefly outline the main features of the complex RAF regulation, conformational transitions and allosteric interactions with RAF inhibitors that are integrated in the model. A detailed list of assumptions, a description of processes and parameters, and a program file that can be processed by the open source software package BioNetGen (Chylek et al., 2014) are given in SI.

***RAF activation cycle.*** Our model recapitulates how the activities of WT RAF kinases are controlled by (*i*) inhibitory phosphorylation on S259 for CRAF and S365 for BRAF, (*ii*) activating phosphorylation on S338 for CRAF, (*iii*) homo- and heterodimerization, and (*iv*) inhibitory feedback phosphorylation by ERK on several sites (including S642 on CRAF and T753 on BRAF), as illustrated in Figs. S2 and 2 (Baljuls et al., 2013; Dhillon et al., 2002; Ritt et al., 2010). RAS-GTP is considered an input to the ERK cascade. In the absence of RAS-GTP, both CRAF and BRAF reside in the cytoplasm in inactive states characterized by pS259 (p denotes phosphorylation) and S338 for CRAF and pS365 for BRAF. Active RAS recruits CRAF and BRAF to the plasma membrane. This is followed by RAF conformational changes, the dissociation of 14-3-3 proteins, dephosphorylation of inhibitory pS259 or pS365, and phosphorylation of S338, resulting in catalytic activity of RAF monomers (Chiloeches et al., 2001; Dhillon et al., 2002), Fig. S2. Strikingly, catalytic activities increase more than 10-fold following RAF heterodimerization (Freeman et al., 2013; Rushworth et al., 2006).

*Influence of ERK feedback on RAF activity.* In the model, ERK phosphorylation affects RAF activities through three different mechanisms (see SI, section 1.6 for details). First, it lowers the binding affinities of both CRAF and BRAF for RAS-GTP (Dougherty et al., 2005; Ritt et al., 2010). Second, it dramatically decreases the activity of CRAF monomers (Dougherty et al., 2005). Third, ERK phosphorylation lowers the affinities of monomers to dimerize. This leads to dissociation of RAF dimers, resulting in a precipitous drop in the total kinase activity (Ritt et al., 2010; Rushworth et al., 2006). Owing to these mechanisms, the activity of RAF kinases is tightly controlled by ERK-mediated feedback in the absence of oncogenic RAS and BRAF mutations (Kholodenko and Birtwistle, 2009; Sturm et al., 2010).

*Oncogenic BRAF mutant.* We model both WT RAF and mutant BRAFV600E heterozygous and homozygous cells (see SI, section 2). In the model BRAFV600E monomers are constitutively active, irrespective of the phosphorylation state of inhibitory S365, as suggested by structural and biochemical studies (Hu et al., 2013). Similar to wild-type, BRAFV600E is recruited to the plasma

membrane by active RAS. The dimerization potential of mutant BRAF is higher than that of wild-type protein, and the stability of BRAFV600E dimers is less affected by ERK feedback phosphorylation than in the case of WT BRAF (Lavoie and Therrien, 2015). A complete list of the relative kinase activities of CRAF, WT BRAF and BRAFV600E monomers and homo- and hetero-dimers is given in SI, section 4, List S4.1.

***Allosteric interactions of RAF monomers and dimers with inhibitors.*** Structurally diverse RAF inhibitors preferentially bind to different specific conformations of RAF molecules. Owing to thermal motions, these conformations can spontaneously transition between IN and OUT positions of the DFG motif and αC-helix (Lavoie and Therrien, 2015; Shao et al., 2017). Therefore, the apparent dissociation constants ($K_d$) of inhibitor binding to RAF monomers and dimers will depend on the equilibrium constants of these transitions, which in turn critically depend on the RAF binding, phosphorylation and dimerization states captured in the model. Distinct inhibitor types differentially stabilize IN or OUT positions of the αC-helix and the DFG motif and allosterically change these equilibrium constants and $K_d$'s (Kholodenko, 2015), see SI, section 3 and Lists S3.2 – S3.4. Thus, a unique feature of our model is its inclusion of conformational transitions of the αC-helix and the DFG motif in kinase monomers and dimers, which are driven by the kinetics of RAF activation cycles, interactions with inhibitors and thermal intramolecular motions (illustrated in Fig. 2, see SI, section 3 for details).

Summarizing, the model describes how the dynamic assortment of different RAF states determines the $K_d$ of inhibitor binding within a cell. These $K_d$ values critically depend on BRAF and RAS oncogenic mutations, thermal RAF motions, and the rate constants of inhibitor binding to different RAF conformations (see SI, section 3). Importantly, structurally diverse RAF inhibitors will have different $K_d$'s for different RAF molecular states, which is a prerequisite for inhibitor synergy or antagonism in cellular dose-responses. Next, using our comprehensive, structure-based model, we will assess which combinations of structurally different RAF inhibitors can effectively suppress ERK signaling in cancer cells with distinct genetic and protein expression background and then test the model predictions in experiments.

## BRAFV600E mutant-driven cells with WT RAS: what combinations of RAF inhibitors are more effective than individual inhibitors?

Signaling by BRAFV600E monomers is successfully blocked by RAF inhibitors that are used in the clinic, such as vemurafenib and dabrafenib. However, these drugs cannot effectively suppress signaling by RAF dimers, leading to paradoxical ERK activation and the emergence of resistance,

when RAF dimerization is increased through different adaptive mechanisms. Importantly, model simulations suggest that in both homo- and heterozygous cells harboring mutant BRAF and WT RAS, BRAFV600E homo- and heterodimers considerably contribute to the total RAF activity (Figs. S3A-S3F). Therefore, synergy between RAF inhibitors will occur if they cooperate to efficiently inhibit RAF dimers (Kholodenko, 2015). Our hypothesis is that two RAF inhibitors binding to alternative conformations of the αC-helix and/or DFG motif could block RAF dimer activity. Binding of a CO/DI inhibitor to an inhibitor-free RAF dimer stabilizes the dimer and the αC-helix of the respective protomer in an OUT position, whereas the αC-helix of the other protomer shifts to an IN position (because two αC-OUT protomer positions are generally incompatible with the dimer structure (Karoulia et al., 2016)). As drugs preferentially binding to an IN position of the αC-helix will select this protomer, a CO/DI and CI/DO inhibitor pair and a CI/DI and CO/DI pair may potentially synergize in the ERK pathway inhibition.

Using the model, we simulated the stationary dependencies of active MEK and ERK on the doses of RAF inhibitors, applied separately or in combination (these dependences are referred to as dose-responses). The levels of active MEK (ppMEK, Figs. 3A-3B) and ERK (ppERK, Fig. S3G) were normalized by their basal levels in growing cells, and drug exposure was simulated for several hours to reach the system steady state. To compare dose-response curves for different inhibitors, doses are commonly normalized by the IC50 values for each drug, which are the doses that inhibit the basal MEK or ERK activity by 50% (or by other ICZ values where $0 \leq Z < 100\%$) (Chou, 2006; Greco et al., 1995; Yeh et al., 2009). Accordingly, normalized dose-response curves for two different inhibitors always cross at the point where the normalized dose of each drug equals one (see blue and green dose-response curves in Fig. 3). Several quantitative metrics exist to estimate if two different inhibitors synergize, antagonize or act independently in suppressing pathway signaling, which are discussed in detail in SI, section 6. The Talalay-Chou combination index (CI) identifies drug synergy, additivity or antagonism, if the CI is smaller than 1, equal 1 or greater than 1, respectively (Chou, 2006). An advantage of using CI is the smaller amount of required data points, as compared with other, more comprehensive drug interaction metrics (see below and also SI, section 6 for more details).

Our simulations suggest that in BRAFV600E/WT RAS cells, two structurally distinct RAF inhibitors can synergize, if they preferably bind to protomers with different orientations of the αC-helix in a dimer (see the inserts in Fig. 3 panels showing that the CI is smaller than 1 over a range of doses). A combination of CO/DI and CI/DO inhibitors is most effective, suppressing ppERK with almost no paradoxical activation, whereas a combination of CO/DI and CI/DI inhibitors that can also be

synergistic shows substantial paradoxical activation mainly induced by a CI/DI inhibitor (Fig. 3C and S3H). Also, in BRAFV600E/WT RAS cells, CI/DI and CI/DO inhibitors will not be synergistic (Fig S3J where the CI is greater than 1 over a range of doses), because BRAFV600E homodimers and BRAFV600E-BRAF dimers will be ineffectively inhibited by this drug pair. A comparison of the calculated dose-responses (Fig. 3A) with experimentally measured response curves in A375 ($BRAF^{V600E/V600E}$, WT RAS) cells (Fig. 3B) demonstrates that the model accurately predicts synergistic inhibition of the ERK pathway by B0R (CO/DI) and sorafenib (CI/DO).

The synergy between CI/DO and CO/DI inhibitors increases, if a CO/DI inhibitor has a low dissociation rate constant ($k_{off}$ ), as, e.g., LGX818 with $1/k_{off} \geq 2$hrs (Yao et al., 2015). Strikingly, this low $k_{off}$ does not change the efficiency of this inhibitor applied separately, but it markedly enhances the synergistic effect of the drug combination (Fig. 3D, cf. the CI values in Fig. 3C and 3D). Intriguingly, if a CI/DO drug has a low $k_{off}$, this almost does not affect the efficacy of this drug applied separately or in combination with a CO/DI drug (Fig. S3I).

## Inhibition of mutant RAS-driven cells with WT BRAF by combinations of RAF inhibitors: systematic search for synergy.

Specific RAF inhibitors used in the clinic are ineffective against tumors harboring oncogenic RAS mutations (Heidorn et al., 2010; Zhang et al., 2015). A combination of a RAF inhibitor (dabrafenib or vemurafenib) and a MEK inhibitor (trametinib) is standard of care for BRAFV600E-driven metastatic melanoma (Grob et al., 2015; Larkin et al., 2014). However, our model simulations suggest that this drug combination does not synergize to inhibit ERK signaling in oncogenic mutant RAS and WT BRAF cells (Figs. 4A and S4A). In fact, the model predicts that this combination increases the ppERK signal compared to MEK inhibitor alone (Fig. 4A). We tested this prediction using the oncogenic RAS mutant-driven melanoma cell line MEL-JUSO ($NRAS^{Q61L/WT}$ and $HRAS^{G13D/G13D}$ (Forbes et al., 2015)). The experimental results corroborate model predictions, demonstrating that in MEL-JUSO cells the addition of dabrafenib to trametinib (at the doses that do not fully inhibit ERK activation) increases rather than decreases ERK signaling (Fig. 4B). Therefore next, we explore whether RAF inhibitor combinations can effectively suppress ERK signaling in RAS mutant-driven cells.

***Combination of CI/DI and CI/DO RAF inhibitors: model predictions***. Oncogenic RAS increases the abundance of BRAF-CRAF dimers. Because in a dimer, the BRAF protomer is dephosphorylated on S365, the equilibrium position of its DFG motif is shifted to the DFG-IN conformation. Consequently, CI/DI inhibitors preferentially bind to this BRAF protomer, stabilizing the DFG-IN

conformation. Experimental data suggest that in growing cells the CRAF protomer is not phosphorylated on S338 in a considerable fraction of BRAF-CRAF dimers (Dhillon et al., 2002; Diaz et al., 1997), which is recapitulated in our simulations (Fig. S5A). Consequently, the DFG-motif of this CRAF protomer has a higher probability to be in an OUT position than in an IN position. As a result, this protomer will preferentially bind a CI/DO inhibitor, underpinning a potential synergy between CI/DI and CI/DO inhibitors. Importantly, this mechanism of synergy does not depend on which type of inhibitor binds first to a heterodimer; a CI/DI inhibitor would predominantly bind to a BRAF S365 protomer, whereas a CI/DO inhibitor would predominantly bind to a CRAF S259, S338 protomer. The model suggests that a substantial fraction of fully inhibited CRAF-BRAF heterodimers will contain a pair of CI/DO and CI/DI inhibitor molecules instead of two copies of either inhibitor (see Fig. S5B). The simulated dose-responses show that either inhibitor induces a strong paradoxical ERK activation, Fig. 5A (data for ppMEK are shown in Fig. S5C). In agreement with experimental studies (Karoulia et al., 2016), CI/DI inhibitors are predicted to show a higher paradoxical ERK activation than CI/DO inhibitors. Notably, the concentration ranges in which inhibitors lead to paradoxical activation become wider with increasing RAS-GTP levels (Fig. S5D).

The inhibitory effect of a two drug combination can be comprehensively assessed by calculating or measuring the ppERK response across a two-dimensional plane of drug doses, Fig. 5B (Keith et al., 2005; Yeh et al., 2009). Lines of constant ppERK inhibition are termed Loewe isoboles (Greco et al., 1995) (IC20, IC50 and IC80 isoboles are shown in Fig. 5B). For non-interacting drugs, these isoboles are straight lines. If two inhibitors synergize, Loewe isoboles are concave, since lesser doses result in the same inhibitory effect. Convex isoboles indicate antagonism between inhibitors, because their combinations require increased doses to achieve the same inhibition. Importantly, these distinctive features of Loewe isoboles do not depend on the normalization method (any ICZ value can be used), or even absolute, non-normalized inhibitor doses can be plotted (see SI, section 6). The blue and green dose-response curves for separate inhibitors in Fig. 5A correspond to directions along the axes of the response plane in Fig. 5B, whereas different directions inside the plane correspond to different ratios of inhibitor doses in a combination, Fig. S5E. Different ratios result in different total doses for achieving the same ppERK inhibition. For each desired inhibition level (Z) there is a minimal total dose determined by an optimal ratio of drug doses, which together achieve the Z level of inhibition (a method for deriving optimal inhibitor ratios is given in SI, section 6.3). Therefore, the commonly used 1:1 ratio of normalized inhibitor doses can be suboptimal for desired inhibition

levels, which suggests that in preclinical studies, a two-dimensional plane of inhibitor doses might need to be analyzed.

Whereas in BRAFV600E/WT RAS cells, a combination of CI/DI and CI/DO inhibitors does not show synergy (Fig S3J), this combination synergistically suppresses ERK activity in oncogenic RAS mutant, WT BRAF cells, Figs. 5A and Fig. S5C. The combined response shown in Fig. 5A corresponds to the 2.2:1 ratio of normalized doses of CI/DI and CI/DO inhibitors. The response plane in Fig. 5B shows that this ratio is optimal for achieving 80% inhibition of ppERK at the minimal total dose of both inhibitors (see SI, section 6 and Scheme S6.2). Following paradoxical ERK activity increase, the inhibitor combination becomes more effective than either inhibitor, starting at the doses around 1/2 of the IC50. For instance, when the sum of two inhibitor doses equals 1 (i.e., when each inhibitor is added at 0.5 of its IC50), the ppERK level drops more than 2-fold, compared to the level when each inhibitor is applied separately at the IC50 dose. At the same time, this inhibitor combination failed to considerably reduce paradoxical activation, suggesting that other inhibitor type combinations need to be also analyzed.

Synergy between CI/DI and CI/DO inhibitors strengthens when a CI/DO inhibitor has a low dissociation rate constant, $k_{off}$, such as TAK-632 and AZ-628 with $1/k_{off} \geq 2$ hrs (Hatzivassiliou et al., 2010; Okaniwa et al., 2013). After this CI/DO inhibitor binds to inactive RAF monomers, it facilitates RAF dimerization and remains bound, because of its low $k_{off}$. This leads to the accumulation of heterodimers where one RAF protomer is bound to a CI/DO inhibitor, whereas the other protomer is inhibitor-free (Kholodenko, 2015). An inhibitor-bound and kinase-inactive RAF protomer in a dimer allosterically transactivates the free RAF protomer, which then assumes an active DFG-IN conformation and has higher affinity for a CI/DI inhibitor than for the second CI/DO inhibitor molecule. Our modeling results demonstrate that lowering $k_{off}$ of a CI/DO inhibitor (while keeping the $K_d$ value the same) markedly enhances synergy between CI/DI and CI/DO inhibitors (Fig. 5C) but does not considerably change the efficiency of this inhibitor as a single agent.

***Testing modeling predictions for oncogenic RAS mutant cells.*** To test model predictions, we conducted experiments in the MEL-JUSO ($NRAS^{Q61L/WT}$ and $HRAS^{G13D/G13D}$) melanoma cell line (Figs. 5D-E and S5F-H). In these cells, we measured the dose-responses of active MEK and ERK to increasing doses of SB-590885 (CI/DI RAF inhibitor (Heidorn et al., 2010)) and sorafenib (CI/DO RAF inhibitor (Heidorn et al., 2010; Holderfield et al., 2014)) added separately or in combination. Experimental data allowed reconstruction of a substantial part of the dose-response plane across multiple inhibitor combinations (Figs. 5D and S5G). The data along the axes correspond to ppERK

responses to each inhibitor applied separately, also shown by blue and green dose-response curves in Figs. 5E and S5G. Responses to each inhibitor show marked paradoxical ERK activation, extending into the micromolar range for either inhibitor, while in *in vitro* kinase assays both inhibitors inhibit all RAF isoforms in the low nM range (King et al., 2006; Wan et al., 2004; Wilhelm et al., 2004). Because in mutant NRAS and HRAS MEL-JUSO cells, SB-590885 did not suppress ERK activity (in the dose range we used), we could not normalize inhibitor doses by commonly used IC50 levels, and plot responses versus absolute inhibitor doses. Therefore, for each ppERK response to a combination of SB-590885 and sorafenib shown on the dose-response plane in Fig. 5D, the total inhibitor dose is the sum of the absolute SB-590885 and sorafenib concentrations (that can be found by projections of the corresponding ERK response point onto axes). The concave shapes of the Loewe isoboles (lines of constant ppERK inhibition) in Figs. 5D confirm our model predictions, demonstrating marked synergy for the combination of SB-590885 with sorafenib. The optimal ratio of sorafenib to SB-590885 doses to achieve 75% ppERK inhibition was about 1.5:1. The section of the dose-response plane corresponding to this ratio is shown in Fig. 5E demonstrating that a combination of SB-590885 and sorafenib substantially inhibits ERK signaling in MEL-JUSO cells at the same total doses, for which either inhibitor on its own is unable to suppress ERK activity efficiently.

When the number of data points across the two-dimensional plane of inhibitor doses is insufficient to reconstruct the Loewe isoboles, the combination index CI is commonly used to identify synergy or antagonism (Chou, 2006). For any particular drug combination ratio, the CI detects if at this ratio the Loewe isoboles will be concave (under a straight line of non-interacting drugs), in which case $CI < 1$, or convex (above this line), in which case $CI > 1$, see SI, section 6. Importantly, the classic metrics for assessing drug interactions, such as the Chou combination index or Loewe isoboles cannot apply to the range of doses, at which individual inhibitors and their combinations paradoxically activate a pathway. An objective measure of suppressing pathway signaling is the area under the dose response curves for each inhibitor taken separately and in combination (Kholodenko, 2015), see SI, section 6. Inserts to Fig. 5A, 5C and 5E demonstrate that this area and therefore, resistance to inhibition, substantially diminishes for a combination of CI/DI and CI/DO inhibitors.

***Combination of CI/DO and CO/DI RAF inhibitors.*** Next, in oncogenic RAS mutant cells we analyzed combinations of RAF inhibitors that preferably bind distinct orientations of both DFG motif and αC-helix. These drugs, and also inhibitors that preferentially bind only distinct αC-helix orientations, can potentially synergize in both BRAFV600E/WT RAS cells (Fig. 3 and S3) and in RAS mutant cells. Yet, model simulations show that the best combination for RAS mutant cells is a

pair of CI/DO and CO/DI inhibitors (Fig. 6A,B), whereas a pair of CI/DI and CO/DI inhibitors induces marked MEK/ERK paradoxical activation (Fig. S6A,B). Experiments in MEL-JUSO ($NRAS^{Q61L/WT}$, $HRAS^{G13D/G13D}$) and SKMEL2 ($NRAS^{Q61R/WT}$) cells, bearing an activating RAS mutations and WT BRAF, have collaborated modeling predictions that combinations of CO/DI and CI/DO inhibitors are more efficient than either of inhibitors alone (see Fig. 6C for ppERK dose-responses in SKMEL2 cells treated with B0R (CO/DI), sorafenib (CI/DO) and their combination, and Fig. 6D for ppERK dose-responses in MEL-JUSO cells treated with vemurafenib (CO/DI), sorafenib (CI/DO) and their combination).

In SKMEL2 cells, following marked paradoxical activation of ERK by B0R or sorafenib (a peak value of 8 to 10 times of the basal level), none of these drugs on their own could decrease the ppERK signal back to the basal level. The best inhibition was 250% of the basal level. Therefore, the drug doses were normalized by the doses corresponding to 250% activation (also referred to as $IC_{-250}$). Fig. 6C shows that the dose-response curve for the combination of inhibitors is lower than the dose-response curves of these inhibitors on their own. For example, although the maximal concentration of sorafenib and B0R each resulted in 2.5-fold higher activation of ERK than the basal level, when these drugs were combined, the same total dose reduced the ppERK signal more than 2.5-fold compared to each drug alone. Although this drug combination dramatically decreases paradoxical ERK activation, it fails to significantly decrease the basal ERK activity in SKMEL2 cells. Our simulations suggest that if a CO/DI inhibitor has a low $k_{off}$ (e.g. LGX818 (Yao et al., 2015)), it will increase the residence time of this inhibitor binding to a RAF dimer, promoting binding of a CI/DO or a CI/DI inhibitor (Fig. 6C). This will increase synergy between inhibitors (Figs. 6A and 6B). Remarkably, decreasing $k_{off}$ for CI/DO and CI/DI inhibitors does not facilitate their potential synergy with a CO/DI inhibitor (Fig. S6G).

Interestingly, vemurafenib applied in doses up to 50 μM could only activate ppERK in MEL-JUSO cells (Fig. 6C), as reported for other RAS-mutant cancer cells (Adelmann et al., 2016; Karoulia et al., 2016). Sorafenib applied separately could only slightly inhibit ppERK at high doses (12 μM), following paradoxical activation. Remarkably, a combination of vemurafenib and sorafenib could effectively inhibit the ERK pathway (following paradoxical ERK activation) at the total doses over 8 μM (5 μM vemurafenib and 3 μM sorafenib). In line with our model predictions, even RAF inhibitors, which on their own only activated ERK signaling, could inhibit the pathway when given in a proper combination.

***Inhibition of oncogenic RAS signaling correlates with reduced cell proliferation and colony formation.***

A combination of CI/DO and CO/DI RAF inhibitors blocked oncogenic RAS signaling in MEL-JUSO cells. Therefore, next we explored how these combinations affect cell proliferation and colony formation potential, which tests for the ability of a single cell to survive and grow into a colony. Both vemurafenib and sorafenib applied individually inhibited MEL-JUSO cell proliferation with the GI50 (a dose inhibiting cell proliferation by 50%) of 32 μM and 8 μM, respectively (Fig. 6E). At 1:1 ratio, a combination of these drugs synergistically inhibited proliferation. When both drugs were combined at 50% of the corresponding GI50 dose, the combination inhibited the cell growth 2-fold more efficiently than each drug at its GI50 dose. Moreover, both drug synergy metrics, the CI and AUC, demonstrated a pronounced synergy between vemurafenib and sorafenib in inhibiting MEL-JUSO cell proliferation (insert to Fig. 6E demonstrates that the CI for inhibition of proliferation was smaller than 0.6 over a range of doses). Likewise, a combination of vemurafenib and sorafenib synergistically inhibited colony formation in MEL-JUSO cells (Fig. 6F). Our data demonstrate that oncogenic RAS signaling, proliferation and the ability to form colonies were synergistically inhibited by a combination of CI/DO and CO/DI RAF inhibitors in MEL-JUSO cells ($NRAS^{Q61L/WT}$, $HRAS^{G13D/G13D}$).

## Combinations of RAF inhibitors suppress ERK signaling in cells bearing both oncogenic RAS and BRAFV600E mutations

One of the common mechanisms of resistance to RAF inhibitors in BRAFV600E melanomas is the appearance of a secondary NRAS mutation in the ERK pathway (Johnson et al., 2015; Lito et al., 2013; Nazarian et al., 2010). Some melanoma patients develop secondary malignancies from cells harboring pre-existing RAS mutations, whereas for others, RAS mutations frequently occur during treatments with BRAF inhibitors (Nazarian et al., 2010). Instructively, the model predicts that inhibitor combinations that synergistically suppress ERK signaling in RAS mutant cells also synergistically inhibit ppERK in co-mutated RAS and BRAF600E cells (Fig. 7A-D). This model prediction is explained by the enhanced RAF dimerization and the fact that emerging dimers can be effectively inhibited only by a combination of RAF inhibitors. A combination of a CI/DO inhibitor with a low $k_{off}$ CO/DI inhibitor is predicted to be particularly effective in suppressing ERK activity in these cells (Fig. 7C).

To test these predictions, we treated parental ($BRAF^{V600E/WT}$/WT RAS) and vemurafenib resistant M249 ($BRAF^{V600E/WT}$/$NRAS^{Q61K/WT}$) cells (Nazarian et al., 2010) with vemurafenib alone, sorafenib alone and the combination of these drugs. The data confirm that a combination of CI/DO and CO/DI inhibitors effectively suppresses ERK signaling in cells bearing both RAS and RAF oncogenic mutations (Fig. 7E). NRAS mutation results in about 3.5-fold increase in the basal ppERK level compared to parental cells (Fig. 7E). After treatment with 3 μM vemurafenib, the ppERK level in resistant M249 cells reaches the value equal to the basal level in the parental cells. Increasing the doses of vemurafenib from 3 to 10 μM does not substantially decrease the ppERK level in M249 cells. Although resistant to vemurafenib, ERK signaling is effectively inhibited in these cells by a 1:1 molar combination of vemurafenib and sorafenib starting from a total drug concentration of 3 μM. These results support model predictions.

***How robust are model predictions?*** The predictive power of our structure-based, dynamic model of ERK signaling and inhibitor – kinase interactions was tested against experiments and corroborated by the resulting data. Yet, a question arises of how robust these model predictions are, when we go beyond the possibilities of direct experimental testing. To answer this question, we carried out the sensitivity analysis of model-predicted drug interaction metrics to the changes in model parameters. We explored how the area under dose-response curves (AUC, an objective measure of pathway inhibition for a range of drug doses), and the Talalay-Chou combination index (CI) are sensitive to parameter changes, by calculating the response coefficients, $R_p^{AUC}$ and $R_p^{CI}$. These response coefficients (also known as the control or sensitivity coefficients, see, e.g., (Kholodenko et al., 1987; Kholodenko et al., 1997; Kholodenko and Westerhoff, 1995)) determine the fractional change in the AUC and CI brought about by a small fractional change in a model parameter *p*, which in the limit of infinitesimal changes reads, $R_p^X = \lim((\Delta X/X)/(\Delta p/p)) = d\ln X\,/d\ln p\,,\ X = \{AUC,\ CI\}$. Thus, $R_p^{AUC}$ and $R_p^{CI}$ are essentially equal the % changes in the AUC and CI caused by a 1% change in a parameter. If $R_p^{AUC}$ and $R_p^{CI}$ are substantially smaller than 1, the model predictions are robust to the changes in the corresponding parameter.

We explored robustness of model predictions for two types of drug resistant melanoma cells, harboring either oncogenic RAS mutations and WT BRAF (MEL-JUSO, SKMEL2) or bearing both oncogenic RAS and heterozygous BRAFV600E mutations (vemurafenib resistant M249 cells). Figs. 7F-G and S7I-J illustrate the distribution of the response coefficients $R_p^{CI}$ and $R_p^{AUC}$ to the parameter changes. Strong responses were induced by the changes in the parameters describing the kinase activity of RAF isoforms and formation of RAF dimers. These results are not surprising, because our

model suggests that the prerequisite to pronounced synergy between different types of RAF inhibitors is their cooperation to efficiently inhibit RAF homo- and heterodimers. For cells bearing both mutant oncogenic RAS and heterozygous BRAFV600E, the largest responses were induced by changing the kinase activity of semi-inhibited (harboring only one RAF inhibitor molecule) BRAFV600E homo-dimers. The AUC and CI decreased by about 0.6% (corresponding to a 0.6% increase in drug synergy) with the increase in this kinase activity by 1%. Likewise, synergy between CO/DI and CI/DO RAF inhibitors was also controlled by (*i*) the thermodynamic factors that quantify the facilitation of RAF dimerization by inhibitors, (*ii*) the parameter describing a decrease in the apparent $K_d$'s of RAF homo-/heterodimerization due to the spatial co-localization of both RAF molecules bound to RAS-GTP, and (*iii*) the affinities of BRAFV600E binding to RAS-GTP and BRAFV600E dimerization and the parameters describing decreases in these affinities following RAF feedback phosphorylation by active ERK (Fig. 7 and S7). The most sensitive responses to the protein abundance changes were found for the abundances of mutant BRAFV600E, ERK, and oncogenic RAS.

Cells bearing oncogenic RAS mutations and WT BRAF exhibited a similar distribution of CI and AUC responses to parameter changes (excluding those related to BRAFV600E). In the absence of BRAFV600E, the CI and AUC were sensitive to the parameters describing (*i*) the spatial co-localization effects on the affinities of BRAF and CRAF dimerization and binding to RAS-GTP, (*ii*) decreases in these affinities following RAF feedback phosphorylation by active ERK, and (*iii*) BRAF abundance and its (de)phosphorylation on S365. Similar as above, synergy between CO/DI and CI/DO RAF inhibitors was also strongly controlled by the thermodynamic factors that quantify the facilitation of RAF dimerization by inhibitors and, additionally, by potential cooperativity between IN/OUT transitions of the DFG-motif and the αC-helix (see Section 3, SI). Also, in the absence of strong signaling by mutant BRAFV600E monomers, the parameters that affect the signal transfer between MEK and ERK (such as the abundances of MEK and ERK phosphatases) more substantially influence drug synergy for oncogenic RAS and WT BRAF cells than for double RAS and BRAFV600E mutant cells. The absolute sensitivity values of the AUC and CI to the remaining parameters were smaller than 0.2, Fig. 7 and S7. We, therefore, conclude that our model predictions are robust and the highest sensitivities to parameter changes can be predicted by their influence on the RAF dimer formation.

## DISCUSSION

Intrinsic or acquired resistance to kinase inhibitors, including RAF inhibitors in melanoma and other cancers remains a pressing clinical problem. While different combinations of kinase inhibitors are routinely tested in clinical trials, it is unclear how the best combinations can be chosen. A plethora of confounding factors, including allosteric drug–kinase interactions, phosphorylation-induced conformational changes and kinase dimerization, multiple feedback loops and diverse cell mutational and expression profiles hamper intuitive reasoning about optimal drug combinations. Understanding each drug's mode of action and the mode of their combined actions at the network level would enable a systematic and robust design of the best combinations. Different dynamics of phosphorylation responses to inhibitors that preferentially bind to active or inactive conformations were previously reported (Kleiman et al., 2011). To describe the experimental data the authors designed a simplified kinetic model that correlates changes in phosphorylation of the EGFR with drug binding without elaborating the underlying molecular mechanisms. Here we present a next-generation pathway model that allows mechanistic and predictive analysis by dynamically integrating thermodynamics and kinetics of drug interactions, structural elements, PTMs, mutational status and pathway regulation. This model unravels salient features of the systems-level dose-responses to different types of RAF inhibitors that show similar inhibition of isolated RAF kinases, but preferentially bind to alternative conformations of the DFG motif and αC-helix adopted by RAF kinases as a result of different oncogenic activation mechanisms. Previous attempts of predicting dose-responses failed (Costello et al., 2014; de Gramont et al., 2015; Prasad, 2016; Saez-Rodriguez et al., 2015), because both the employed network models and machine learning methods could not embrace highly dynamic nature of allosteric interactions of structurally different drugs with multiple kinase conformations governed by thermal motions and posttranslational modifications (Nussinov et al., 2013). The type of next-generation models presented here can be instrumental in the future analysis of mechanisms of drug actions and the design of efficacious combinations. For instance, this approach could be extended to optimize combinations of RAF and MEK inhibitors.

Although our model explores RAF inhibitor combinations, it is based on general principles applicable to any kinases that undergo dimerization during activation (Bessman et al.). The model makes a surprising prediction that two drugs targeting the same protein pocket can synergize, while normally they would compete, as known from enzyme kinetics. However, a reason for potential synergy is asymmetry of protomer conformations that is induced by PTMs and/or binding of the first inhibitor molecule to a dimer (Jambrina et al., 2016; Kholodenko, 2015). These unexpected results would not have been discovered without mathematical and structural modeling, accounting for the asymmetry of protomer conformations in a kinase dimer. The model precisely predicts for which

mutational profiles and which drugs will preferentially bind different protomers in a kinase dimer and together completely inhibit these dimers. This suggests an alternative principle that two structurally different inhibitors, which target the same kinase, but in different conformations, can be synergistic.

Different mechanisms of intrinsic or acquired resistance in melanoma have a common feature of the increased abundance of RAF dimers. Moreover, recent clinical sequencing of 10,000 metastatic cancers (Zehir et al., 2017) not only revealed the relatively common co-occurrence of NRAS and BRAF mutations that increase RAF dimerization, but also BRAF in-frame deletions, which produce isoforms predicted to enable RAS-independent BRAF dimerization similar to the BRAF splice variants previously associated with acquired resistance to vemurafenib (Poulikakos et al., 2011). Whereas pharmacological research concentrated on creating RAF inhibitors that do not induce RAF dimers and thereby avoid paradoxical ERK activation (Zhang et al., 2015), our model suggested exploiting structural and thermodynamic features of dimer-drug interactions to completely inhibit RAF dimers. Based on model predictions, we showed that both BRAFV600E monomers and RAF dimers are best inhibited together by specific combinations of RAF inhibitors, even when each inhibitor is ineffective on its own. Importantly, the total dose of two combined drugs is considerably smaller than the dose of each inhibitor, which could substantially reduce toxicity resulting from off-target effects.

Experiments corroborate model predictions. In cancer cells bearing BRAFV600E mutation and WT RAS (A375 cell line, Fig. 3), BRAFV600E and NRAS Q61K co-mutations (resistant M249 cell line, Fig. 7) or oncogenic RAS and WT BRAF (MEL-JUSO cells, Fig. 6), a combination of CI/DO and CO/DI inhibitors showed pronounced synergy, effectively inhibiting ERK activation. The results suggest that for mutant BRAFV600E-driven cells, adding a CI/DO inhibitor (e.g., sorafenib, AZ-628, TAK-632, LY3009120) to a standardly used CO/DI inhibitor (vemurafenib, dabrafenib or encorafenib) can be beneficial not only because of more effective inhibition of ERK signaling in WT RAS cancer cells, but also because of synergistic inhibition of signaling in pre-existing or emerging resistant cancer cell clones with both BRAFV600E and RAS mutations. For these mutational profiles, especially for cells with mutant BRAF600E and WT RAS, a combination of CI/DI and CI/DO inhibitors is predicted to show additive rather than synergistic effects (Figs. S3J and S7). Almost counterintuitively, the model predicts, and experiments confirm that the same combination of CI/DI and CI/DO inhibitors is markedly synergistic in oncogenic RAS mutant cells with WT BRAF (MEL-JUSO cells, $NRAS^{Q61L/WT}$ and $HRAS^{G13D/G13D}$), Figs. 5 and Fig. S5. The combinations of RAF inhibitors described above can also be effective in suppressing RAF/ERK signaling in cells

with other mechanisms of resistance, such as CRAF/BRAF overexpression and BRAF splicing variants that enable RAS-independent BRAF dimerization (see SI, section 8 and Figs. 7F-7H). Summarizing, although in cells bearing oncogenic RAS mutations, individual RAF inhibitors are commonly ineffective, proper combinations of RAF inhibitors with particular modes of action efficiently inhibit ERK signaling. Biologically, this effective ERK inhibition is accompanied by a synergistic suppression of proliferation and colony formation in MEL-JUSO cells (Fig. 6).

Similarly, modeling can also address the open question whether RAF inhibitors increase the affinity of RAF kinases for RAS. RAF inhibitors increase the amount of RAS-RAF complexes (Hatzivassiliou et al., 2010; Karoulia et al., 2016), which was interpreted as the facilitation of RAF binding to RAS-GTP by these drugs. Although this explanation is plausible, structural evidence is lacking. Moreover, the model demonstrates that allosteric inhibitor effects resulting in enhancement of RAF dimerization can fully explain the increase in RAS-RAF complexes without an assumption that RAF inhibitors increase RAF affinities for RAS-GTP (Fig. S7E). Because each of the RAF protomers in a RAF dimer is bound to RAS in the narrow layer near the membrane, the apparent affinity of RAF for RAS increases due to spatial localization effects. Also, recent data on RAS dimerization (Nan et al., 2015) suggest that the increase in the apparent affinity of RAF for RAS can be explained by spatial localization. To further illustrate the interconnection between RAF dimerization and RAF binding to RAS, we developed a toy model (see SI, section 7) that shows how spatial localization effects result in an inhibitor-induced increase in the RAS-RAF complexes. If the structural mechanisms for the RAF dimerization-independent induction of RAS-RAF interactions are elucidated, these mechanisms can be readily incorporated into the model.

In summary, the type of next generation dynamic model presented here can address salient issues in drug targeting as well as help discover new aspects of drugs mode of action. These insights can be exploited to rationally design drug combinations that would be difficult to find through trial-and-error approach.

## Materials and Methods

### RAF inhibitors

Vemurafenib (PLX4032) was obtained from Selleckchem (Cat No. S1267). Sorafenib tosylate and SB-590885 were purchased from Axon Medchem (Axon 1397) and R&D Systems (2650/10), respectively. B0R (2,6-difluoro-N-(3-methoxy-2H-pyrazolo[3,4-b]pyridin-5-yl)-3-[(propylsulfonyl) amino]benzamide) (Wenglowsky et al., 2011) was kindly provided by Genentech. All inhibitors

were dissolved in DMSO to yield 10 mM stocks and stored at -20ºC.

**Cell culture**

Cell lines were either purchased from ATCC (SKMEL2, A375) or DSMZ (MEL-JSUO). M249 cells and the isogenic Vemurafenib-resistant cell line M249R were kindly provided by Antoni Ribas (Nazarian et al., 2010). All cells were grown in RPMI (Gibco) supplemented with 2 mM L-glutamine and 10% (v/v) fetal bovine serum in a humidified atmosphere of 5% $CO_2$ at 37ºC. Cells were seeded in 12-well plates (Greiner CELLSTAR dishes) at the density of $10^5$ cells per well. After reaching sufficient confluency, cells were treated with different concentrations of inhibitors and DMSO as control as indicated. To prepare the protein lysates, plates were transferred on ice, washed with ice-cold PBS and harvested by scraping in specific ELISA buffers as indicated below.

**MSD Multi-Spot Assay ELISA System:**

ERK and MEK activation was assessed by ELISA using the MESOSCALE MSD Phospho/Total ERK1/2 assay whole cell lysate Kit [phospho(Thr202/Tyr204; Thr185/Tyr187)/Total ERK1/2 Assay Whole Cell Lysate Kit, K15107D] or MEK kit [Phospho(Ser217/221)/Total MEK1/2 Assay Whole Cell Lysate Kit, K15129D] according to the manufacturer's instructions. Briefly, following the addition of complete MSD lysis buffer and scraping the cells from the surface of the dish, the cellular debris was removed from the lysate by centrifugation at 10000xg at 4ºC for 10 min. Protein concentration was determined using the BCA test according to the manufacturer's instructions (Pierce™ BCA Protein Assay Kit). Lysates were adjusted to 0.1 μg/μL protein concentrations for ERK kit and 0.8 μg/mL for MEK kit and relative MEK and ERK activation assessed according to the manufacturer's instructions using the MSD Sector Imager 2400 (model 1250).

**xMAP assays:**

Following the addition of complete Luminex lysis buffer and scraping the cells from the surface of the dish, the cellular debris was removed from the lysate by centrifugation at 10000xg at 4ºC for 10 min. The pellet was discarded and the protein concentration of lysates was adjusted to 0.3 μg/μL using the BCA assay kit. xMAP assays were performed on a Luminex-3D platform (Luminex, Austin, TX) using commercially available phosphoprotein antibody-coupled beads (ProtATonce, Athens, Greece). A custom multiplex phosphoprotein assay was used to determine the levels of test phosphoproteins in cell lysates: dual specificity mitogen-activated protein kinase kinase-1 (MEK1) with phosphorylation site S217/S221, and extracellular signal-regulated kinase-1 (ERK1) with

phosphorylation site T202/Y204. Additionally, for loading control the levels of glyceraldehyde 3-phosphate dehydrogenase (GAPDH) protein were analyzed in a separate setting. Custom antibody-coupled beads were technically validated as described before (Poussin et al., 2014).

**Western blot:**

Cells were transferred on ice, scraped using lysis buffer (10mM Tris pH 7.5, 150mM NaCl, and 0.5% (v/v) NP-40) complemented with protease and phosphatase inhibitors, and the cellular debris removed from the lysate by centrifugation at 10,000xg at 4$^{o}$C for 10 min. Protein concentration was determined using the BCA test according to the manufacturer's instructions (Pierce™ BCA Protein Assay Kit). Lysates were then resolved by SDS PAGE (12%) and transferred on a polyvinylidene difluoride membrane (Millipore). Protein visualization was performed in combination with horseradish peroxidase–conjugated secondary antibodies (Cell Signalling Technologies) and the enhanced chemiluminescence system (GE Healthcare) using the Advanced Molecular Vision Chemi Image Unit associated with ChemoStar Imager (INTAS Science Imaging Instruments GmbH) for the following antibodies: Polyclonal rabbit anti-human mitogen-activated protein (MAP) kinase [extra-cellular signal-regulated kinase (ERK) 1 and ERK2] antibody (Sigma), monoclonal mouse anti-human MAP kinase activated (diphosphorylated ERK1 and ERK2) antibody (Sigma).

**Cell proliferation assay**

Cell proliferation was analyzed by CellTiter 96 Aqueous One Solution Cell Proliferation Assay (MTS; Promega) according to manufacturer's instructions. For this, 5,000 cells were plated per well of 96-well tissue culture plates (in 200 µL of medium). Proliferation and viability of inhibitor- and control-treated cells was assayed after 96 hrs. The results represent the mean ±SD of triplicate samples, expressed as a percentage of control.

**Colony formation assay**

For colony formation assay, 1,000 cells per well were seeded into 6-well plates and on the next day drug treatments were performed. Two weeks after the treatment, cells were fixed and stained using the Fixing / Staining solution (Crystal Violet (0.05% w/v), Formaldehyde (1%), PBS (1X), Methanol (1%)). Washed and air dried dishes were scanned and analysed by eye and using Clono-Counter software package (Niyazi et al., 2007).

**Molecular Dynamics Simulations.**

We previously modeled the ATP-pBRAF homodimer using atomistic molecular dynamics (MD) simulations (Jambrina et al., 2016). We run longer simulation and analyzed the dynamic adjustment of the αC-helix position by defining the ω angle via the C and N terminal residues of the αC-helix (Cα atoms of Q493 and T508), the anchoring αF-helix (Cα atom of A641).

Our initial conformation for the molecular dynamics (MD) simulation was based on the PDB structures 4E26 (Qin et al., 2012) corresponding to the active forms of the BRAF kinase domain. The ATP and the two $Mg^{2+}$ ions were docked in the active site based on the 4DFX structure (Bastidas et al., 2012). The initial coordinates of the missing residues (439-447, and 604-609) were modeled using the M4T server (Fernandez-Fuentes et al., 2007a; Fernandez-Fuentes et al., 2007b; Rykunov et al., 2009). The homodimer system included a short, 20 amino acid-long substrate-like peptide (SP20 (Bastidas et al., 2012)) bound in the active site of each monomer. The ATP-pBRAF homodimer has the following phosphorylated activating residues: S446 in the NtA motif, T599 and S602 in the activation loop, and S579 in the catalytic domain. The initial model was essentially symmetrical, the all-atom RMSD between the protomers was 0.07 Å and the dimer interactions are remarkably similar (all-atom RMSD = 0.7 Å obtained for the alignment of the dimer but with the positions of the protomers inter-switched).

The simulation was performed using explicit water with the CHARMM-27 force field (MacKerell et al., 1998; Mackerell et al., 2004) at constant temperature (298 K) and pressure (1 bar). Langevin dynamics was used with a Langevin damping coefficient of 1 $ps^{-1}$. For long range electrostatics treatment, the non-bonded switching distance was set to 10 Å and a cut off distance of 12 Å was used. The ShakeH algorithm (Ryckaert et al., 1977) was used with 2 fs time steps. The trajectory was saved every 0.2 ns.

**Mathematical model.**

The RAS/RAF/MEK/ERK pathway mathematical model was formulated using a rule-based approach (Chylek et al., 2014), in which protein-protein interactions are represented by rules. Each rule is associated with a rate law and defines a class of reactions related by a common transformation. The model was specified using BNGL, a formal language for writing rule-based models (Faeder et al., 2009). The model specification file, supplied in electronic format in the supplemental online material, was processed by the BioNetGen software package (Blinov et al., 2004; Harris et al., 2016) to derive the reaction network and the corresponding system of coupled ordinary differential equations (ODEs) implied by the rules. The ODEs were numerically integrated

using BioNetGen's default algorithmic parameter settings and interface to CVODE in the SUNDIALS software package (Hindmarsh et al., 2005). Sensitivity coefficients of the model-predicted drug interaction metrics (CI and AUC) were calculated as the fractional change in the AUC or CI divided by the fractional parameter change (variation of the parameter change between 1 and 5% practically did not affect the sensitivity values).

Methods to assess additivity, synergy or antagonism between two drugs are presented in SI, section 6. Details of activating and inhibiting phosphorylation sites for each protein in the model, kinetic, thermodynamic and spatial localization parameters are provided in the SI.

**Acknowledgement.**

We thank Poulikos Poulikakos, Colm Ryan, Lan Nguyen and Dirk Fey for insightful discussions and UCD IT services for providing access to UCD Sonic computational cluster. Also, thanks are given to the Irish Centre for High-End Computing (ICHEC) for the provision of computational facilities. This work was supported by the by the EU H2020 grants MSCA-IF-2016 SAMNets (Grant no. 750688), SmartNanoTox (Grant no. 686098), NanoCommons (Grant no. 731032), Science Foundation Ireland (Grant no.14/IA/2395), NIH/NIGMS grant R01GM111510 and the JDACS4C program of DOE and NCI.

**Author contribution**

B.N.K., O.S.R., J.Ra. and W.K. conceived the study. B.N.K., O.S.R., W.S.H. and R.G.P. developed a model with the input from W.K., D.M., N.R. and J.Ra. E.R. and S.G. performed analysis of RAF protomer structures and carried out MD simulations. B.N.K., O.S.R., W.K., N.R. and J.Ra. designed wet-lab experiments. F.K., N.R., J.Ra., J.Ro., L.A., A.K., O.S.R. and C.F. carried out the experiments. B.N.K. wrote the manuscript with input from all authors, especially from O.S.R., J.Ra. and W.K. All authors read and approved the final version of the manuscript.

**Conflict of interests.**

L.A. is a founder of ProtaTonce, a biomarker discovery and compound assessment company.

**Figure legends**

**Fig. 1. Asymmetry of BRAF homodimers.** (**A**) Definitions of the αC-helix angle (ω) IN (ω > 54º) or OUT (ω < 52º) positions (Jambrina et al., 2014) as well as the DFG-motif IN (*d* < 7 Å) or OUT (*d* > 9.5 Å) conformations via the L505-F595 distance (*d*). The structure is illustrated using the PDB structure 3TV4. (**B**) Molecular dynamics simulation showing that the αC-helix positions of two RAF protomers in a dimer dynamically adjust to asymmetric positions in BRAF homodimers (blue – αC-IN, red – αC-OUT). (**C**) Distribution of the αC-helix conformations in 92 BRAF kinase domain protomers based on the analysis of 46 BRAF dimer structures deposited in PDB. (Insert) Distribution of the αC-helix positions in BRAF dimers with only one inhibitor molecule bound, based on 6 PDB structures: 3OG7, 3Q4C, 4FK3, 4H58, 4XV1, 4XV3. (**D**) Distribution of the αC-helix and DFG motif conformations in the 90 BRAF protomers analyzed. Among 45 analyzed RAF dimer PDB structures, 6 of the structures contain only 1 inhibitor molecule, and the rest have two inhibitors molecules bound to the dimer. See also Figure S1.

**Figure 2. Rule-based modeling of binding and phosphorylation reactions and concomitant conformational changes of RAF kinases.** (**A**) Illustration of rules governing RAF binding to RAS and RAF activation and dimerization cycles. Protein domains and phosphosites that are phosphorylated (p) or dephosphorylated are shown by rectangles. Switch is the RAS switch domain. RBD and DIM are the RAS-binding and dimerization domains; bI and cI are the inhibitor binding sites on BRAF and CRAF. The domains that are bound in a protein complex are colored. In the S338 rectangle the asterisk (*) indicates that the S338 phosphorylation state does not influence the CRAF association/dissociation reactions with RAS-GTP, whereas the rates of those reactions are affected by the states of the RAF residues (pS642 and pT753) that are phosphorylated by ERK. (**B**) Simplified BRAF-CRAF (B-C) dimerization cycle and allosteric inhibitor (I) interactions with RAF monomers and dimers. (**C**) The reaction of inhibitor (I) binding to BRAF (reaction 2) is expanded into 12 reactions that take into account possible positions of the DFG-motif and αC-helix. See also Figure S2.

**Figure 3. Combination of CO/DI and CI/DO drugs synergistically inhibits the ERK pathway in cells bearing BRAFV600E mutation and WT RAS.** (**A**) Model-predicted responses of MEK signaling to CO/DI and CI/DO inhibitors and their combinations in cells with homozygous BRAFV600E mutation. [RAS-GTP]=25 nM, [$BRAF^{V600E}$]=50 nM, [$BRAF^{WT}$]=0, basal ppMEK level is 609 nM. (**B**) MEK signaling responses of growing A375 (WT RAS, $BRAF^{V600E/V600E}$) cells to B0R and sorafenib and their combination measured using MESOSCALE system, 1 hr, IC50 of B0R

is 0.075 μM, IC50 of sorafenib is 44 μM, in a combination the ratio of B0R and sorafenib is 1.2:1. (**C**-**D**) Simulated responses of ERK signaling to CO/DI and CI/DO inhibitors and their combination are presented for cells with heterozygous BRAFV600E mutation. The residence times $1/k_{off}$ of CO/DI inhibitor are 1 s (**C**) and $10^4$ s (**D**). [RAS-GTP]=25 nM, [$BRAF^{V600E}$]=25 nM, [$BRAF^{WT}$]=25 nM, basal ppERK level is 1363 nM. (**A**, **C**-**D**) In each combination, the ratio of CO/DI and CI/DO inhibitor doses is 1.2:1. The remaining parameters are given in Lists S4.1 and S5.1 in SI. In each panel, the insert assesses drug synergy using the Talalay-Chou combination index (CI). See also Figure S3.

**Figure 4. A combination of dabrafenib and trametinib shows antagonism in cells harboring oncogenic RAS mutation and WT BRAF.** (**A**) Simulated responses of ERK signaling to individual drugs and their combination. Inhibitor doses are normalized by IC50. [RAS-GTP]=250 nM, [$BRAF^{WT}$]=50 nM, [$BRAF^{V600E}$]=0, basal ppERK level is 480 nM. The ratio of CO/DI RAF (dabrafenib) and MEK inhibitor (trametinib) normalized doses applied in combination is 1:6.4. (**B**) ERK signaling responses of growing MEL-JUSO cells ($NRAS^{Q61L/WT}$, $HRAS^{G13D/G13D}$, $BRAF^{WT/WT}$) to dabrafenib (CO/DI RAF inhibitor), trametinib (MEK inhibitor) and their combination measured using Western Blot, 1 hr. See also Figure S4.

**Figure 5. Combination of CI/DI and CI/DO inhibitors synergistically inhibits the ERK pathway in cells harboring oncogenic RAS mutations and WT BRAF.** (**A**-**C**) Simulated stationary responses of ERK signaling to individual drugs and their combinations. The residence time $t_{off} \sim 1/k_{off}$ of CI/DO inhibitor is 1 s (**A**-**B**) and $10^4$ s (**C**). Inhibitor doses are normalized by IC50, the total doses shown for the combination correspond to the optimal ratios of CI/DI and CI/DO doses. [RAS-GTP]=250 nM, [$BRAF^{V600E}$]=0, [$BRAF^{WT}$]=50 nM, basal ppERK level is 480 nM, the ratios of CI/DI and CI/DO inhibitor doses applied in combination are 2.2:1 (**A**) and 2.6:1 (**C**). (**D**-**E**) ERK signaling responses of growing MEL-JUSO cells ($NRAS^{Q61L/WT}$, $HRAS^{G13D/G13D}$, $BRAF^{WT/WT}$) to SB-590885 (CI/DI), sorafenib (CI/DO) and their combination measured using LUMINEX system, 24 hr. In a combination, the ratio of SB590885 to sorafenib is 1:1.5. The ppERK responses are plotted vs the absolute concentrations of inhibitors applied separately and vs the sum of absolute concentrations for their combination. Areas under the dose-response curves that assess efficiency of inhibitor combination are presented as inserts (**A, C, E**). See also Figure S5.

**Figure 6. Combination of CI/DO and CO/DI inhibitors synergistically inhibits ERK signaling, proliferation, and colony formation in cells bearing oncogenic RAS mutations and WT BRAF. (A, B)** Simulated responses of ERK signaling to CO/DI and CI/DO inhibitors and their combination.

The residence time $t_{off} \sim 1/k_{off}$ of a CO/DI inhibitor is 1 s (**A**) and $10^4$ s (**B**). Inhibitor doses are normalized by IC50, the total doses shown for the combination correspond to the optimal dose ratio that is nearly 1:1. [RAS-GTP]=250 nM, [$BRAF^{V600E}$]=0, [$BRAF^{WT}$]=50 nM, basal ppERK level is 484 nM. (**C**) ERK signaling responses of growing SKMEL2 ($NRAS^{Q61R/WT}$, $BRAF^{WT/WT}$) to B0R (CO/DI), sorafenib (CI/DO) and their combination measured using MESOSCALE system, 24 hr treatment. Doses are normalized by the doses that correspond to 250% of the basal ppERK level (20.7 μM for B0R and 5 μM for Sorafenib). This was the minimal ppERK level, reached by either inhibitor following paradoxical ERK activation. The ratio of B0R and sorafenib applied in combination is 1:1. (**D, E**) ERK signaling (**D**) and cell proliferation (**E**) responses of growing MEL-JUSO cells ($NRAS^{Q61L/WT}$, $HRAS^{G13D/G13D}$, $BRAF^{WT/WT}$) to vemurafenib (CO/DI), sorafenib (CI/DO) and their combination measured using MESOSCALE system, 24 hr treatment. Doses are normalized by GI50 levels, i.e. by the levels of 50% inhibition of cellular growth. The ratio of vemurafenib and sorafenib applied in combination is 1:1. (**E**) Error bars are calculated using 4 biological replicates. The Talalay-Chou combination index (CI) assessing drug synergy in inhibiting cell proliferation is shown as insert. Areas under the dose-response curves (AUC) that assess efficiency of inhibitor combinations are presented as inserts (**A**-**E**). (**F**) Colony formation of MEL-JUSO cells treated with vemurafenib (VEM) and sorafenib (SOR) applied separately and in combination, a representative of 3 biological replicates. See also Figure S6.

**Figure 7. Combinations of RAF inhibitors can synergistically inhibit ERK signaling in cells bearing both oncogenic RAS and BRAFV600E mutations.** (**A**-**D**) Model-predicted stationary responses of ERK signaling to CI/DO and CO/DI inhibitors and their combinations. The residence time $t_{off} \sim 1/k_{off}$ of a CO/DI inhibitor is 1 s (**A**) and $10^4$ s (**C**), and the residence time of a CI/DO inhibitor is 1 s (**B**) and $10^4$ s (**D**). Inhibitor doses are normalized by IC50. In combinations, the ratio of CO/DI and CI/DO inhibitor doses are 1:1 (**A, C**), the ratios of CI/DI and CI/CO inhibitor doses are 6:1 (**B**) and 5:1 (**D**). [RAS-GTP]=250 nM, [$BRAF^{V600E}$]=25 nM, [$BRAF^{WT}$]=25 nM, basal ppERK level is 2151 nM. (**E**) ERK signaling responses to vemurafenib (CO/DI), sorafenib (CI/DO) and a combination measured using MESOSCALE system, 24 hr treatment for growing parental ($BRAF^{V600E/WT}$/WT RAS) and resistant ($BRAF^{V600E/WT}$/$NRAS^{Q61K/WT}$) M249 cells. The ppERK response is plotted vs the absolute concentrations of inhibitors applied separately and vs the sum of absolute concentrations for combinations, in which the ratio of vemurafenib and sorafenib doses is 1:1. (**A**-**E**) Inserts assess drug synergy using the Talalay-Chou combination index (CI). **(F-G)** Sensitivity analysis of the Talalay-Chou combination index (CI). The response coefficients of the CI (calculated for 50% inhibition of ERK signaling) to a change in each model parameter are

determined for a combination of CO/DI (inhibitor a) and CI/DO (inhibitor b) RAF inhibitors for cells bearing both oncogenic RAS and BRAFV600E mutations (**F**) or only oncogenic RAS and WT BRAF (**G**). The CI is most sensitive to the changes in: (**F**) BRAFV600, ERK, and oncogenic RAS abundances (cyan ■); Spatial co-localization of RAF and RAS-GTP (yellow ■); BRAFV600E affinities for dimerization and RAS-GTP and the decrease in these affinities after ERK feedback phosphorylation of RAF (magenta ■); Facilitation of RAF dimerization by inhibitors (green ■); Kinase activity of semi-inhibited BRAFV600E homo-dimers (red ■); (**G**) BRAF abundance and kinetic parameters of BRAF (de)phosphorylation on S365 (cyan ■ ); Parameters of signal transfer between MEK and ERK (dark-purple ■); Decrease in RAF affinity for RAS-GTP after RAF is phosphorylated by ERK (magenta ■); Spatial co-localization of RAF and RAS-GTP (yellow ■); Thermodynamic factors describing (*i*) facilitation of RAF dimerization by inhibitors and (*ii*) cooperativity between IN/OUT transitions of DFG-motif and αC-helix in BRAF (green ■); Kinase activity of RAF dimers (red ■).

## References


Adelmann, C.H., Ching, G., Du, L., Saporito, R.C., Bansal, V., Pence, L.J., Liang, R., Lee, W., and Tsai, K.Y. (2016). Comparative profiles of BRAF inhibitors: the paradox index as a predictor of clinical toxicity. Oncotarget *7*, 30453-30460.

Baljuls, A., Kholodenko, B.N., and Kolch, W. (2013). It takes two to tango--signalling by dimeric Raf kinases. Mol Biosyst *9*, 551-558.

Bastidas, A.C., Deal, M.S., Steichen, J.M., Keshwani, M.M., Guo, Y., and Taylor, S.S. (2012). Role of N-Terminal Myristylation in the Structure and Regulation of cAMP-Dependent Protein Kinase. Journal of molecular biology *422*, 215-229.

Bessman, Nicholas J., Bagchi, A., Ferguson, Kathryn M., and Lemmon, Mark A. Complex Relationship between Ligand Binding and Dimerization in the Epidermal Growth Factor Receptor. Cell reports *9*, 1306-1317.

Blinov, M.L., Faeder, J.R., Goldstein, B., and Hlavacek, W.S. (2004). BioNetGen: software for rule-based modeling of signal transduction based on the interactions of molecular domains. Bioinformatics.

Borisov, N.M., Chistopolsky, A.S., Faeder, J.R., and Kholodenko, B.N. (2008). Domain-oriented reduction of rule-based network models. IET Syst Biol *2*, 342-351.

N., Weinstein, J.N., Collisson, E.A., Mills, G.B., Shaw, K.R., Ozenberger, B.A., Ellrott, K., Shmulevich, I., Sander, C., and Stuart, J.M. (2013). The Cancer Genome Atlas Pan-Cancer analysis project. Nat Genet *45*, 1113-1120.

Caunt, C.J., Sale, M.J., Smith, P.D., and Cook, S.J. (2015). MEK1 and MEK2 inhibitors and cancer therapy: the long and winding road. Nature reviews Cancer *15*, 577-592.

Chiloeches, A., Mason, C.S., and Marais, R. (2001). S338 phosphorylation of Raf-1 is independent of phosphatidylinositol 3-kinase and Pak3. Mol Cell Biol *21*, 2423-2434.

Chou, T.C. (2006). Theoretical basis, experimental design, and computerized simulation of synergism and antagonism in drug combination studies. Pharmacol Rev *58*, 621-681.

Chylek, L.A., Harris, L.A., Tung, C.-S., Faeder, J.R., Lopez, C.F., and Hlavacek, W.S. (2014). Rule-based modeling: a computational approach for studying biomolecular site dynamics in cell signaling systems. Wiley Interdisciplinary Reviews: Systems Biology and Medicine *6*, 13-36.

Costello, J.C., Heiser, L.M., Georgii, E., Gonen, M., Menden, M.P., Wang, N.J., Bansal, M., Ammad-ud-din, M., Hintsanen, P., Khan, S.A., *et al.* (2014). A community effort to assess and improve drug sensitivity prediction algorithms. Nat Biotech *32*, 1202-1212.

de Gramont, A., Watson, S., Ellis, L.M., Rodon, J., Tabernero, J., de Gramont, A., and Hamilton, S.R. (2015). Pragmatic issues in biomarker evaluation for targeted therapies in cancer. Nat Rev Clin Oncol *12*, 197-212.

Dhillon, A.S., Meikle, S., Yazici, Z., Eulitz, M., and Kolch, W. (2002). Regulation of Raf-1 activation and signalling by dephosphorylation. EMBO J *21*, 64-71.

Diaz, B., Barnard, D., Filson, A., MacDonald, S., King, A., and Marshall, M. (1997). Phosphorylation of Raf-1 serine 338-serine 339 is an essential regulatory event for Ras-dependent activation and biological signaling. Mol Cell Biol *17*, 4509-4516.

Dougherty, M.K., Muller, J., Ritt, D.A., Zhou, M., Zhou, X.Z., Copeland, T.D., Conrads, T.P., Veenstra, T.D., Lu, K.P., and Morrison, D.K. (2005). Regulation of Raf-1 by direct feedback phosphorylation. Mol Cell *17*, 215-224.

Fabbro, D. (2015). 25 years of small molecular weight kinase inhibitors: potentials and limitations. Mol Pharmacol *87*, 766-775.

Faeder, J.R., Blinov, M.L., and Hlavacek, W.S. (2009). Rule-Based Modeling of Biochemical Systems with BioNetGen. In Systems Biology, I.V. Maly, ed. (Totowa, NJ: Humana Press), pp. 113-167.

Fernandez-Fuentes, N., Madrid-Aliste, C.J., Rai, B.K., Fajardo, J.E., and Fiser, A. (2007a). M4T: a comparative protein structure modeling server. Nucleic Acids Research *35*, W363-W368.

Fernandez-Fuentes, N., Rai, B.K., Madrid-Aliste, C.J., Eduardo Fajardo, J., and Fiser, A. (2007b). Comparative protein structure modeling by combining multiple templates and optimizing sequence-to-structure alignments. Bioinformatics *23*, 2558-2565.

Forbes, S.A., Beare, D., Gunasekaran, P., Leung, K., Bindal, N., Boutselakis, H., Ding, M., Bamford, S., Cole, C., Ward, S., *et al.* (2015). COSMIC: exploring the world's knowledge of somatic mutations in human cancer. Nucleic Acids Res *43*, D805-811.

Freeman, A.K., Ritt, D.A., and Morrison, D.K. (2013). Effects of Raf dimerization and its inhibition on normal and disease-associated Raf signaling. Mol Cell *49*, 751-758.

Garnett, M.J., Rana, S., Paterson, H., Barford, D., and Marais, R. (2005). Wild-type and mutant B-RAF activate C-RAF through distinct mechanisms involving heterodimerization. Mol Cell *20*, 963-969.

Greco, W.R., Bravo, G., and Parsons, J.C. (1995). The search for synergy: a critical review from a response surface perspective. Pharmacol Rev *47*, 331-385.

Grob, J.J., Amonkar, M.M., Karaszewska, B., Schachter, J., Dummer, R., Mackiewicz, A., Stroyakovskiy, D., Drucis, K., Grange, F., Chiarion-Sileni, V., *et al.* (2015). Comparison of dabrafenib and trametinib combination therapy with vemurafenib monotherapy on health-related quality of life in patients with unresectable or metastatic cutaneous BRAF Val600-mutation-positive melanoma (COMBI-v): results of a phase 3, open-label, randomised trial. The Lancet Oncology *16*, 1389-1398.

Harris, L.A., Hogg, J.S., Tapia, J.-J., Sekar, J.A.P., Gupta, S., Korsunsky, I., Arora, A., Barua, D., Sheehan, R.P., and Faeder, J.R. (2016). BioNetGen 2.2: advances in rule-based modeling. Bioinformatics *32*, 3366-3368.

Hatzivassiliou, G., Song, K., Yen, I., Brandhuber, B.J., Anderson, D.J., Alvarado, R., Ludlam, M.J., Stokoe, D., Gloor, S.L., Vigers, G., *et al.* (2010). RAF inhibitors prime wild-type RAF to activate the MAPK pathway and enhance growth. Nature *464*, 431-435.

Heidorn, S.J., Milagre, C., Whittaker, S., Nourry, A., Niculescu-Duvas, I., Dhomen, N., Hussain, J., Reis-Filho, J.S., Springer, C.J., Pritchard, C., *et al.* (2010). Kinase-dead BRAF and oncogenic RAS cooperate to drive tumor progression through CRAF. Cell *140*, 209-221.

Hindmarsh, A.C., Brown, P.N., Grant, K.E., Lee, S.L., Serban, R., Shumaker, D.E., and Woodward, C.S. (2005). SUNDIALS: Suite of nonlinear and differential/algebraic equation solvers. ACM Trans Math Softw *31*, 363-396.

Holderfield, M., Deuker, M.M., McCormick, F., and McMahon, M. (2014). Targeting RAF kinases for cancer therapy: BRAF-mutated melanoma and beyond. Nature reviews Cancer *14*, 455-467.

Hu, J., Stites, E.C., Yu, H., Germino, E.A., Meharena, H.S., Stork, P.J., Kornev, A.P., Taylor, S.S., and Shaw, A.S. (2013). Allosteric activation of functionally asymmetric RAF kinase dimers. Cell *154*, 1036-1046.

Jambrina, P.G., Bohuszewicz, O., Buchete, N.V., Kolch, W., and Rosta, E. (2014). Molecular mechanisms of asymmetric RAF dimer activation. Biochem Soc Trans *42*, 784-790.

Jambrina, P.G., Rauch, N., Pilkington, R., Rybakova, K., Nguyen, L.K., Kholodenko, B.N., Buchete, N.V., Kolch, W., and Rosta, E. (2016). Phosphorylation of RAF Kinase Dimers Drives Conformational Changes that Facilitate Transactivation. Angew Chem Int Ed Engl *55*, 983-986.

Johnson, D.B., Menzies, A.M., Zimmer, L., Eroglu, Z., Ye, F., Zhao, S., Rizos, H., Sucker, A., Scolyer, R.A., Gutzmer, R., *et al.* (2015). Acquired BRAF inhibitor resistance: A multicenter meta-analysis of the spectrum and frequencies, clinical behaviour, and phenotypic associations of resistance mechanisms. European Journal of Cancer *51*, 2792-2799.

Karoulia, Z., Wu, Y., Ahmed, T.A., Xin, Q., Bollard, J., Krepler, C., Wu, X., Zhang, C., Bollag, G., Herlyn, M., *et al.* (2016). An Integrated Model of RAF Inhibitor Action Predicts Inhibitor Activity against Oncogenic BRAF Signaling. Cancer Cell *30*, 485-498.

Keith, C.T., Borisy, A.A., and Stockwell, B.R. (2005). Multicomponent therapeutics for networked systems. Nat Rev Drug Discov *4*, 71-78.

Kholodenko, B., Zilinskiene, V., Borutaite, V., Ivanoviene, L., Toleikis, A., and Praskevicius, A. (1987). The role of adenine nucleotide translocators in regulation of oxidative phosphorylation in heart mitochondria. FEBS Lett *223*, 247-250.

Kholodenko, B.N. (2015). Drug resistance resulting from kinase dimerization is rationalized by thermodynamic factors describing allosteric inhibitor effects. Cell reports *12*, 1939-1949.

Kholodenko, B.N., and Birtwistle, M.R. (2009). Four-dimensional dynamics of MAPK information processing systems. Wiley Interdiscip Rev Syst Biol Med *1*, 28-44.

Kholodenko, B.N., Demin, O.V., and Westerhoff, H.V. (1997). Control Analysis of Periodic Phenomena in Biological Systems. The Journal of Physical Chemistry B *101*, 2070-2081.

Kholodenko, B.N., Hoek, J.B., and Westerhoff, H.V. (2000). Why cytoplasmic signalling proteins should be recruited to cell membranes. Trends Cell Biol *10*, 173-178.

Kholodenko, B.N., and Westerhoff, H.V. (1995). The macroworld versus the microworld of biochemical regulation and control. Trends in Biochemical Sciences *20*, 52-54.

King, A.J., Patrick, D.R., Batorsky, R.S., Ho, M.L., Do, H.T., Zhang, S.Y., Kumar, R., Rusnak, D.W., Takle, A.K., Wilson, D.M., *et al.* (2006). Demonstration of a Genetic Therapeutic Index for Tumors Expressing Oncogenic <em>BRAF</em> by the Kinase Inhibitor SB-590885. Cancer research *66*, 11100.

Kleiman, L.B., Maiwald, T., Conzelmann, H., Lauffenburger, D.A., and Sorger, P.K. (2011). Rapid phospho-turnover by receptor tyrosine kinases impacts downstream signaling and drug binding. Mol Cell *43*, 723-737.

Larkin, J., Ascierto, P.A., Dreno, B., Atkinson, V., Liszkay, G., Maio, M., Mandala, M., Demidov, L., Stroyakovskiy, D., Thomas, L., *et al.* (2014). Combined vemurafenib and cobimetinib in BRAF-mutated melanoma. The New England journal of medicine *371*, 1867-1876.

Lavoie, H., and Therrien, M. (2015). Regulation of RAF protein kinases in ERK signalling. Nat Rev Mol Cell Biol *16*, 281-298.

Lito, P., Rosen, N., and Solit, D.B. (2013). Tumor adaptation and resistance to RAF inhibitors. Nat Med *19*, 1401-1409.

MacKerell, A.D., Bashford, D., Bellott, M., Dunbrack, R.L., Evanseck, J.D., Field, M.J., Fischer, S., Gao, J., Guo, H., Ha, S., *et al.* (1998). All-Atom Empirical Potential for Molecular Modeling and Dynamics Studies of Proteins. The Journal of Physical Chemistry B *102*, 3586-3616.

Mackerell, A.D., Feig, M., and Brooks, C.L. (2004). Extending the treatment of backbone energetics in protein force fields: Limitations of gas-phase quantum mechanics in reproducing protein conformational distributions in molecular dynamics simulations. Journal of Computational Chemistry *25*, 1400-1415.

Nan, X., Tamguney, T.M., Collisson, E.A., Lin, L.J., Pitt, C., Galeas, J., Lewis, S., Gray, J.W., McCormick, F., and Chu, S. (2015). Ras-GTP dimers activate the Mitogen-Activated Protein Kinase (MAPK) pathway. Proc Natl Acad Sci U S A *112*, 7996-8001.

Nazarian, R., Shi, H., Wang, Q., Kong, X., Koya, R.C., Lee, H., Chen, Z., Lee, M.K., Attar, N., Sazegar, H., *et al.* (2010). Melanomas acquire resistance to B-RAF(V600E) inhibition by RTK or N-RAS upregulation. Nature *468*, 973-977.

Niyazi, M., Niyazi, I., and Belka, C. (2007). Counting colonies of clonogenic assays by using densitometric software. Radiation Oncology *2*, 4.

Nussinov, R., Tsai, C.-J., and Ma, B. (2013). The Underappreciated Role of Allostery in the Cellular Network. Annual Review of Biophysics *42*, 169-189.

Okaniwa, M., Hirose, M., Arita, T., Yabuki, M., Nakamura, A., Takagi, T., Kawamoto, T., Uchiyama, N., Sumita, A., Tsutsumi, S., *et al.* (2013). Discovery of a selective kinase inhibitor (TAK-632) targeting pan-RAF inhibition: design, synthesis, and biological evaluation of C-7-substituted 1,3-benzothiazole derivatives. J Med Chem *56*, 6478-6494.

Pawson, T., and Nash, P. (2003). Assembly of cell regulatory systems through protein interaction domains. Science *300*, 445-452.

Poulikakos, P.I., Persaud, Y., Janakiraman, M., Kong, X., Ng, C., Moriceau, G., Shi, H., Atefi, M., Titz, B., Gabay, M.T., *et al.* (2011). RAF inhibitor resistance is mediated by dimerization of aberrantly spliced BRAF(V600E). Nature *480*, 387-390.

Poulikakos, P.I., Zhang, C., Bollag, G., Shokat, K.M., and Rosen, N. (2010). RAF inhibitors transactivate RAF dimers and ERK signalling in cells with wild-type BRAF. Nature *464*, 427-430.

Poussin, C., Mathis, C., Alexopoulos, L.G., Messinis, D.E., Dulize, R.H.J., Belcastro, V., Melas, I.N., Sakellaropoulos, T., Rhrissorrakrai, K., Bilal, E., *et al.* (2014). The species translation challenge—A systems biology perspective on human and rat bronchial epithelial cells. *1*, 140009.

Prasad, V. (2016). Perspective: The precision-oncology illusion. Nature *537*, S63-S63.

Prior, I.A., Lewis, P.D., and Mattos, C. (2012). A comprehensive survey of Ras mutations in cancer. Cancer research *72*, 2457-2467.

Qin, J., Xie, P., Ventocilla, C., Zhou, G., Vultur, A., Chen, Q., Liu, Q., Herlyn, M., Winkler, J., and Marmorstein, R. (2012). Identification of a Novel Family of BRAFV600E Inhibitors. Journal of Medicinal Chemistry *55*, 5220-5230.

Rahman, M.A., Salajegheh, A., Smith, R.A., and Lam, A.K. (2014). BRAF inhibitors: From the laboratory to clinical trials. Crit Rev Oncol Hematol *90*, 220-232.

Rauch, N., Rukhlenko, O.S., Kolch, W., and Kholodenko, B.N. (2016). MAPK kinase signalling dynamics regulate cell fate decisions and drug resistance. Current Opinion in Structural Biology *41*, 151-158.

Ritt, D.A., Monson, D.M., Specht, S.I., and Morrison, D.K. (2010). Impact of feedback phosphorylation and Raf heterodimerization on normal and mutant B-Raf signaling. Mol Cell Biol *30*, 806-819.

Romano, D., Nguyen, L.K., Matallanas, D., Halasz, M., Doherty, C., Kholodenko, B.N., and Kolch, W. (2014). Protein interaction switches coordinate Raf-1 and MST2/Hippo signalling. Nat Cell Biol *16*, 673-684.

Roskoski, R., Jr. (2016). Classification of small molecule protein kinase inhibitors based upon the structures of their drug-enzyme complexes. Pharmacol Res *103*, 26-48.

Rubinstein, B.Y., Mattingly, H.H., Berezhkovskii, A.M., and Shvartsman, S.Y. (2016). Long-term dynamics of multisite phosphorylation. Molecular Biology of the Cell *27*, 2331-2340.

Rushworth, L.K., Hindley, A.D., O'Neill, E., and Kolch, W. (2006). Regulation and role of Raf-1/B-Raf heterodimerization. Mol Cell Biol *26*, 2262-2272.

Ryckaert, J.-P., Ciccotti, G., and Berendsen, H.J.C. (1977). Numerical integration of the cartesian equations of motion of a system with constraints: molecular dynamics of n-alkanes. Journal of Computational Physics *23*, 327-341.

Rykunov, D., Steinberger, E., Madrid-Aliste, C.J., and Fiser, A. (2009). Improved scoring function for comparative modeling using the M4T method. Journal of Structural and Functional Genomics *10*, 95-99.

Saez-Rodriguez, J., MacNamara, A., and Cook, S. (2015). Modeling Signaling Networks to Advance New Cancer Therapies. Annu Rev Biomed Eng *17*, 143-163.

Sanchez-Laorden, B., Viros, A., Girotti, M.R., Pedersen, M., Saturno, G., Zambon, A., Niculescu-Duvaz, D., Turajlic, S., Hayes, A., Gore, M., *et al.* (2014). BRAF Inhibitors Induce Metastasis in RAS Mutant or Inhibitor-Resistant Melanoma Cells by Reactivating MEK and ERK Signaling. Science Signaling *7*, ra30.

Shao, Q., Xu, Z., Wang, J., Shi, J., and Zhu, W. (2017). Energetics and structural characterization of the "DFG-flip" conformational transition of B-RAF kinase: a SITS molecular dynamics study. Phys Chem Chem Phys *19*, 1257-1267.

Shi, H., Moriceau, G., Kong, X., Lee, M.K., Lee, H., Koya, R.C., Ng, C., Chodon, T., Scolyer, R.A., Dahlman, K.B., *et al.* (2012). Melanoma whole-exome sequencing identifies (V600E)B-RAF amplification-mediated acquired B-RAF inhibitor resistance. Nat Commun *3*, 724.

Stephen, Andrew G., Esposito, D., Bagni, Rachel K., and McCormick, F. Dragging Ras Back in the Ring. Cancer Cell *25*, 272-281.

Sturm, O.E., Orton, R., Grindlay, J., Birtwistle, M., Vyshemirsky, V., Gilbert, D., Calder, M., Pitt, A., Kholodenko, B., and Kolch, W. (2010). The mammalian MAPK/ERK pathway exhibits properties of a negative feedback amplifier. Sci Signal *3*, ra90.

Varga, A., Ehrenreiter, K., Aschenbrenner, B., Kocieniewski, P., Kochanczyk, M., Lipniacki, T., and Baccarini, M. (2017). RAF1/BRAF dimerization integrates the signal from RAS to ERK and ROKalpha. Sci Signal *10*.

Wan, P.T.C., Garnett, M.J., Roe, S.M., Lee, S., Niculescu-Duvaz, D., Good, V.M., Project, C.G., Jones, C.M., Marshall, C.J., Springer, C.J., *et al.* (2004). Mechanism of Activation of the RAF-ERK Signaling Pathway by Oncogenic Mutations of B-RAF. Cell *116*, 855-867.

Weber, C.K., Slupsky, J.R., Kalmes, H.A., and Rapp, U.R. (2001). Active Ras Induces Heterodimerization of cRaf and BRaf. Cancer research *61*, 3595.

Wenglowsky, S., Ren, L., Ahrendt, K.A., Laird, E.R., Aliagas, I., Alicke, B., Buckmelter, A.J., Choo, E.F., Dinkel, V., Feng, B., *et al.* (2011). Pyrazolopyridine Inhibitors of B-RafV600E. Part 1: The Development of Selective, Orally Bioavailable, and Efficacious Inhibitors. ACS Medicinal Chemistry Letters *2*, 342-347.

Wilhelm, S.M., Carter, C., Tang, L., Wilkie, D., McNabola, A., Rong, H., Chen, C., Zhang, X., Vincent, P., McHugh, M., *et al.* (2004). BAY 43-9006 Exhibits Broad Spectrum Oral Antitumor Activity and Targets the RAF/MEK/ERK Pathway and Receptor Tyrosine Kinases Involved in Tumor Progression and Angiogenesis. Cancer research *64*, 7099.

Yaktapour, N., Meiss, F., Mastroianni, J., Zenz, T., Andrlova, H., Mathew, N.R., Claus, R., Hutter, B., Frohling, S., Brors, B., *et al.* (2014). BRAF inhibitor-associated ERK activation drives development of chronic lymphocytic leukemia. J Clin Invest *124*, 5074-5084.

Yao, Z., Torres, N.M., Tao, A., Gao, Y., Luo, L., Li, Q., de Stanchina, E., Abdel-Wahab, O., Solit, D.B., Poulikakos, P.I., *et al.* (2015). BRAF Mutants Evade ERK-Dependent Feedback by Different Mechanisms that Determine Their Sensitivity to Pharmacologic Inhibition. Cancer Cell *28*, 370-383.

Yeh, P.J., Hegreness, M.J., Aiden, A.P., and Kishony, R. (2009). Drug interactions and the evolution of antibiotic resistance. Nat Rev Microbiol *7*, 460-466.

Zehir, A., Benayed, R., Shah, R.H., Syed, A., Middha, S., Kim, H.R., Srinivasan, P., Gao, J., Chakravarty, D., Devlin, S.M., *et al.* (2017). Mutational landscape of metastatic cancer revealed from prospective clinical sequencing of 10,000 patients. Nat Med *23*, 703-713.

Zhang, C., Spevak, W., Zhang, Y., Burton, E.A., Ma, Y., Habets, G., Zhang, J., Lin, J., Ewing, T., Matusow, B., *et al.* (2015). RAF inhibitors that evade paradoxical MAPK pathway activation. Nature *526*, 583-586.

Figure 1

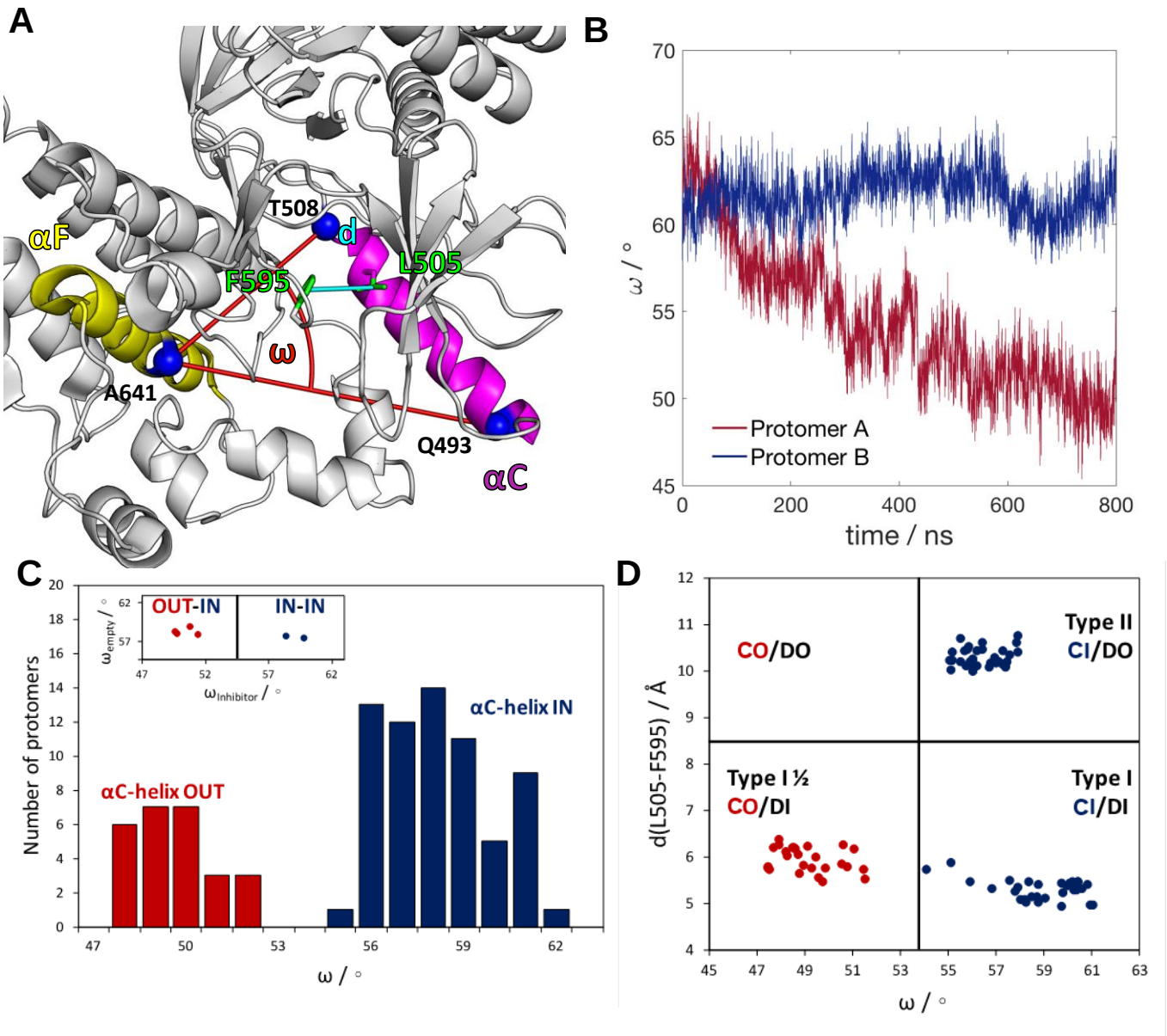
A
αF
T508
d
L505
F595
ω
A641
Q493
αC
B
ω / °
time / ns
Protomer A
Protomer B
C
Number of protomers
ω / °
OUT-IN
IN-IN
ω_empty / °
ω_Inhibitor / °
αC-helix OUT
αC-helix IN
D
d(L505-F595) / Å
ω / °
CO/DO
Type II
CI/DO
Type I ½
CO/DI
Type I
CI/DI

Figure 2

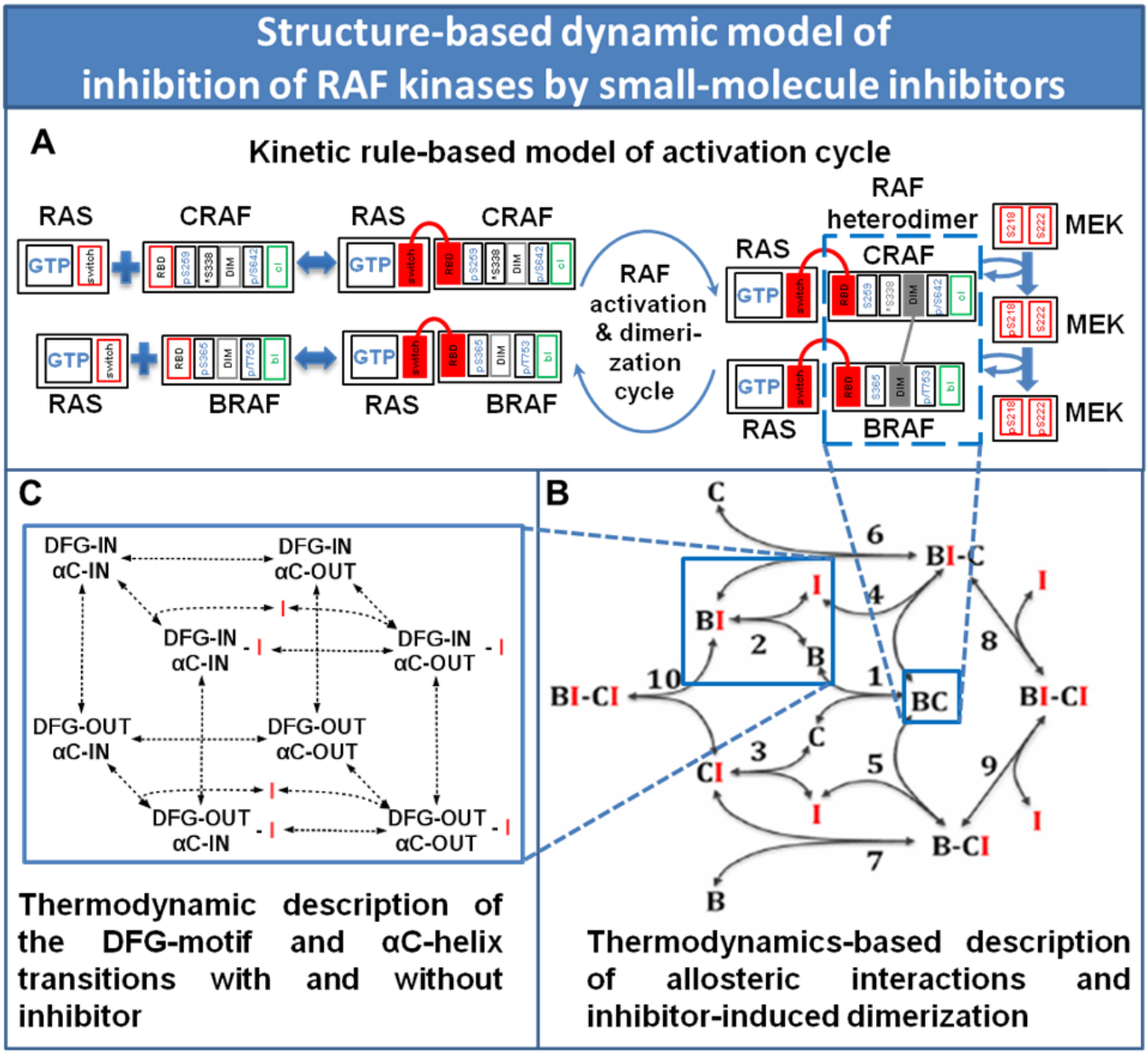
Structure-based dynamic model of inhibition of RAF kinases by small-molecule inhibitors
A
Kinetic rule-based model of activation cycle
RAS
CRAF
BRAF
GTP
switch
RBD
CR1
CR2
CR3
DIM
RAF activation & dimeri-zation cycle
RAF heterodimer
MEK
pS218
pS222
C
DFG-IN αC-IN
DFG-IN αC-OUT
DFG-OUT αC-IN
DFG-OUT αC-OUT
Thermodynamic description of the DFG-motif and αC-helix transitions with and without inhibitor
B
BI-C
BI
BC
BI-CI
CI
B-CI
Thermodynamics-based description of allosteric interactions and inhibitor-induced dimerization

Figure 3

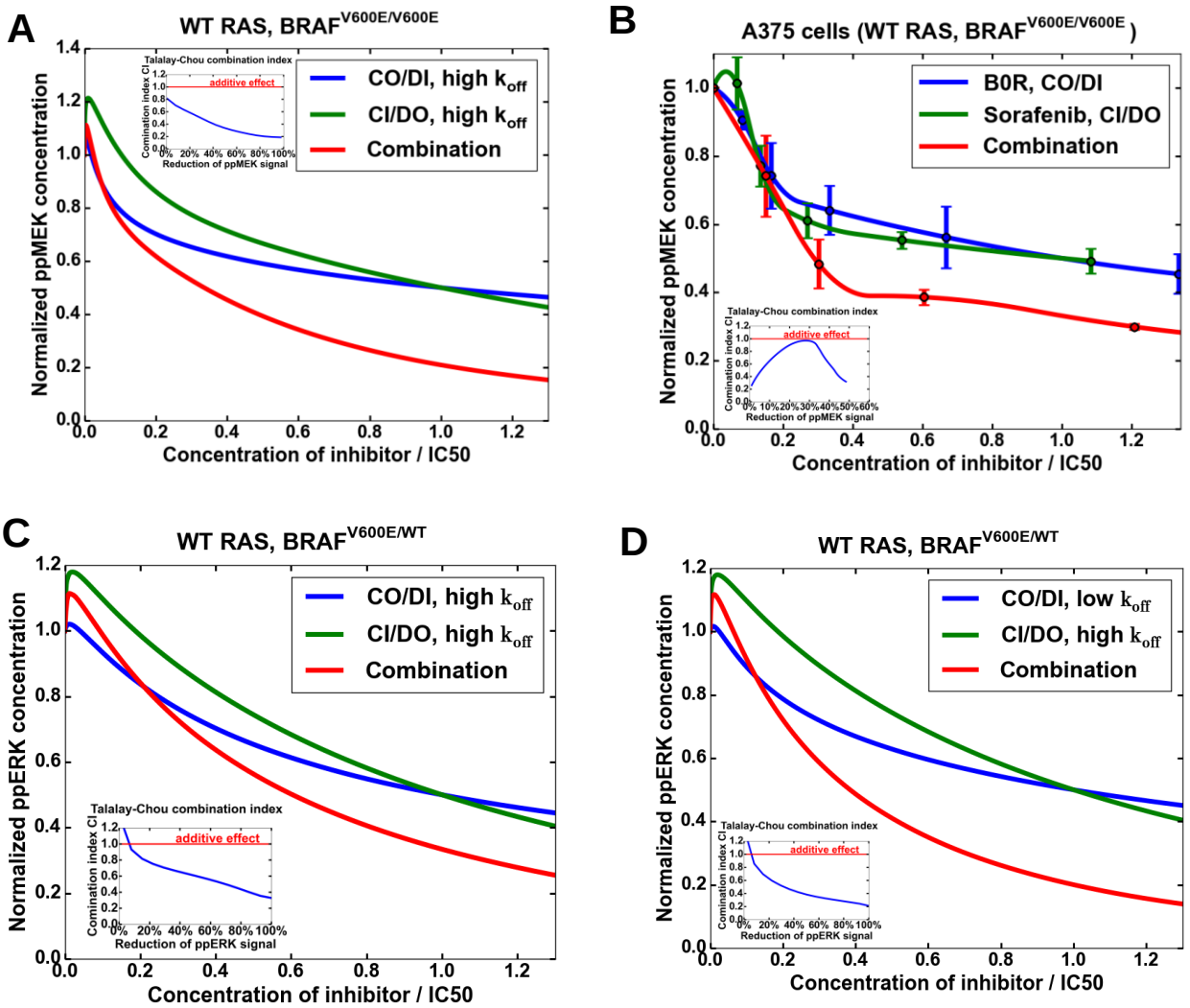
A
WT RAS, BRAF V600E/V600E
Normalized ppMEK concentration
Concentration of inhibitor / IC50
CO/DI, high k off
CI/DO, high k off
Combination
Talalay-Chou combination index
Comination index CI
additive effect
Reduction of ppMEK signal
B
A375 cells (WT RAS, BRAF V600E/V600E )
Normalized ppMEK concentration
Concentration of inhibitor / IC50
B0R, CO/DI
Sorafenib, CI/DO
Combination
Talalay-Chou combination index
Comination index CI
additive effect
Reduction of ppMEK signal
C
WT RAS, BRAF V600E/WT
Normalized ppERK concentration
Concentration of inhibitor / IC50
CO/DI, high k off
CI/DO, high k off
Combination
Talalay-Chou combination index
Comination index CI
additive effect
Reduction of ppERK signal
D
WT RAS, BRAF V600E/WT
Normalized ppERK concentration
Concentration of inhibitor / IC50
CO/DI, low k off
CI/DO, high k off
Combination
Talalay-Chou combination index
Comination index CI
additive effect
Reduction of ppERK signal

Figure 4

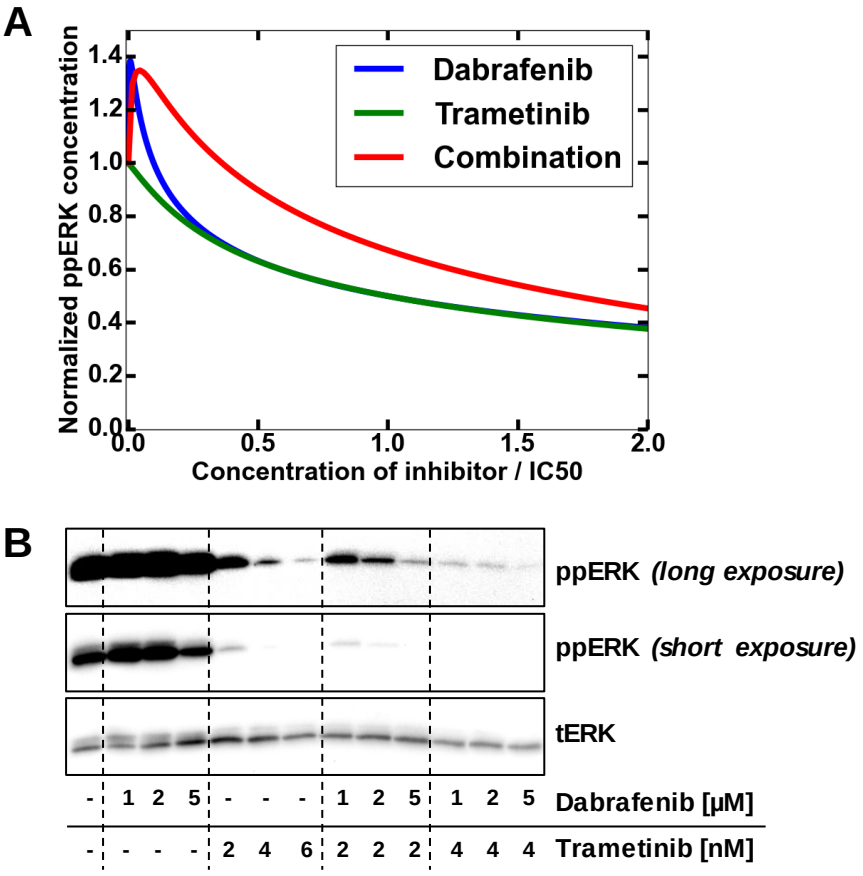
A
Normalized ppERK concentration
1.4
1.2
1.0
0.8
0.6
0.4
0.2
0.0
0.0
0.5
1.0
1.5
2.0
Concentration of inhibitor / IC50
Dabrafenib
Trametinib
Combination
B
ppERK (long exposure)
ppERK (short exposure)
tERK
- 1 2 5 - - - 1 2 5 1 2 5
Dabrafenib [μM]
- - - - 2 4 6 2 2 2 4 4 4
Trametinib [nM]

Figure 5

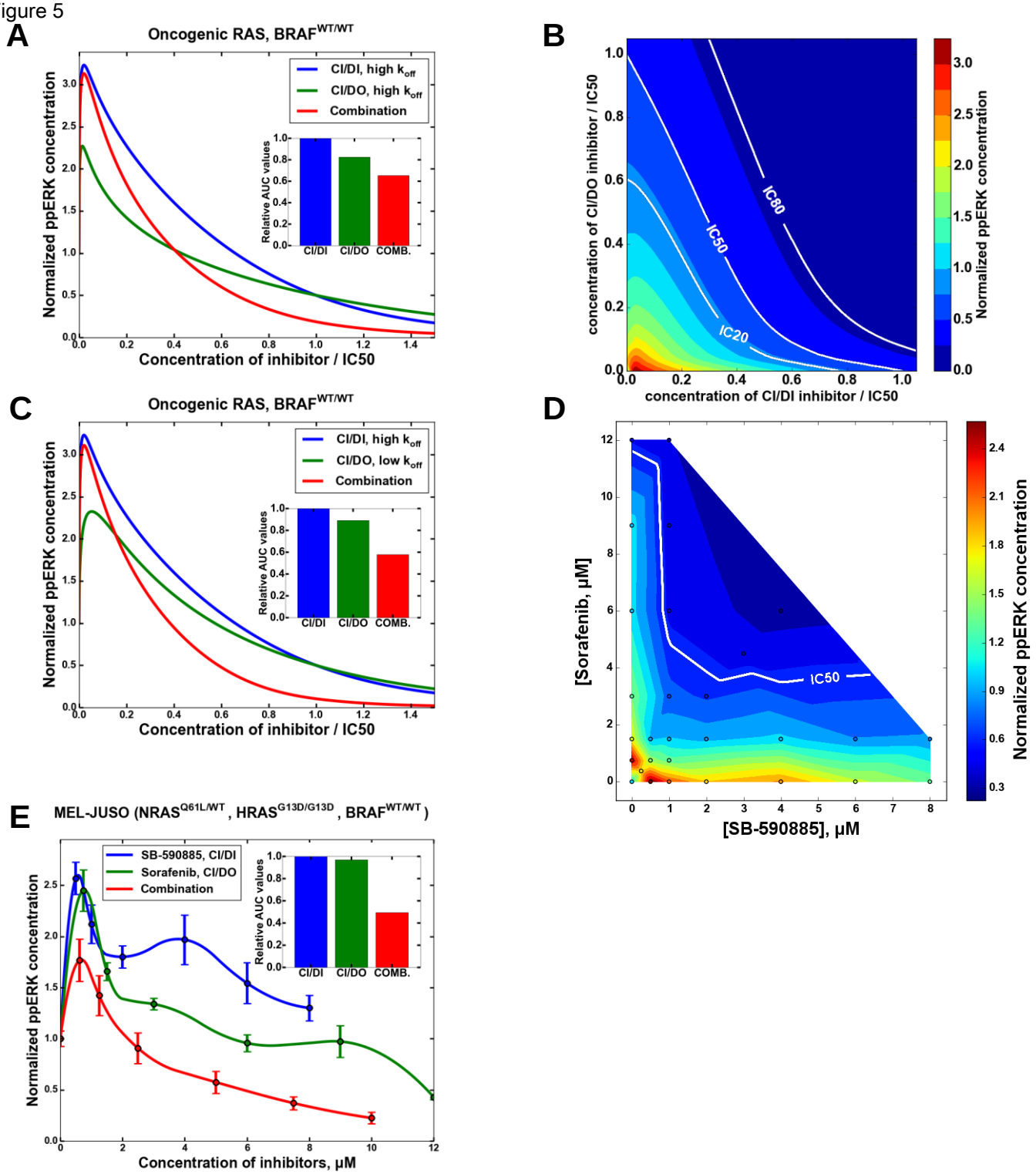
A
Oncogenic RAS, BRAF^WT/WT
CI/DI, high k_off
CI/DO, high k_off
Combination
Normalized ppERK concentration
Concentration of inhibitor / IC50
Relative AUC values
CI/DI
CI/DO
COMB.
B
concentration of CI/DO inhibitor / IC50
concentration of CI/DI inhibitor / IC50
IC80
IC50
IC20
Normalized ppERK concentration
C
Oncogenic RAS, BRAF^WT/WT
CI/DI, high k_off
CI/DO, low k_off
Combination
Normalized ppERK concentration
Concentration of inhibitor / IC50
Relative AUC values
CI/DI
CI/DO
COMB.
D
[Sorafenib, µM]
[SB-590885], µM
IC50
Normalized ppERK concentration
E
MEL-JUSO (NRAS^Q61L/WT, HRAS^G13D/G13D, BRAF^WT/WT)
SB-590885, CI/DI
Sorafenib, CI/DO
Combination
Normalized ppERK concentration
Concentration of inhibitors, µM
Relative AUC values
CI/DI
CI/DO
COMB.

Figure 6

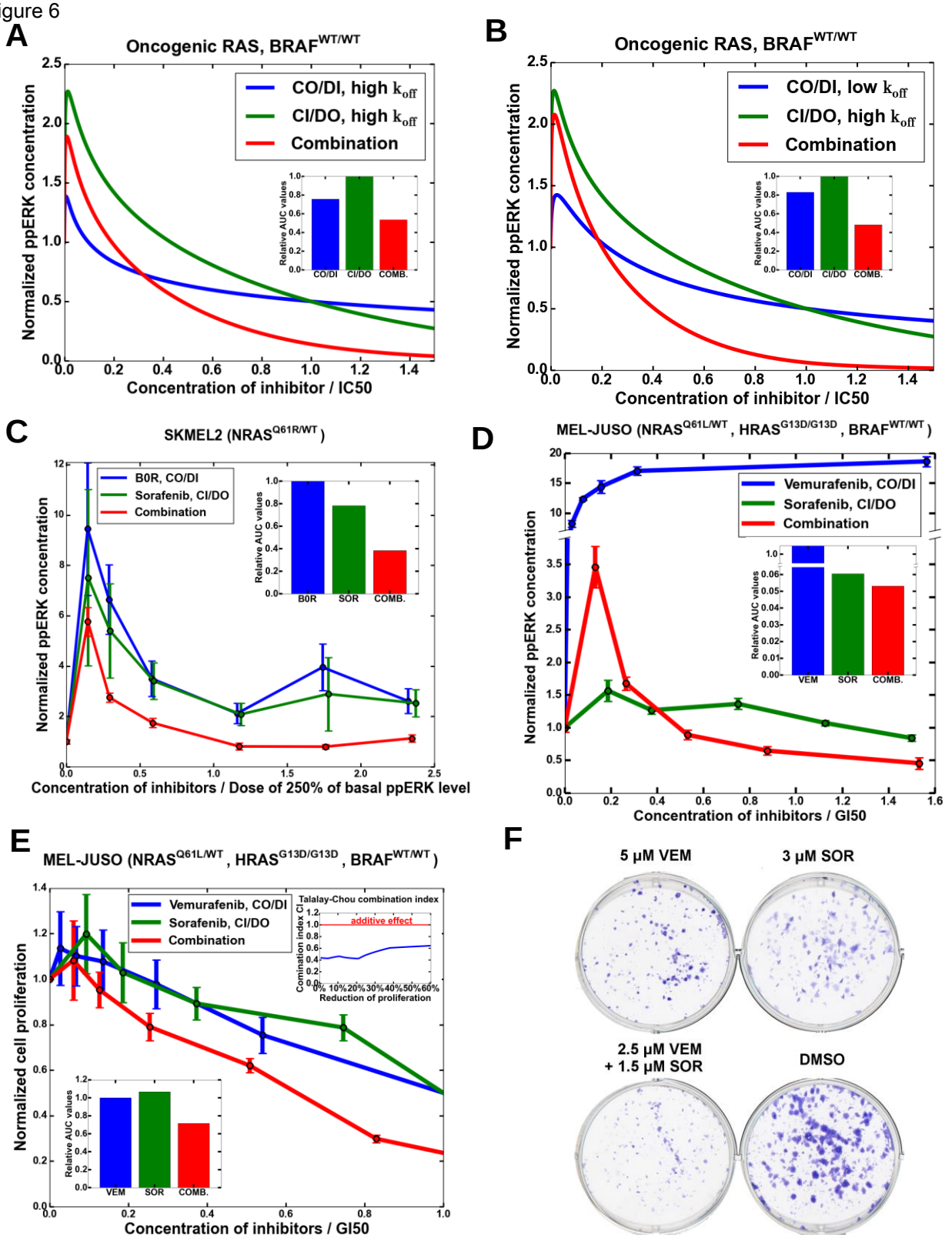
A
Oncogenic RAS, BRAF^WT/WT
CO/DI, high k_off
CI/DO, high k_off
Combination
Normalized ppERK concentration
Concentration of inhibitor / IC50
Relative AUC values
CO/DI
CI/DO
COMB.
B
Oncogenic RAS, BRAF^WT/WT
CO/DI, low k_off
CI/DO, high k_off
Combination
Normalized ppERK concentration
Concentration of inhibitor / IC50
C
SKMEL2 (NRAS^Q61R/WT)
B0R, CO/DI
Sorafenib, CI/DO
Combination
Normalized ppERK concentration
Concentration of inhibitors / Dose of 250% of basal ppERK level
B0R
SOR
COMB.
D
MEL-JUSO (NRAS^Q61L/WT, HRAS^G13D/G13D, BRAF^WT/WT)
Vemurafenib, CO/DI
Sorafenib, CI/DO
Combination
Normalized ppERK concentration
Concentration of inhibitors / GI50
VEM
SOR
COMB.
E
MEL-JUSO (NRAS^Q61L/WT, HRAS^G13D/G13D, BRAF^WT/WT)
Vemurafenib, CO/DI
Sorafenib, CI/DO
Combination
Talalay-Chou combination index
additive effect
Comination index CI
Reduction of proliferation
Normalized cell proliferation
Concentration of inhibitors / GI50
VEM
SOR
COMB.
F
5 μM VEM
3 μM SOR
2.5 μM VEM
+ 1.5 μM SOR
DMSO

Figure 7

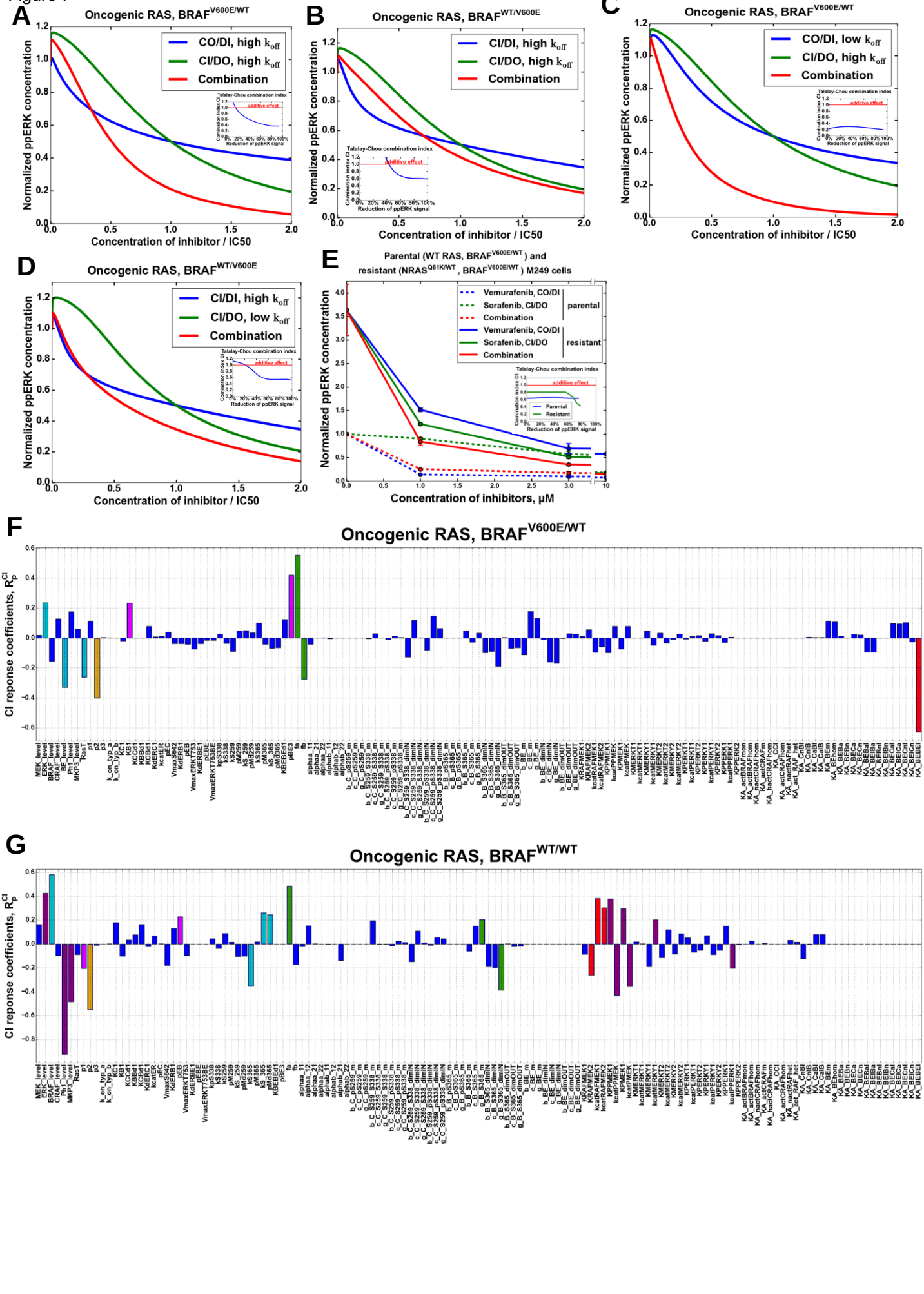
A
Oncogenic RAS, BRAF^V600E/WT
CO/DI, high k_off
CI/DO, high k_off
Combination
Normalized ppERK concentration
Concentration of inhibitor / IC50
B
Oncogenic RAS, BRAF^WT/V600E
CI/DI, high k_off
CI/DO, high k_off
Combination
C
Oncogenic RAS, BRAF^V600E/WT
CO/DI, low k_off
CI/DO, high k_off
Combination
D
Oncogenic RAS, BRAF^WT/V600E
CI/DI, high k_off
CI/DO, low k_off
Combination
E
Parental (WT RAS, BRAF^V600E/WT) and
resistant (NRAS^Q61K/WT, BRAF^V600E/WT) M249 cells
Vemurafenib, CO/DI
Sorafenib, CI/DO
Combination
parental
Vemurafenib, CO/DI
Sorafenib, CI/DO
Combination
resistant
Concentration of inhibitors, μM
Talalay-Chou combination index
additive effect
Reduction of ppERK signal
F
Oncogenic RAS, BRAF^V600E/WT
CI reponse coefficients, R_p^CI
G
Oncogenic RAS, BRAF^WT/WT
CI reponse coefficients, R_p^CI

**Supplemental Information.**

# Dissecting RAF inhibitor resistance by structure-based modeling reveals ways to overcome oncogenic RAS signaling

Oleksii S. Rukhlenko, Fahimeh Khorsand, Aleksandar Krstic, Jan Rozanc, Leonidas G. Alexopoulos, Nora Rauch, William S. Hlavacek, Richard G. Posner, Silvia Gómez-Coca, Edina Rosta, Cheree Fitzgibbon, David Matallanas, Jens Rauch, Walter Kolch, Boris N. Kholodenko

## Content

**Table S1 related to Figures 1 and 2. Summary of the structural properties of RAF inhibitors**

| Type of inhibitor | Orientation of αC-helix | Orientation of DFG-motif | Abbreviation | Examples of inhibitors |
|---|---|---|---|---|
| I | IN | IN | CI/DI | SB590885, GDC-0879 |
| I½ | OUT | IN | CO/DI | vemurafenib, B0R, dabrafenib, LGX818 |
| II | IN | OUT | CI/DO | sorafenib, AZ-628, TAK-632, LY3009120 |

## Supplemental Figures

**Figure S1 related to Figure 1.** (**A**) Overlay of two structures, one of which is αC-helix-IN (4YHT, blue color), and the other is αC-helix-OUT (3TV4, red color). The αC-helix angle ω, which defines IN (ω > 54$^o$) or OUT (ω < 52$^o$) positions is highlighted in blue and red. (**B**) Overlay of the 46 BRAF dimer structures analysed showing the αC-helix IN and OUT in blue and red respectively. (**C**) Overlay of two structures one of which is DFG-IN (4YHT, blue color) and the other is DFG-OUT (4DBN, red color). The L505-F595 distance, which defines IN (d < 7 Å) and OUT (d > 9.5 Å) conformations, is depicted in blue and red lines, respectively. (**D**) Overlay of the 45 BRAF dimer structures analysed showing the DFG IN (blue) and OUT (red) (3C4C was not included because it has a different DFG conformation). (**E**) Distribution of the DFG conformations in 90 BRAF kinase domain protomers based on the analysis of 45 BRAF dimer structures deposited in PDB.

**Figure S2 related to Figure 2.** Kinetic schemes of the rules governing: (**A**) CRAF binding to RAS and CRAF activation cycle; (**B**) BRAF binding to RAS and BRAF activation cycle; (**C**) Influence of ERK feedback phosphorylation on binding of RAF kinases to RAS; (**D**) RAF hetero-dimerization cycle; (**E**) Influence of ERK feedback phosphorylation on CRAF-BRAF hetero-dimerization. Protein domain designations are the same as in Fig. 2. Parameter notations on the arrows are explained in the SI, sections 1 and 2, see also List S5.1.

**Figure S3 related to Figure 3.** (**A-F**) Model-predicted relative contribution of kinase activity of RAF monomers and dimers into the total RAF kinase activity during treatment with CO/DI (**A, D**), CI/DO (**B, E**) and CI/DI (**C, F**) inhibitors and in the absence of inhibitors (inserts) for cells with heterozygous (**A-C**) and homozygous (**D-F**) BRAFV600E mutation and WT RAS. **(G-J**) Model-predicted response of MEK and ERK signaling to: CO/DI and CI/DO inhibitors and their combination (**G, I**), CI/DI and CO/DI inhibitors and their combination (**H**), and CI/DI and CI/DO inhibitors and their combination (**J**) in cells with homozygous (**G**) and heterozygous (**H-J**) BRAFV600E mutation. Inhibitor doses are normalized by IC50. The residence time $1/k_{off}$ of CO/DI and CI/DI inhibitors is 1 s. The residence times $1/k_{off}$ of CI/DO inhibitor are 1 s (**B, E, G, J**) and $10^4$ s (**I**). In each combination, the ratio of CO/DI and CI/DO inhibitor doses is 1.2:1, the ratio of CI/DI and CO/DI inhibitor doses is 1.2:1, and the ratio of CI/DI and CI/DO inhibitor doses is 1.2:1. Parameters for (**A-C**) and (**H-J**) are: [RAS-GTP]=25 nM, [$BRAF^{V600E}$]=25 nM, [$BRAF^{WT}$]=25 nM. Parameters for (**D-F**) and (**G**) are: [RAS-GTP]=25 nM, [$BRAF^{V600E}$]=50 nM, [$BRAF^{WT}$]=0 nM. The remaining parameters are given in Lists S4.1 and S5.1 in SI. In panels (**G-J**), the inserts assess synergy, additivity or antagonism, using the Talalay-Chou combination index (CI).

**Figure S4 related to Figure 4.** Predictive simulations of Loewe isoboles demonstrate antagonism rather than synergy of inhibiting ERK signaling by combinations of CO/DI RAF inhibitor and MEK inhibitor in cells bearing oncogenic RAS and WT BRAF (cf. Figs. S5 and 5). [RAS-GTP]=250 nM, [$BRAF^{V600E}$]=0, [$BRAF^{WT}$]=50 nM, basal ppERK level is 480 nM.

**Figure S5 related to Figure 5. (A-E**) Model predicted stationary responses to CI/DI and CI/DO inhibitors and their combination of: **(A)** CRAF phosphorylation on S259 and S338; **(B)** RAF heterodimers bound with two molecules of RAF inhibitor; **(C)** MEK signaling; **(D-E)** ERK signaling. (**C**) Talalay-Chou index for MEK and ERK inhibition is presented on the insert. [RAS-GTP]=250 nM (**A-E**), [RAS-GTP]=100 nM (**D**), [$BRAF^{V600E}$]=0, [$BRAF^{WT}$]=50 nM, basal ppERK levels are 480 nM (**A-E**) and 279 nM (**D**), the ratio of CI/DI and CI/DO inhibitor doses applied in combination is 2.2:1 (**A-E**). (**F-I**). ERK (**F-G, I**) and MEK (**H**) signaling responses in growing MEL-JUSO ($NRAS^{Q61L/WT}$, $HRAS^{G13D/G13D}$, $BRAF^{WT/WT}$) cells to SB-590885 (CI/DI), sorafenib (CI/DO) and their combination, which are measured

using MESOSCALE (**F**) and LUMINEX (**G-H**) systems, and Western Blot (**I**), 24 hr. The Western Blots (**I**) are taken from a single membrane which was obtained using multistrip western blotting (Aksamitiene et al., 2007). For inhibitor combinations, the ratio of SB590885 to sorafenib is 1:1.5. The ppERK responses are plotted vs the absolute concentrations of inhibitors applied separately and vs the sum of the absolute concentrations for their combination.

**Figure S6 related to Figure 6.** Model-predicted responses of MEK (**B-C**, **E-F**) and ERK (**A**, **D**, **G**) signaling to CI/DI, CO/DI inhibitors and their combination (**A-B**, **D-E**) and to CO/DI, CI/DO inhibitors and their combination (**C**, **F**, **G**). The residence times $t_{off} \sim 1/k_{off}$ of CO/DI inhibitor are 1 s (**A-C, G**) and $10^4$ s (**D-F**). Inserts assess synergy, additivity or antagonism, using the AUC (**A, D, G**) and CI (**B, C, E-G**).The residence times of CI/DO inhibitor are 1 s (**C, F**) and $10^4$ s (**G**). Inhibitor doses are normalized by IC50, the total doses shown for the combination correspond to the optimal ratios of inhibitor doses. [RAS-GTP]=250 nM, [$BRAF^{V600E}$]=0, [$BRAF^{WT}$]=50 nM, basal ppERK level is 484 nM. The ratios of CI/DI and CO/DI inhibitor doses applied in combination are 3:5 (**A-B**) and 1:1 (**D-E**). The ratios of CO/DI and CI/DO inhibitor doses applied in combination are 1:1 (**C, F, G**).

**Figure S7 related to Figure 7.** (**A-D**) Model-predicted stationary responses of ERK (**A-B**) and MEK (**C-D**) signaling in cells with oncogenic RAS mutation and heterozygous BRAFV600E mutation to: CI/DI and CO/DI inhibitors and their combination (**A-B**), CO/DI and CI/DO inhibitors and their combination (**C**), and CI/DI and CI/DO inhibitors and their combination (**D**). The residence time $t_{off} \sim 1/k_{off}$ of all inhibitors is 1 s. Inhibitor doses are normalized by IC50. In combinations, the ratio of CI/DI and CO/DI inhibitor doses are 1:1 (**A**) and 2.2:1 (**B**), the ratio of CO/DI and CI/DO inhibitor doses is 1:1 (**C**), and the ratio of CI/DI and CI/DO inhibitor doses is 6:1 (**D**). [RAS-GTP]=250 nM, [$BRAF^{V600E}$]=25 nM, [$BRAF^{WT}$]=25 nM, basal ppERK level is 2151 nM. (**E**) Model-predicted response of RAS-RAF complexes concentration to different RAF inhibitors in cells with WT BRAF and oncogenic RAS. [RAS-GTP]=250 nM, [$BRAF^{V600E}$]=0, [$BRAF^{WT}$]=50 nM, basal ppERK level is 480 nM. (**F**) Model-predicted stationary response of ERK signaling to CO/DI, CI/DO inhibitors and their combination in cells with WT RAS and p61 splice variant of heterozygous BRAFV600E. [RAS-GTP]=25 nM, [$BRAF^{V600E}$]=0, [$p61BRAF^{V600E}$]=25 nM, [$BRAF^{WT}$]=25 nM, basal ppERK level is 1627 nM. Inhibitor doses are normalized by IC50. In combination, the ratio of CO/DI and CI/DO inhibitor doses is 7:1. (**A**, **B**, **F**) Inserts assess drug synergy using the Talalay-Chou combination index (CI). **G-H**. Model-predicted stationary responses of ERK signaling in cells with WT RAS, heterozygous BRAFV600E mutation and CRAF overexpression to: CI/DI, CI/DO inhibitors and their combination, and to CO/DI, CI/DO inhibitors and their combination. Inhibitor doses are normalized by IC50 (**G**) and IC30 (**H**). [RAS-GTP]=25 nM, [$BRAF^{V600E}$]=25 nM, [$BRAF^{WT}$]=25 nM, [CRAF]=250 nM, basal ppERK level is 2603 nM. (**I–J**) Sensitivities of the areas under dose-response curves (AUC) to parameter changes for a combination of CO/DI (inhibitor a) and CI/DO (inhibitor b) RAF inhibitors in cells bearing both oncogenic RAS and BRAFV600E mutations (**I**) or only oncogenic RAS and WT BRAF (**J**).

## Supplemental Experimental Procedures

### 1. A model of the RAF kinase activation cycle.

### 1.1. CRAF and BRAF phosphorylation sites and binding domains considered in the model

The model monitors the states of the three phosphorylation sites on CRAF **(**S259, S338 and S642) and two phosphorylation sites on BRAF (S365 and T753). S259 on CRAF and S365 on BRAF are inhibitory sites (Roskoski, 2010). Phosphorylation of these sites (yielding pS259 and pS365) and binding of 14-3-3 protein stabilize the inactive conformations of CRAF and BRAF (Dhillon and Kolch, 2002; Dhillon et al., 2002; Leicht et al., 2007; Roskoski, 2010). S338 is an activating site on CRAF (Dhillon and Kolch, 2002; Leicht et al., 2007). Phosphorylation of inhibitory S259 and phosphorylation of activating S338 sites on CRAF are mutually exclusive (Chiloeches et al., 2001). Following S259 dephosphorylation, CRAF requires S338 phosphorylation for full activation in the model. Next, the model includes sites of feedback phosphorylation by ERK, S642 and T753, on CRAF and BRAF, respectively (Ritt et al., 2010).

Binding and dimerization of RAF kinases is described in the model through the RAS Binding Domain (RBD), MEK-Binding domain (MEKB), dimerization domain (DIM) and Inhibitor-binding pocket (CI and BI on CRAF and BRAF). The rates of these reactions depend on the particular CRAF and BRAF phosphorylation states and the spatial localization of these molecules. Binding and dissociation reactions are described by mass-action rate laws in the model. When the available data suggest that (de)phosphorylation reactions are far from saturation, they are described by first order kinetics, otherwise (de)phosphorylation reactions are described by Michaelis – Menten kinetics (see below)

### 1.2. Binding of CRAF monomers to RAS-GTP and (de)phosphorylation of S259 and S338

In the absence of the RAS-GTP signal, CRAF mainly resides in the cytoplasm where it is phosphorylated on S259 (the inhibiting residue), and dephosphorylated on S338 (the residue has to be phosphorylated for full activation) and S642 (the site of feedback phosphorylation by ERK). The rate constant of phosphorylation of CRAF on S259 in the cytoplasm is kS259. The model assumes that there is a low basal rate of dephosphorylation of CRAF on S259 in the cytoplasm, described by the rate constant kS_259. The values of all parameters in the model are given in List S5.1.

CRAF is activated by binding to RAS-GTP leading to the CRAF recruitment to plasma membrane. The data suggest that both CRAF phosphorylated on S259 and CRAF dephosphorylated on S259 can bind to RAS-GTP (Jaumot and Hancock, 2001). The rate constants for association of CRAF with RAS-GTP and dissociation are kC1 and kC_1, respectively.

After binding of CRAF to RAS-GTP, the rate of dephosphorylation of CRAF on S259 is much faster, whereas the rate of its phosphorylation on S259 is much slower than the corresponding rates in the cytoplasm, due to that the dissociation of 14-3-3 proteins (Matallanas et al., 2011). In the model the corresponding rate constants are multiplied by parameters pMd259 and pM259 (List S5.1). Because 14-3-3 proteins are highly abundant in the cell, and their abundance does not change under the conditions analyzed in the paper, the model does not explicitly consider these proteins. CRAF can be phosphorylated on S259 both in a monomeric form and as a protomer in a dimer. If CRAF is phosphorylated on S259 when it is a protomer in a dimer with another RAF molecule, the dimer quickly dissociates. We assume that S338 phosphorylation on CRAF occurs only at the membrane when CRAF is bound to RAS-GTP (the rate constant kpS338), while S338 dephosphorylation occurs both at the membrane (i.e. when CRAF is bound to RAS-GTP) and in the cytoplasm (the rate constant kS338).

### 1.3. Binding of wild-type BRAF monomers and BRAF homodimers to RAS-GTP and (de)phosphorylation of S365

In the absence of the RAF-GTP signal, BRAF mainly resides in the cytoplasm where it is phosphorylated on S365 (the inhibiting residue), and dephosphorylated on T753 (the site of feedback phosphorylation by ERK). We assume that both BRAF phosphorylated on S365 and BRAF dephosphorylated on S365 can bind to RAS-GTP. The rate constants for association of BRAF with RAS-GTP and dissociation are kB1 and kB_1, respectively. Literature data suggest that the dissociation constant for BRAF binding to RAS-GTP is less than this constant for CRAF binding to RAS-GTP (Fischer et al., 2007).

The rate constants of phosphorylation and dephosphorylation of BRAF on S365 in the cytoplasm are kS365 and kS_365. On the plasma membrane (i.e., when BRAF is bound to RAS-GTP), the phosphorylation of BRAF on S365 is slower and its dephosphorylation is faster than in the cytoplasm, which is described by the parameters pM365 and pMd365 (List S5.1). We also assume that BRAF can be phosphorylated on S365 both in a monomeric form and as a protomer in a dimer. If BRAF is phosphorylated on S365 when it is a protomer in a dimer with another RAF molecule, the dimer quickly dissociates described in the model by a process coupled to the S365 phosphorylation on BRAF protomer.

### 1.4. CRAF and BRAF dimerization.

When RAF kinases are in active conformations, they form dimers (Lavoie and Therrien, 2015). Accordingly, in the model only CRAF dephosphorylated on S259 and BRAF dephosphorylated on S365 can participate in dimerization reactions. As mentioned above, if CRAF gets phosphorylated on S259 in a homo/hetero dimer, or BRAF gets phosphorylated on S365 in a homo/hetero dimer, the dimer rapidly dissociates. Influence of feedback phosphorylation of CRAF and BRAF by ERK on dimerization reactions is explained in Section 1.6. The rate constants for association and dissociation of BRAF homodimers are kBBd1 and kBBd_1, respectively; the rate constants for CRAF homodimer association and dissociation are kCCd1 and kCCd_1, respectively (List S5.1). The rate constants of association and dissociation of BRAF-CRAF heterodimers in the model are kCBd1 and kCBd_1 respectively. The literature data suggest that the dissociation constants of WT BRAF homodimers and CRAF-BRAF heterodimers are slightly less (by a factor of 2) than the dissociation constant for CRAF homodimers (Rajakulendran et al., 2009). The data also suggest that the phosphorylation state of S338 does not influence the rates of CRAF dimerization but substantially affects the activity of the dimer (Garnett et al., 2005).

In our model all intracellular concentrations are based on to the cytoplasmic water volume. The values of dissociation constants for RAF dimers in the cytoplasm are high compared to the BRAF/CRAF abundances (Lavoie and Therrien, 2015; Rajakulendran et al., 2009). As a result, RAF dimers are nearly absent in the cytoplasm. However, if RAF molecules are bound to RAS-GTP, they are localized on the plasma membrane, and all interactions take place in a much smaller volume, localized near the membrane. Because the effective local concentrations of RAF molecules become much higher than in the cytoplasm (Kholodenko, 2006; Kholodenko et al., 2000; Lamson et al., 2006), the apparent $K_d$'s of RAF homo-/heterodimerization dramatically decrease of both RAF molecules are bound to RAS-GTP(Kholodenko et al., 2000; Markevich et al., 2004). In the model, the association rate constants for RAF homo-/heterodimerization are increased by a factor of $p_2$ if both RAF molecules are bound to RAS-GTP and the corresponding dissociation constant is decreased by a factor of $p_2$. Thus, $p_2^2$ reflects a ratio of volumes (Kholodenko et al., 2000; Markevich et al., 2004).

### 1.5. Binding of CRAF and BRAF homo- and heterodimers to RAS-GTP

The spatial co-localization effect also affects the binding of RAF to RAS-GTP. If at least one protomer in a RAF dimer is bound to RAS, the dimer is localized in the plasma membrane compartment, and therefore the other RAF protomer has a higher propensity to bind the second RAS-GTP (Kholodenko, 2006; Kholodenko et al., 2000). To account for this effect, the corresponding kinetic constants describing binding of RAF to RAS-GTP were rescaled as follows (Kholodenko et al., 2000; Markevich et al., 2004). The association rate constants for RAF binding to RAS-GTP are increased by a factor of $p_2$ if a RAF molecule is in a dimer that is bound to RAS-GTP via one of its protomers. The corresponding dissociation constants are decreased by a factor of $p_2$. Thus, $p_2^2$ reflects a ratio of volumes (Kholodenko et al., 2000; Markevich et al., 2004).

### 1.6. Feedback phosphorylation of CRAF and BRAF monomers by active ERK and dephosphorylation by phosphatases.

It is known that ERK-mediated feedback strongly affects RAF kinase activities by inhibiting RAS-GTP binding and RAF dimerization (Dougherty et al., 2005; Ritt et al., 2010). For the sake of simplicity, the inhibitory sites that are phosphorylated on RAFs by ERK are represented by just one site S642 on CRAF and T753 on BRAF. We assume that only active ERK (where Y and T sites on ERK are phosphorylated) can bind to RAF monomers and phosphorylate them. Computational analysis of ERK binding sites on RAF molecules performed using ScanSite (Ehrenberger et al., 2015; Obenauer et al., 2003) suggests that active ERK binds to RAFs via the domain that overlaps with the RAF dimerization interface (Dm); this rules out ERK feedback phosphorylation of RAF homo- and heterodimers. Thus, in the model, ERK can bind to and phosphorylate only RAF monomers.

Based on experimental data (Dougherty et al., 2005; Ritt et al., 2010), our model considers that if CRAF is phosphorylated on S642, the rate constants for CRAF-RAS association become $p_1$-fold lower, and the dissociation rate constants become $p_1$-fold higher (see figure S1C) than the corresponding values before CRAF phosphorylation by ERK. As a result, the equilibrium dissociation constant increases by a factor $p_1^2$, List S5.1. Similarly, if BRAF is phosphorylated on T753 the rate constants for BRAF-RAS association are $p_1$-fold lower, and the corresponding dissociation rate constants are $p_1$-fold higher (see figure S1C). Likewise, when CRAF is phosphorylated on S642, the association rate constants for CRAF homo- and heterodimerization become $p_3$-fold lower and the dissociation rate constants become $p_3$-fold higher (Ritt et al., 2010). Similarly, if BRAF is phosphorylated on T753 the association rate constants for BRAF homo- and heterodimerization become $p_3$-fold lower and the corresponding dissociation rate constants become $p_3$-fold higher. The influence of the different modifiers (such as $p_1$, $p_2$, $p_3$, etc.) can be multiplicative. For instance, when a CRAF monomer that is bound to RAS-GTP and phosphorylated on S642 dimerizes with a BRAF monomer that is bound to RAS-GTP and phosphorylated on T753, the association rate constant becomes $kCBd1 \cdot p_2/p_3^2$, and the corresponding dissociation rate constant becomes $kCBd\_1 \cdot p_3^2/p_2$.

### 1.7. Kinase activity of RAF monomers and dimers.

A BRAF monomer dephosphorylated on S365 is catalytically active, whereas the kinase activity of CRAF monomers that are dephosphorylated on S259 depends on additional S338 phosphorylation (see List S4.1). The kinase activity of active BRAF monomers is five times higher than the activity of active CRAF monomers phosphorylated on S338 (Rushworth et al., 2006). ERK feedback phosphorylation of CRAF on S642 dramatically suppresses CRAF activity (Dougherty et al., 2005; Ritt et al., 2010) (see

List S4.1). ERK feedback phosphorylation of BRAF on T753 does not directly affect BRAF kinase activity (Dougherty et al., 2005; Ritt et al., 2010).

Kinase activity of RAF homodimers is the sum of activities of the corresponding RAF protomers. The literature data suggest that kinase activity of CRAF-BRAF heterodimers is 15-times higher than the activity of BRAF homodimers (Freeman et al., 2013; Rushworth et al., 2006). The data show that when in a dimer S338 on CRAF is not phosphorylated, the dimer activity is only about 40-50% of the full activity of the dimer with CRAF phosphorylated on S338 (Garnett et al., 2005). Kinase activities of all monomer and dimer forms are summarized in List S4.1.

**2. Oncogenic BRAFV600E mutant.**

We assume that the S365 state does not influence BRAFV600E, and thus the model does not track the S365 state on BRAFV600E. The model monitors only the state of the ERK feedback phosphorylation site, T753, on BRAFV600E. BRAFV600E monomers are assumed to have higher kinase activity than WT BRAF monomers, and dimers containing BRAFV600E have higher kinase activity than dimers with WT BRAF or CRAF (see List S4.1).

Binding and dimerization of BRAFV600E kinase is described in the model in the same way as for CRAF and BRAF. The following binding sites are taken into account for BRAFV600E: RAS Binding Domain (RBD), MEK-Binding domain (MEKB), dimerization domain (DIM) and Inhibitor-binding pocket (EI).

The rate constants for association and dissociation of BRAFV600E and RAS-GTP are assumed to be similar to the rate constants for WT BRAF. The dimerization rate constants for BRAFV600E are assumed to be the same as the dimerization rate constants for BRAF dephosphorylated on S365. We assume that the feedback phosphorylation by ERK less affects BRAFV600E than WT BRAF. Accordingly, the changes in the corresponding association/dissociation rate constants are described by the parameters pBE1 and pBE3, which are smaller than the parameters $p_1$ and $p_3$ for WT BRAF (see List S5.1).

**3. Core model for allosteric interactions of RAF monomers and dimers with inhibitors.**

Each state of a RAF molecule is characterized by the phosphorylation states of key amino acid residues, which control RAF conformational changes and activity, S259, S338 and S642 for CRAF and S365 and T753 for BRAF. Furthermore, the RAF conformational and activity state depends on binding to RAS-GTP, another RAF molecule in a dimer or an inhibitor. For any particular phosphorylation state and set of binding partners there exists a thermodynamic equilibrium for the kinase in active and inactive conformations due to thermal motions of the molecule (Arora and Brooks, 2007; Daily et al., 2010; Hakulinen and Puranen, 2016; Lavoie and Therrien, 2015; Shao et al., 2017). Structurally, the state of a RAF molecule is described by the positions of the DFG motif and αC-helix, which in turn depend on phosphorylation and its binding partner. Because of thermal motions, in each phosphorylation and binding state, a RAF molecule can switch between DFG-IN and DFG-OUT positions of the DFG-motif, and between αC-IN and αC-OUT positions of αC-helix.

A RAF inhibitor generally binds to different conformations of RAF molecule with different microscopic $K_d$'s. The smallest $K_d$ corresponds to the preferential RAF conformation for this inhibitor. Because of the thermal motions, a RAF molecule can spontaneously switch between different conformations. This dynamic equilibrium is described by the equilibrium constants of conformational transitions, which in turn depend on the phosphorylation and dimerization state of a molecule. As a result, inhibitor binding is determined by the apparent dissociation constant ($K_d^{app}$) whose difference with the smallest microscopic

$K_d$ depends on both thermal transition equilibrium constants and factors that describe the inhibitor preference for different RAF conformations. Here we set to derive the relationships that express the apparent $K_d^{app}$ in terms of the microscopic $K_d$'s, the equilibrium constants of DFG-IN/DFG-OUT transitions, αC-IN/αC-OUT transitions and factors that describe the inhibitor preference for different conformational states of RAF molecules. In each kinetic scheme below, it is assumed that the phosphorylation and dimerization states of a RAF molecule shown do not change during thermal movements of the DFG motif and αC-helix between their IN and OUT positions. For simplicity, we first consider only DFG-IN and DFG-OUT transitions (sections A1 and A2) and then analyze the general case of thermal motions of both the DFG motif and αC-helix (section B).

## 3.1 Thermodynamics of binding of structurally diverse RAF inhibitors to DFG-IN/OUT RAF conformations.

### *3.1.1. DFG-IN inhibitors.*

A kinetic scheme of a DFG-IN inhibitor binding to RAF and the thermal transitions between DFG-OUT and DFG-IN conformations of free and inhibitor-bound RAF molecules are shown in Scheme S3.1. For simplicity, Scheme S3.1 assumes that the illustrated RAF molecule states maintain the preferred αC-helix position for binding of this DFG-IN inhibitor.

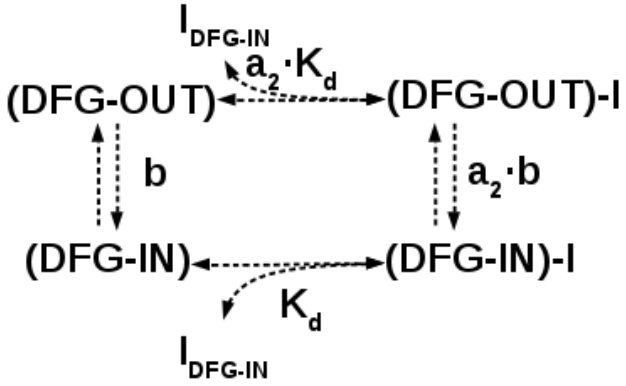


Scheme S3.1.

Here $K_d$ is the smallest microscopic equilibrium dissociation constant for a DFG-IN inhibitor binding to a specific RAF form in a DFG-IN conformation, and $b$ is the equilibrium constant for a transition of this RAF form (which is free of inhibitor) from a DFG-OUT conformation to a DFG-IN conformation. A DFG-IN inhibitor can also bind the same RAF form in a DFG-OUT conformation, but the corresponding dissociation constant is larger because of the assumed preference of the inhibitor for the DFG-IN conformation. This constant equals the smallest microscopic dissociation constant $K_d$ multiplied by a preference factor $a_2 > 1$, i.e., $a_2 \cdot K_d$. The equilibrium relationships between the concentrations of free and inhibitor-bound RAF molecules in each conformational state are given in Eq. S3.1,

$$[DFG-IN] = b \cdot [DFG-OUT]$$
$$[(DFG-IN)-I_{DFG-IN}] = \frac{[DFG-IN] \cdot I_{DFG-IN}}{K_d} \quad \text{(S3.1)}$$
$$[(DFG-OUT)-I_{DFG-IN}] = \frac{1}{b} \cdot \frac{[DFG-IN] \cdot I_{DFG-IN}}{a_2 K_d}$$

The kinetic diagram in Scheme S3.1 contains a cyclic route composed of reversible binding/dissociation reactions and thermal transitions between DFG-IN/OUT conformations. According to the law of microscopic reversibility, the total free energy change equals zero along this cyclic path. This leads to the so-called detailed balance equation that requires the product of the equilibrium constants along the cycle to be equal to 1 (see, e.g, (Kholodenko et al., 1999; Kholodenko et al., 1998)). As a result, the equilibrium constant for a transition of the inhibitor-bound RAF from the DFG-OUT conformation to the DFG-IN conformation equals $a_2 \cdot b$ (as shown in Scheme S3.1).

$$\frac{[(DFG-IN)-I_{DFG-IN}]}{[(DFG-OUT)-I_{DFG-IN}]} = \frac{[DFG-IN]}{[DFG-OUT]} \cdot \frac{[(DFG-IN)-I_{DFG-IN}]}{[DFG-IN]\cdot I_{DFG-IN}} \cdot \frac{[DFG-OUT]\cdot I_{DFG-IN}}{[(DFG-OUT)-I_{DFG-IN}]} = a_2 b \quad \text{(S3.2)}$$

Using the microscopic $K_d$'s and the equilibrium constants of conformational transitions, $b$ and $a_2 \cdot b$, the apparent dissociation constant of DFG-IN inhibitor binding to RAF molecules (that reside in the same αC-helix position as the preferred position for binding of this DFG-IN inhibitor) can be expressed as follows,

$$K_d^{app} = \frac{([DFG-OUT]+[DFG-IN])\cdot[I_{DFG-IN}]}{[(DFG-OUT)-I_{DFG-IN}]+[(DFG-IN)-I_{DFG-IN}]} = \frac{b+1}{b+\frac{1}{a_2}} K_d \quad \text{(S3.3)}$$

Here $[DFG-OUT]+[DFG-IN]$ and $[(DFG-OUT)-I_{DFG-IN}]+[(DFG-IN)-I_{DFG-IN}]$ are the sums of the equilibrium concentrations of free and inhibitor-bound RAF molecules, respectively. The concentrations of RAF molecules in each conformational state are related by the equilibrium constants, as shown in Eqs. S3.1 and S3.2. Note that because the IN/OUT spontaneous thermal motions of the DFG-motif can occur in any state of a RAF molecule (monomeric or dimeric, bound to inhibitor or free), the equilibrium constant $b$ for these transitions depends on the specific state of a RAF molecule. For example, $b$ depends on thermodynamic factors describing the allosteric inhibitor interactions with RAF monomers and dimers (see below).

If the preference factor $a_2$ for binding of a DFG-IN inhibitor to a DFG-OUT conformation is very large, $a_2 \to \infty$, meaning that this DFG-IN inhibitor poorly binds to a DFG-OUT conformation, Eq. (S3.3) simplifies as follows,

$$K_d^{app} \xrightarrow{a_2 \to \infty} \left(1+\frac{1}{b}\right)\cdot K_d \quad \text{(S3.4)}$$

### 3.1.2. *DFG-OUT inhibitors.*

A kinetic scheme for a DFG-OUT inhibitor binding to RAF and the thermal transitions between DFG-OUT and DFG-IN conformations of free and inhibitor-bound RAF molecules is presented in Scheme S3.2. We assume that the RAF molecule states included in Scheme S3.2 maintain the preferred αC-helix position for binding of this DFG-OUT inhibitor.

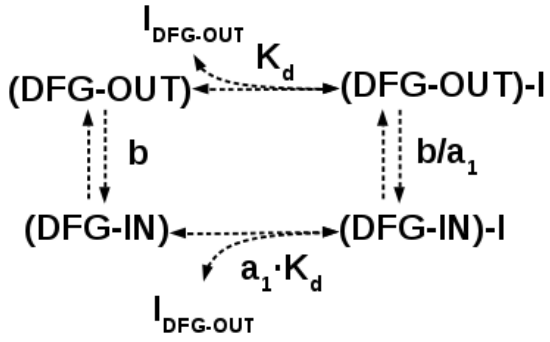


Scheme S3.2

Here, $K_d$ is the smallest microscopic equilibrium dissociation constant for the DFG-OUT inhibitor binding to a specific RAF form in a DFG-OUT conformation, $a_1 \cdot K_d$ is the dissociation constant for the DFG-OUT inhibitor binding to the same RAF form in a DFG-IN conformation (this constantequals the smallest microscopic $K_d$ for DFG-OUT conformation multiplied by a preference factor $a_1 > 1$), and $b$ is the equilibrium constant for a transition of this RAF form (which is free of inhibitor) from a DFG-OUT conformation to a DFG-IN conformation.

As discussed above, from the detailed balance equation it follows that the apparent dissociation constant for DFG-OUT inhibitor binding to RAF molecules can be expressed as follows (in these illustrative examples, we are assuming that the aC-helix conformation does not change, corresponding to preferential inhibitor binding),

$$K_d^{app} = \frac{([DFG-OUT]+[DFG-IN]) \cdot [I_{DFG-OUT}]}{[(DFG-OUT)-I_{DFG-OUT}]+[(DFG-IN)-I_{DFG-OUT}]} = \frac{b+1}{\frac{b}{a_1}+1} K_d \qquad \text{(S3.5)}$$

If the preference factor $a_1$ for binding of a DFG-OUT inhibitor to a DFG-IN conformation is very large, $a_1 \to \infty$, meaning that this inhibitor poorly binds to a DFG-IN conformation, Eq. S3.5 simplifies as follows,

$$K_d^{app} \xrightarrow{a_1 \to \infty} (b+1) \cdot K_d \qquad \text{(S3.6)}$$

### 3.2. Taking into account the thermal motions of both the DFG-motif and αC-helix to calculate the apparent $K_d$'s for binding of structurally diverse RAF inhibitors.

A kinetic diagram for an inhibitor binding to a RAF molecule and the thermal transitions between eight possible DFG-IN/OUT and αC-helix IN/OUT conformations of free and inhibitor-bound RAF forms is shown in Scheme S3.3.

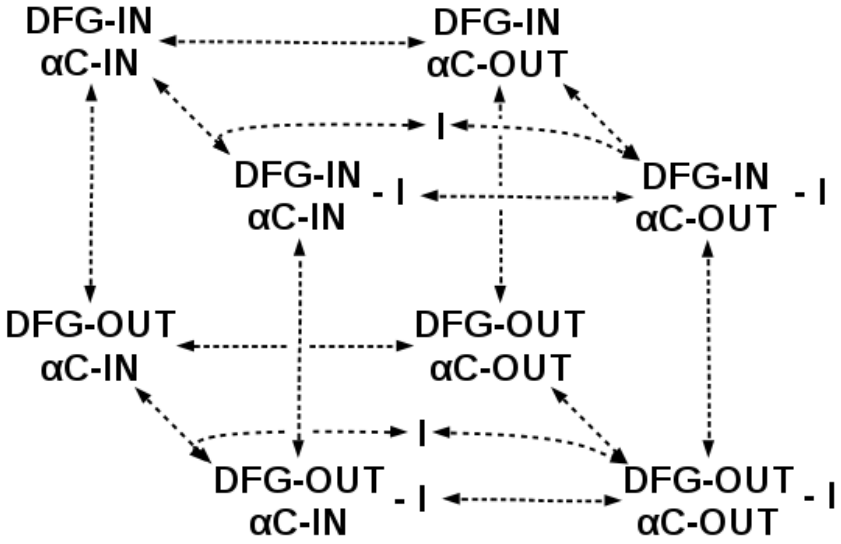


Scheme S3.3.

We will denote the equilibrium constants for IN/OUT transitions of the DFG-motif at the fixed IN or OUT position of the αC-helix by $b_1$ and $b_2$, respectively. Similarly, we will denote the equilibrium constants for IN/OUT transitions of the αC-helix for the different IN or OUT states of the DFG-motif by $c_1$ and $c_2$, respectively. In other words, we have

$$b_1 = \frac{[DFG-IN, \alpha C-IN]}{[DFG-OUT, \alpha C-IN]} \qquad b_2 = \frac{[DFG-IN, \alpha C-OUT]}{[DFG-OUT, \alpha C-OUT]} \tag{S3.7}$$

$$c_1 = \frac{[DFG-IN, \alpha C-IN]}{[DFG-IN, \alpha C-OUT]} \qquad c_2 = \frac{[DFG-OUT, \alpha C-IN]}{[DFG-OUT, \alpha C-OUT]} \tag{S3.8}$$

The detailed balance principle imposes the following constraints

$$\frac{b_1}{b_2} = \frac{c_1}{c_2} \tag{S3.9}$$

If $b_1=b_2$ then movements of the DFG-motif and αC-helix are independent. If $b_1>b_2$ cooperativity exists between DFG and αC motions. Following Eq. S3.9, we introduce the cooperativity coefficient $\gamma$ and make the following substitutions:

$$\begin{aligned} b_1 &= \gamma b \\ b_2 &= b \\ c_1 &= \gamma c \\ c_2 &= c \end{aligned} \tag{S3.10}$$

At present, researchers have produced and tested three types of RAF inhibitors that preferably bind to (1) DFG-IN, αC-IN (CI/DI), (2) DFG-OUT, αC-IN (CI/DO) or (3) DFG-IN, αC-OUT (CO/DI) conformations of RAF molecules. Each inhibitor type binds preferably to one out of the possible four DFG-IN/OUT, αC-IN/OUT conformations. Preferential binding is described by the smallest microscopic $K_d$, but each inhibitor can also bind to other conformations (Park et al., 2012), yet with larger $K_d$'s. For each known RAF inhibitor type, List S3.1 presents the coefficients that multiply the smallest microscopic $K_d$ to obtain the $K_d$'s for binding of this inhibitor type to less preferable DFG and αC-helix conformations. For instance, the first row in List S3.1 shows that a CI/DI inhibitor ($I^{CI/DI}$) binds with the smallest microscopic $K_d$ to the preferred DFG-IN, αC-IN RAF conformation, but its $K_d$ for binding to the DFG-

OUT, αC-IN conformation equals $a_{21}^{CI/DI}K_d$, its $K_d$ of binding to DFG-IN, αC-OUT conformation equals $a_{12}^{CI/DI}K_d$, and its binding $K_d$ to DFG-OUT, αC-OUT conformation equals $a_{22}^{CI/DI}K_d$.

**List S3.1. Binding Kds to different RAF conformations for three types of RAF inhibitors**

| **Type of RAF inhibitor** | ***Kd* for binding to DFG-IN, αC-IN conformation** | ***Kd* for binding to DFG-OUT, αC-IN conformation** | ***Kd* for binding to DFG-IN, αC-OUT conformation** | ***Kd* for binding to DFG-OUT, αC-OUT conformation** |
|---|---|---|---|---|
| DFG-IN, αC-IN ($I^{CI/DI}$) | $K_d$ | $a_{21}^{CI/DI}K_d$ | $a_{12}^{CI/DI}K_d$ | $a_{22}^{CI/DI}K_d$ |
| DFG-OUT, αC-IN ($I^{CI/DO}$) | $a_{11}^{CI/DO}K_d$ | $K_d$ | $a_{12}^{CI/DO}K_d$ | $a_{22}^{CI/DO}K_d$ |
| DFG-IN, αC-OUT ($I^{CO/DI}$) | $a_{11}^{CO/DI}K_d$ | $a_{21}^{CO/DI}K_d$ | $K_d$ | $a_{22}^{CO/DI}K_d$ |

Interactions of different types of inhibitors (I) with each possible conformation (DFG-IN/OUT, αC-helix-IN/OUT) of a RAF molecule are shown in Schemes S3.4a, S3.4b and S3.4c for $I^{CI/DI}$ (S3.4a), $I^{CI/DO}$ (S3.4b) and $I^{CO/DI}$ (S3.4c) inhibitors. The microscopic dissociation constants and the equilibrium constants for conformational changes are indicated. As above, we assume that any specific phosphorylation state and binding partner(s) of this RAF molecule do not change over the reactions shown in these Schemes.

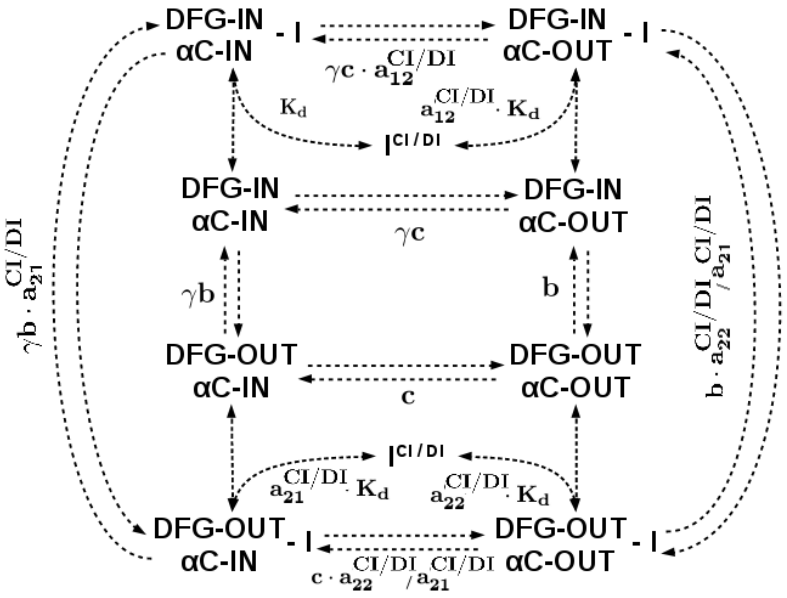


Scheme S3.4a for $I^{CI/DI}$

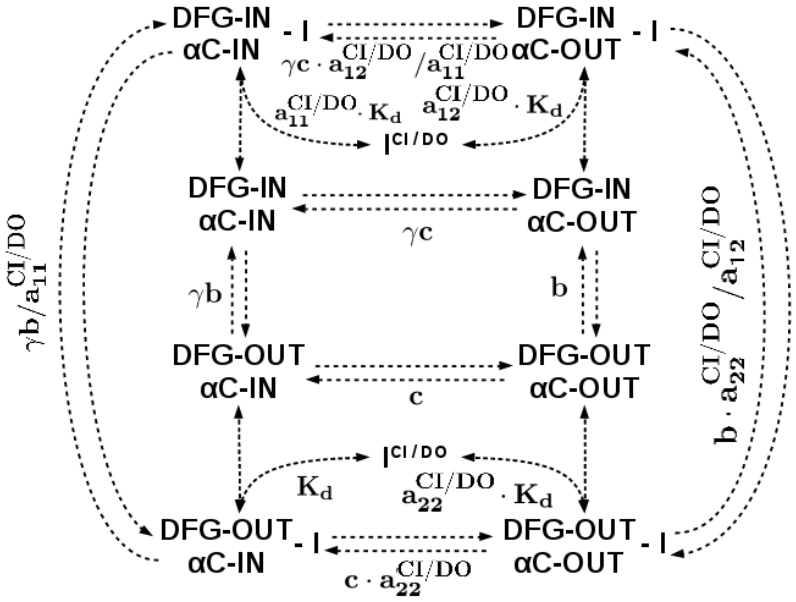


Scheme S3.4b for $I^{CI/DO}$

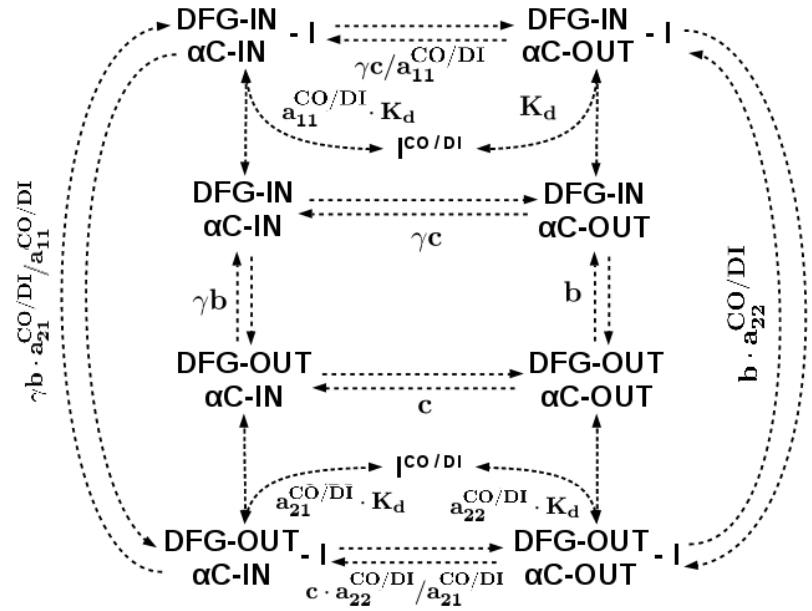


Scheme S3.4c for $I^{CO/DI}$

These schemes are valid for every BRAF molecule and CRAF molecule appearing in the model. For example, in the BRAF-CRAF dimerization cycle and allosteric inhibitor interactions with RAF monomers and dimers shown in the lumped reaction Scheme S3.5 at the left, the binding of inhibitor to a BRAF molecule is expanded into 12 reactions that take into account all possible positions of the DFG-motif and αC-helix.

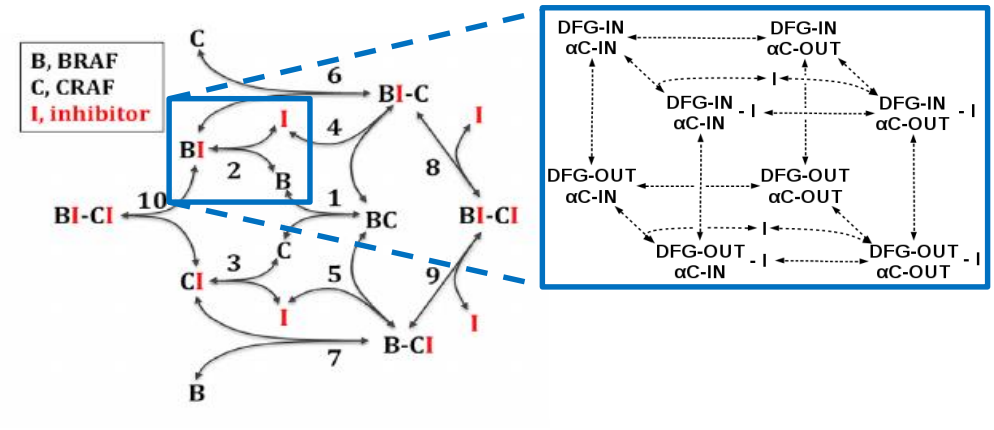


Scheme S3.5

For a cycle of the 12 inhibitor binding and thermal motion reactions shown in Schemes S3.3-S3.5, we can write the following equations which capture the relationships between the equilibrium concentrations of RAF molecules that have different positions for the DFG motif and αC-helix and that are bound to different inhibitor types,

$$\frac{[DFG-IN,\alpha C-IN]}{[DFG-IN,\alpha C-OUT]}=\gamma\cdot c \qquad \frac{[DFG-IN,\alpha C-IN]}{[DFG-OUT,\alpha C-IN]}=\gamma\cdot b$$

$$\frac{[DFG-OUT,\alpha C-IN]}{[DFG-OUT,\alpha C-OUT]}=c \qquad \frac{[DFG-IN,\alpha C-IN]}{[DFG-OUT,\alpha C-OUT]}=\gamma\cdot b\cdot c$$

$$[(DFG-IN,\alpha C-IN)-I^{CI/DI}]=[DFG-IN,\alpha C-IN]\cdot[I^{CI/DI}]/K_d$$

$$[(DFG-IN,\alpha C-OUT)-I^{CI/DI}]=\frac{[DFG-IN,\alpha C-IN]\cdot[I^{CI/DI}]/K_d}{\gamma c\cdot a_{12}^{CI/DI}}$$

$$[(DFG-OUT,\alpha C-IN)-I^{CI/DI}]=\frac{[DFG-IN,\alpha C-IN]\cdot[I^{CI/DI}]/K_d}{\gamma b\cdot a_{21}^{CI/DI}}$$

$$[(DFG-OUT,\alpha C-OUT)-I^{CI/DI}]=\frac{[DFG-IN,\alpha C-IN]\cdot[I^{CI/DI}]/K_d}{\gamma bc\cdot a_{22}^{CI/DI}} \qquad \text{(S3.11)}$$

$$[(DFG-IN,\alpha C-IN)-I^{CI/DO}]=\frac{[DFG-IN,\alpha C-IN]\cdot[I^{CI/DO}]/K_d}{a_{11}^{CI/DO}}$$

$$[(DFG-IN,\alpha C-OUT)-I^{CI/DO}]=\frac{[DFG-IN,\alpha C-IN]\cdot[I^{CI/DO}]/K_d}{\gamma c\cdot a_{12}^{CI/DO}}$$

$$[(DFG-OUT,\alpha C-IN)-I^{CI/DO}]=\frac{[DFG-IN,\alpha C-IN]\cdot[I^{CI/DO}]/K_d}{\gamma b}$$

$$[(DFG-OUT,\alpha C-OUT)-I^{CI/DO}]=\frac{[DFG-IN,\alpha C-IN]\cdot[I^{CI/DO}]/K_d}{\gamma bc\cdot a_{22}^{CI/DO}}$$

$$[(DFG-IN,\alpha C-IN)-I^{CO/DI}]=\frac{[DFG-IN,\alpha C-IN]\cdot[I^{CO/DI}]/K_d}{a_{11}^{CO/DI}}$$

$$[(DFG-IN,\alpha C-OUT)-I^{CO/DI}]=\frac{[DFG-IN,\alpha C-IN]\cdot[I^{CO/DI}]/K_d}{\gamma c}$$

$$[(DFG-OUT,\alpha C-IN)-I^{CO/DI}]=\frac{[DFG-IN,\alpha C-IN]\cdot[I^{CO/DI}]/K_d}{\gamma b\cdot a_{21}^{CO/DI}}$$

$$[(DFG-OUT,\alpha C-OUT)-I^{CO/DI}]=\frac{[DFG-IN,\alpha C-IN]\cdot[I^{CO/DI}]/K_d}{\gamma bc\cdot a_{22}^{CO/DI}}$$

For any inhibitor type ($I^{Cx/Dx}$), the apparent dissociation constant ($K_{d\,Cx/Dx}^{app}$) for inhibitor binding to a RAF molecule in a particular phosphorylation and dimerization state can be expressed as follows,

$$K_{d\,Cx/Dx}^{app}=\frac{([DFG-IN,\alpha C-IN]+[DFG-OUT,\alpha C-IN]+}{[(DFG-IN,\alpha C-IN)-I^{Cx/Dx}]+[(DFG-OUT,\alpha C-IN)-I^{Cx/Dx}]+}\\ \frac{+[DFG-IN,\alpha C-OUT]+[DFG-OUT,\alpha C-OUT])\cdot I}{+[(DFG-IN,\alpha C-OUT)-I^{Cx/Dx}]+[(DFG-OUT,\alpha C-OUT)-I^{Cx/Dx}]} \quad \text{(S3.12)}$$

Here, $[DFG-IN,\alpha C-IN]$, $[DFG-IN,\alpha C-OUT]$, $[DFG-OUT,\alpha C-IN]$, $[DFG-OUT,\alpha C-OUT]$, $\left[(DFG-IN,\alpha C-IN)-I^{Cx/Dx}\right]$, $\left[(DFG-OUT,\alpha C-IN)-I^{Cx/Dx}\right]$, $\left[(DFG-IN,\alpha C-OUT)-I^{Cx/Dx}\right]$ and $\left[(DFG-OUT,\alpha C-OUT)-I^{Cx/Dx}\right]$ are the equilibrium concentrations of free and inhibitor-bound RAF molecules, respectively, that retain particular states of the DFG motif and αC-helix positions. These concentrations are related by the equilibrium constants of thermal transitions and the microscopic dissociation constants, as presented in Eqs. S3.11. Using Eqs. S3.11 and S3.12, the apparent dissociation constant for inhibitor binding to a RAF molecule in any particular phosphorylation and dimerization state can be expressed through the microscopic dissociation constants, the factors that describe the inhibitor preference for different conformational states of RAF molecules, and the equilibrium constants of IN/OUT transitions of the DFG-motif and αC-helix.

For a DFG-IN, αC-IN inhibitor type ($I^{CI/DI}$), the apparent dissociation constant is expressed, as follows,

$$K_{d\,CI/DI}^{app}=\frac{\gamma bc+b+c+1}{\gamma bc+\frac{b}{a_{12}^{CI/DI}}+\frac{c}{a_{21}^{CI/DI}}+\frac{1}{a_{22}^{CI/DI}}}\cdot K_d \quad \text{(S3.13a)}$$

For a DFG-OUT, αC-IN inhibitor type ($I^{CI/DO}$), the apparent dissociation constant is expressed, as follows,

$$K_{d\,CI/DO}^{app}=\frac{\gamma bc+b+c+1}{\frac{\gamma bc}{a_{11}^{CI/DO}}+\frac{b}{a_{12}^{CI/DO}}+c+\frac{1}{a_{22}^{CI/DO}}}\cdot K_d \quad \text{(S3.13b)}$$

For a DFG-IN, αC-OUT ($I^{CO/DI}$) inhibitor type, the apparent dissociation constant is expressed, as follows,

$$K_{d\,CO/DI}^{app}=\frac{\gamma bc+b+c+1}{\frac{\gamma bc}{a_{11}^{CO/DI}}+b+\frac{c}{a_{21}^{CO/DI}}+\frac{1}{a_{22}^{CO/DI}}}\cdot K_d \quad \text{(S3.13c)}$$

Assuming that coefficients $a_{xx}^{Cx/Dx}$ that distinguish the dissociation constants of a particular inhibitor between the preferential RAF conformation and other conformations are large, Eqs. S3.13 simplify, as follows:

$$K_{d\ CI/DI}^{app} \xrightarrow{a_{12}^{CI/DI},a_{21}^{CI/DI},a_{22}^{CI/DI}\to\infty} 1+\frac{1}{\gamma c}+\frac{1}{\gamma b}+\frac{1}{\gamma bc} \tag{S3.13d}$$

$$K_{d\ CI/DO}^{app} \xrightarrow{a_{11}^{CI/DO},a_{12}^{CI/DO},a_{22}^{CI/DO}\to\infty} \gamma b+\frac{b}{c}+1+\frac{1}{c} \tag{S3.13e}$$

$$K_{d\ CO/DI}^{app} \xrightarrow{a_{11}^{CO/DI},a_{21}^{CO/DI},a_{22}^{CO/DI}\to\infty} \gamma c+1+\frac{c}{b}+\frac{1}{b} \tag{S3.13f}$$

List S3.2 below shows the estimated value ranges for the coefficients $b$, $c$ and $\gamma$ based on the available literature. The last column gives the names of the apparent equilibrium dissociation constants for inhibitor binding to different states of CRAF and BRAF.

**List S3.2. Estimated ranges for the coefficients $b$, $c$ and $\gamma$ based on the available literature.**

| Different phospho-site states of CRAF and BRAF monomers and dimers | Equilibrium constant for DFG-motif motions, $b$ | Equilibrium constant for αC-helix motions, $c$ | Cooperativity between DFG and αC motions, $\gamma$ | Name of apparent dissociation constant |
|---|---|---|---|---|
| **CRAF** | | | | |
| pS259, monomer | 0.01-0.05 | 0.005-0.01 | 1-10 | $K_d^{mC}$ |
| S259, S338, monomer | 0.1-1 | 0.1-1 | 1-10 | |
| S259, pS338, monomer | 5-10 | 5-10 | 1-10 | |
| S259, S338, bound to CRAF/BRAF, which is either free or bound to a $I^{CI/DI}$ or $I^{CI/DO}$ inhibitor | 5-10 | 5-10 | 1-10 | $K_d^{DIC}$ |
| S259, pS338, bound to CRAF/BRAF, which is either free or bound to a $I^{CI/DI}$ or $I^{CI/DO}$ inhibitor | 10-20 | 10-20 | 1-10 | |
| S259, S338, bound to CRAF/BRAF, which is bound to a $I^{CO/DI}$ inhibitor | 5-10 | 10-100 | 1-10 | $K_d^{DOC}$ |
| S259, pS338, bound to CRAF/BRAF, which is bound to a $I^{CO/DI}$ inhibitor | 10-20 | 40-100 | 1-10 | |
| **BRAF** | | | | |
| pS365, monomer | 0.01-0.05 | 0.005-0.01 | 1-10 | $K_d^{mB}$ |
| S365, monomer | 5-10 | 5-10 | 1-10 | |
| S365, bound to CRAF/BRAF (mutant or WT), which is either free or bound to a $I^{CI/DI}$ or $I^{CI/DO}$ inhibitor | 10-20 | 10-20 | 1-10 | $K_d^{DIB}$ |
| S365, bound to CRAF/BRAF (mutant or WT), which is bound to a $I^{CO/DI}$ inhibitor | 10-20 | 40-100 | 1-10 | $K_d^{DOB}$ |
| **BRAFV600E** | | | | |

| | | | | |
|---|---|---|---|---|
| Monomer | 5-10 | 5-10 | 1-10 | $K_d^{mE}$ |
| Bound to CRAF/BRAF (mutant or WT), which is either free or bound to a $I^{CI/DI}$ or $I^{CI/DO}$ inhibitor | 10-20 | 10-20 | 1-10 | $K_d^{DIE}$ |
| Bound to CRAF/BRAF (mutant or WT), which is bound to a $I^{CO/DI}$ inhibitor | 10-20 | 40-100 | 1-10 | $K_d^{DOE}$ |

List S3.2 does not present the values of the apparent dissociation constants, because they may have the same names but different values for different states of RAF molecules, indicated in the first column of List S3.2. For example, CRAF phosphorylated and dephosphorylated on S338 have different equilibrium constants for both movements of DFG-motif and αC-helix. Moreover, we explore ranges of values for the coefficients $b$, $c$, and $\gamma$ and, hence, the thermodynamic equilibrium constants of thermal motions. Therefore, for each inhibitor type and each RAF state the apparent dissociation constants are automatically calculated from Eqs. S3.13a-c using an Excel spreadsheet "Kds.xlsx" and incorporated into the supplied BioNetGen file "RAF_MEK_ERK.bngl".

From List S3.2, it follows that the probability to observe the DFG-OUT, αC-OUT state of a protomer is less than 1% in RAF dimers. The low probability of this state can explain why there are no reported PDB structures with RAF protomers in DFG-OUT, αC-OUT conformations (see Fig. 1D).There are no known CO/DO inhibitors that would lock a RAF protomer in this conformation.

### 3.3 Relationships between the apparent $K_d$'s and thermodynamic factors that characterize allosteric inhibitor effects.

The equilibrium constants of reactions in each cycle of RAF dimerization and inhibitor binding obey the detailed balance principle. According to this principle, the product of the equilibrium dissociation constants along a closed cycle of binding/dissociation reactions must be equal to 1, since the overall change in free energy is zero. Since the IN/OUT thermal motions include inhibitor-bound RAF states and RAF monomers and dimers, the detailed balance principle imposes constraints on the values of the apparent dissociation constants in the cycle of inhibitor binding and dimerization (see below).

For a cycle of binding of an inhibitor to BRAF (B) and CRAF (C) monomers and a BRAF-CRAF heterodimer (BC), we have the following lumped reaction scheme (which does not elaborate different conformational states, see also Scheme S3.5),

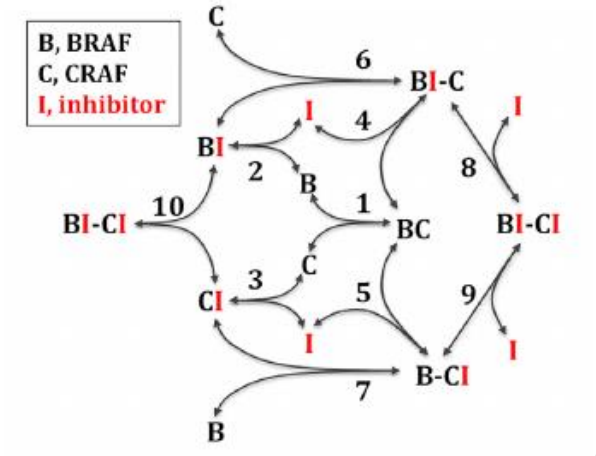


Scheme S3.6

The detailed balance principle requires that the following conditions be satisfied,

$$\frac{K_9 \cdot K_5}{K_4 \cdot K_8} = 1 \qquad \frac{K_5 \cdot K_1}{K_3 \cdot K_7} = 1 \qquad \frac{K_4 \cdot K_1}{K_2 \cdot K_6} = 1 \qquad \frac{K_{10} \cdot K_3}{K_8 \cdot K_6} = 1 \qquad \frac{K_{10} \cdot K_2}{K_7 \cdot K_9} = 1 \qquad \text{(S3.14)}$$

The thermodynamic constraints allow us to express the dissociations constants, $K_4 - K_{10}$, in terms of the dimerization constant $K_1$, inhibitor binding constants $K_2$ and $K_3$ and thermodynamic factors, $f$, $g_1$, and $g_2$ (Kholodenko, 2015). The facilitation factor ($f$), which relates the dimerization constants of free monomers ($K_1$) and inhibitor-bound and free monomers ($K_4$), describes the inhibitor-induced change in dimerization affinity (Kholodenko, 2015). If the facilitation factor $f$ is less than 1, the dimers with only one bound molecule of inhibitor are stabilized by the inhibitor (Kholodenko, 2015). The thermodynamic factor $g_1$ describes the differences in binding of the first inhibitor molecule to different protomers in an asymmetric dimer. The thermodynamic factor $g_2$ connects the dissociation constant $K_5$ for the binding of the second inhibitor molecule to a dimer with one inhibitor molecule bound and the dissociation constant $K_2$ for the inhibitor binding to a monomer. When $g_2 > 1$ the second inhibitor molecule binds to a dimer with one inhibitor molecule bound less effectively than the inhibitor binds to a kinase monomer. The expressions that relate thermodynamic factors and apparent dissociation constants are given in List S3.3.

Equations S3.14 allow us to obtain the following relationships between the thermodynamic factors $g_1$ and $g_2$ and the apparent dissociation constants.

For a $I^{CO/DI}$ inhibitor, these relationships are captured by the following expressions,

$$g_1 = \frac{K_d^{DOC}}{K_d^{DOB}} \cdot \frac{K_d^{mB}}{K_d^{mC}} \qquad g_2 = \frac{K_d^{DOB}}{K_d^{mB}} \qquad \text{(S3.15)}$$

In addition, the detailed balance relationships require that the following condition is satisfied

$$\frac{K_d^{DIB}}{K_d^{DOB}} = \frac{K_d^{DIC}}{K_d^{DOC}} \qquad \text{(S3.16)}$$

Although the values of each apparent dissociation constant are different for different RAF states, they all must satisfy Eqs. S3.16. The $a$-coefficients ($a_{11}^{CI/DI}$, $a_{12}^{CI/DI}$, etc.) are specific for every inhibitor. Coefficients $\gamma$, $b$ and $c$ characterize a given state of a RAF molecule (determined by its binding partners and the phosphorylation status of its phospho-sites). Thus, for specific values of the $a$-coefficients and a given RAF molecule state, Eq. S3.16 imposes thermodynamic constraints on the coefficients, $\gamma$, $b$ and $c$, which are accounted for in the model.

For $I^{CI/DI}$ and $I^{CI/DO}$ inhibitors, the analogs of Eq. S3.15 are the following,

$$g_1 = \frac{K_d^{DIC}}{K_d^{DIB}} \cdot \frac{K_d^{mB}}{K_d^{mC}} \qquad g_2 = \frac{K_d^{DIB}}{K_d^{mB}} \qquad \text{(S3.17)}$$

For each inhibitor type ($I^{\alpha I/DI}$, $I^{\alpha I/DO}$, and $I^{\alpha O/DI}$), Eqs. S3.15, S3.16 or S3.17 relate the thermodynamic factors $g_i$ with the apparent $K_d$'s of inhibitor binding defined in List S3.2.

Eqs. S3.14-S3.17 allow us to relate the phenomenological thermodynamics factors ($g_1$, and $g_2$) with the apparent $K_d$'s of inhibitor binding to different RAF forms. List S3.3 expresses the dissociations constants $K_4 - K_{10}$ in terms of phenomenological factors $f$, $g_1$ and $g_2$ introduced in Ref (Kholodenko, 2015) and in terms of the apparent dissociation constants introduced in List S3.2 and the factor $f$. For each RAF inhibitor, the value of the factor $f$ is a unique feature that is not directly determined by the positions of the αC-helix and DFG motif.

**List S3.3. Reactions and relationships between equilibrium dissociation constants for a model of BRAF-CRAF heterodimerization and allosteric inhibitor effects**

| Reaction Number | Reactions | Equilibrium Dissociation Constants Expressed in Terms of Factors $f$, $g_1$ and $g_2$ | Equilibrium Dissociation Constants Expressed in Terms of Apparent Dissociation Constants and the Factor $f$ |
|---|---|---|---|
| 1 | B + C ↔ B-C | $K_1$ | $K_1$ |
| 2 | B + I ↔ BI | $K_2$ | $K_d^{mB}$ |
| 3 | C + I ↔ CI | $K_3$ | $K_d^{mC}$ |
| 4 | B-C + I ↔ BI-C | $K_4 = f \cdot K_2$ | $K_4 = f \cdot K_d^{mB}$ |
| 5 | B-C + I ↔ B-CI | $K_5 = g_1 \cdot f \cdot K_3$ | $K_5 = \frac{K_d^{DIC}}{K_d^{DIB}} \cdot f \cdot {K_d}^{mB}$ |
| 6 | BI + C ↔ BI-C | $K_6 = f \cdot K_1$ | $K_6 = f \cdot K_1$ |
| 7 | B + CI ↔ B-CI | $K_7 = g_1 \cdot f \cdot K_1$ | $K_7 = f \cdot \frac{K_d^{mB}}{K_d^{mC}} \cdot \frac{K_d^{DIC}}{K_d^{DIB}} \cdot K_1$ |
| 8 | BI-C + I ↔ BI-CI | $K_8 = g_1 \cdot g_2 \cdot K_3$ | For $I^{CO/DI}$, $K_8 = K_d^{DOC}$<br>For $I^{CI/DI}$ and $I^{CI/DO}$: $K_8 = K_d^{DIC}$ |
| 9 | B-CI + I ↔ BI-CI | $K_9 = g_2 \cdot K_2$ | For $I^{CO/DI}$, $K_9 = K_d^{DOB}$<br>For $I^{CI/DI}$ and $I^{CI/DO}$, $K_9 = K_d^{DIB}$ |
| 10 | BI + CI ↔ BI-CI | $K_{10} = f \cdot g_1 \cdot g_2 \cdot K_1$ | For $I^{CO/DI}$, $K_{10} = f \cdot \frac{K_d^{DOC}}{K_d^{mC}} \cdot K_1$<br>For $I^{CI/DI}$ and $I^{CI/DO}$, $K_{10} = f \frac{K_d^{DIC}}{K_d^{mC}} K_1$ |

***Binding of two different inhibitors to RAF molecules.*** Below we analyze the binding of two different inhibitors ($I_1$ and $I_2$) to RAF monomers and dimers in the RAF dimerization cycle. The reaction schemes are presented below,

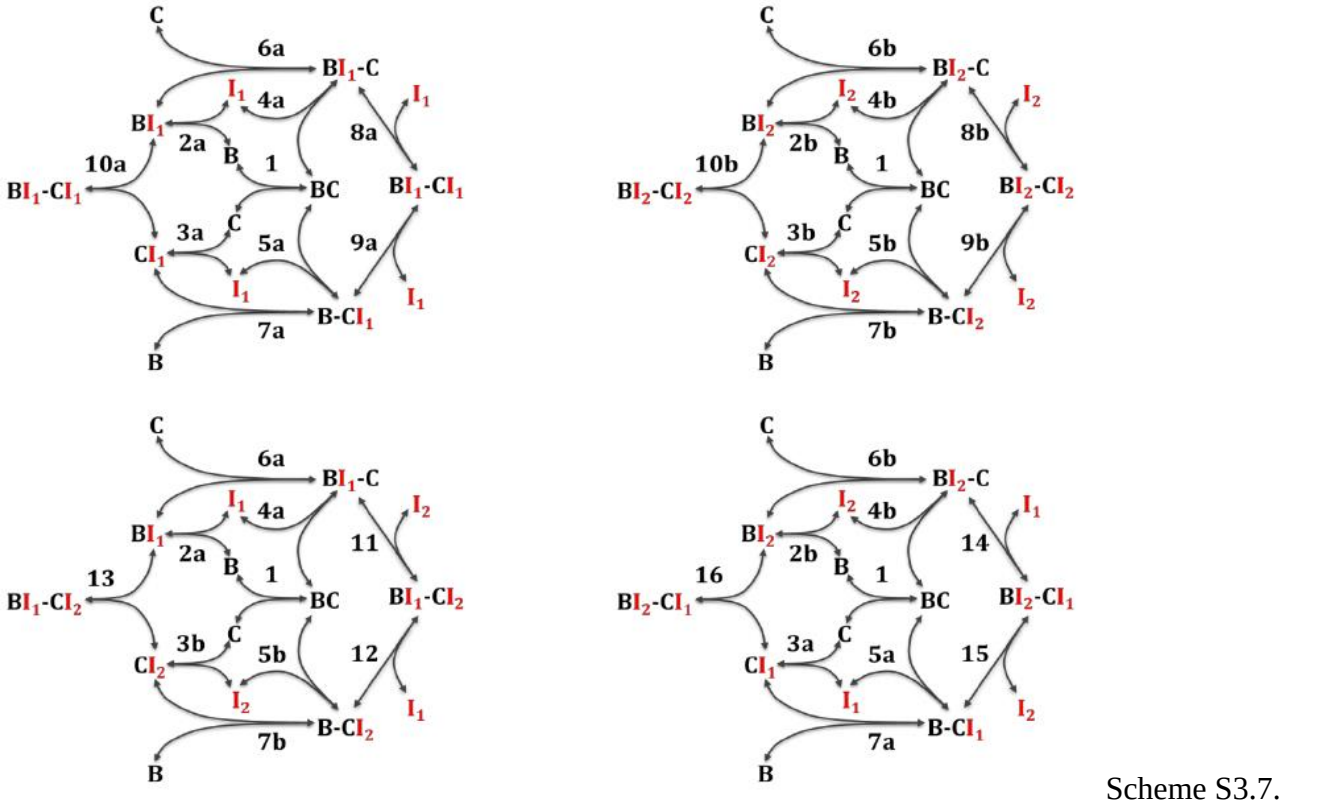


Scheme S3.7.

In Scheme S3.7 and in text below, the subscripts *a* and *b* refer to inhibitors $I_1$ and $I_2$.

Detailed balance principle requires that the following conditions must be satisfied:

$$\begin{aligned}
&\frac{K_{9a}\cdot K_{5a}}{K_{4a}\cdot K_{8a}}=1 \qquad \frac{K_{5a}\cdot K_{1}}{K_{3a}\cdot K_{7a}}=1 \qquad \frac{K_{4a}\cdot K_{1}}{K_{2a}\cdot K_{6a}}=1 \qquad \frac{K_{10a}\cdot K_{3a}}{K_{8a}\cdot K_{6a}}=1\\
&\frac{K_{9b}\cdot K_{5b}}{K_{4b}\cdot K_{8b}}=1 \qquad \frac{K_{5b}\cdot K_{1}}{K_{3b}\cdot K_{7b}}=1 \qquad \frac{K_{4b}\cdot K_{1}}{K_{2b}\cdot K_{6b}}=1 \qquad \frac{K_{10b}\cdot K_{3b}}{K_{8b}\cdot K_{6b}}=1\\
&\frac{K_{12}\cdot K_{5b}}{K_{4a}\cdot K_{11}}=1 \qquad \frac{K_{15}\cdot K_{5a}}{K_{4b}\cdot K_{14}}=1 \qquad \frac{K_{16}\cdot K_{3a}}{K_{6b}\cdot K_{14}}=1 \qquad \frac{K_{13}\cdot K_{3b}}{K_{6a}\cdot K_{11}}=1\\
&\frac{K_{16}\cdot K_{2b}}{K_{7a}\cdot K_{15}}=1 \qquad \frac{K_{10a}\cdot K_{2a}}{K_{7a}\cdot K_{9a}}=1 \qquad \frac{K_{10b}\cdot K_{2b}}{K_{7b}\cdot K_{9b}}=1 \qquad \frac{K_{13}\cdot K_{2a}}{K_{7b}\cdot K_{12}}=1
\end{aligned} \tag{S3.18}$$

Similarly to the one-inhibitor case, the thermodynamic constraints S3.18 allow us to express dissociations constants $K_4$ – $K_{16}$ in terms of the dimerization constant $K_1$, inhibitor binding constants $K_{2a}$, $K_{2b}$, $K_{3a}$ and $K_{3b}$ and thermodynamic factors, $f_a$, $f_b$, $g_{1a}$, $g_{1b}$, $g_{2a}$, $g_{2b}$, $g_{3a}$ and $g_{3b}$. Thermodynamic factors $f_a$, $f_b$, $g_{1a}$, $g_{1b}$, $g_{2a}$, $g_{2b}$ describe the same effects as for the one-inhibitor case, and subscripts *a* and *b* refer to inhibitors $I_1$ and $I_2$. The factor $g_{3a}$ quantifies the difference (normalized on facilitation factors $f_a$ and $f_b$ ) in the dissociation constants of $I_1$ binding to a free RAF monomer versus to the protomer in RAF dimer, when the other protomer is occupied by $I_2$. Likewise, the factor $g_{3b}$ describes the difference (normalized on facilitation factors $f_a$ and $f_b$) in dissociation constants of $I_2$ binding to monomer versus protomer in RAF dimer, when the other protomer is occupied by $I_1$. Note that we have redefined factors $g_{3a}$ and $g_{3b}$ compared to Ref. (Kholodenko, 2015) to make expressions for the dissociation constants $K_{13}$ and $K_{16}$ symmetric with respect to $f_a$ and $f_b$ (see List S3.4). If we denote the factor $g_{3a}$ defined in Ref. (Kholodenko, 2015) as $g^*_{3a}$, it can be expressed via the factor $g_{3a}$ introduced here, as follows, $g^*_{3a} = g_{3a}\cdot\sqrt{f_a/f_b}$. Likewise, the factor $g^*_{3b}$ defined in Ref. (Kholodenko, 2015) is expressed via the factor $g_{3b}$, as follows, $g^*_{3b} = g_{3b}\sqrt{f_b/f_a}$.

Equations S3.18 allow us to obtain the following relationships between the thermodynamic factors $g_{1a}$, $g_{1b}$, $g_{2a}$, and $g_{2b}$ and the apparent dissociation constants. If both $I_1$ and $I_2$ are DFG-IN, αC-OUT inhibitors, these relationships read,

$$\begin{aligned}
g_{1a} &= \frac{K_{da}^{DOC}}{K_{da}^{DOB}}\cdot\frac{K_{da}^{mB}}{K_{da}^{mC}} \qquad & g_{1b} &= \frac{K_{db}^{DOC}}{K_{db}^{DOB}}\cdot\frac{K_{db}^{mB}}{K_{db}^{mC}}\\
g_{2a} &= \frac{K_{da}^{DOB}}{K_{da}^{mB}} \qquad & g_{2b} &= \frac{K_{db}^{DOB}}{K_{db}^{mB}}
\end{aligned} \tag{S3.19}$$

In addition, the detailed balance relationships require the following conditions to be satisfied

$$\frac{K_{da}^{DIB}}{K_{da}^{DOB}}=\frac{K_{da}^{DIC}}{K_{da}^{DOC}}=\frac{K_{db}^{DIB}}{K_{db}^{DOB}}=\frac{K_{db}^{DIC}}{K_{db}^{DOC}} \tag{S3.20}$$

Thermodynamic coefficients for binding of CI/DI and CI/DO inhibitors and their combinations are readily obtained after substituting $K_d^{DOB}$ by $K_d^{DIB}$ and $K_d^{DOC}$ by $K_d^{DIC}$. For example, for a pair of CI/DO (a) and CO/DI (b) inhibitors, Eqns. S3.19 read,

$$g_{1a} = \frac{K_{da}^{DIC}}{K_{da}^{DIB}}\cdot\frac{K_{da}^{mB}}{K_{da}^{mC}} \qquad g_{1b} = \frac{K_{db}^{DOC}}{K_{db}^{DOB}}\cdot\frac{K_{db}^{mB}}{K_{db}^{mC}} \tag{S3.21}$$

$$g_{2a} = \frac{K_{da}^{DIB}}{K_{da}^{mB}} \qquad\qquad g_{2b} = \frac{K_{db}^{DOB}}{K_{db}^{mB}}$$

The detailed balance relationships S3.18 in this case require the following condition to be satisfied

$$\frac{K_{db}^{DIB}}{K_{db}^{DOB}} = \frac{K_{db}^{DIC}}{K_{db}^{DOC}} \tag{S3.22}$$

Eqs. S3.21-S3.22 will be valid for the pair of CI/DI (a) and CO/DI (b) inhibitors as well.

Eqs. S3.18-S3.12 allow us to relate the phenomenological thermodynamics factors ($g_{1a}$, $g_{1b}$, $g_{2a}$ and $g_{2b}$) with the apparent $K_d$'s of inhibhitor binding to different RAF forms. List S3.4 expresses the dissociation constants, $K_4 - K_{16}$ in terms of the phenomenological factors $f_a$, $f_b$, $g_{1a}$, $g_{1b}$, $g_{2a}$, and $g_{2b}$ and also in terms of the apparent dissociation constants introduced in List S3.2 and smaller numbers of free parameters, which are $g_{3a}$, $g_{3b}$, $f_a$ and $f_b$. As above, the value of the factors $g_3$ and $f$ are unique features of each inhibitor that are not directly determined by the positions of the αC-helix and DFG motif.

**List S3.4. Reactions and relationships between equilibrium dissociation constants for a model of BRAF-CRAF heterodimers and two allosteric inhibitors**

| No. | Reactions | Equilibrium dissociation constants expressed in terms of phenomenological thermodynamics factors | Relationships between the $K_d$'s that minimize the number of unknown thermodynamics factors |
|---|---|---|---|
| 1 | B + C ↔ B-C | $K_1$ | $K_1$ |
| 2a | B + $I_1$ ↔ B$I_1$ | $K_{2a}$ | $K_{da}^{mB}$ |
| 2b | B + $I_2$ ↔ B$I_2$ | $K_{2b}$ | $K_{db}^{mB}$ |
| 3a | C + $I_1$ ↔ C$I_1$ | $K_{3a}$ | $K_{da}^{mC}$ |
| 3b | C + $I_2$ ↔ C$I_2$ | $K_{3b}$ | $K_{db}^{mC}$ |
| 4a | B-C + $I_1$ ↔ B$I_1$-C | $K_{4a} = f_a \cdot K_{2a}$ | $K_{4a} = f_a \cdot K_{da}^{mB}$ |
| 4b | B-C + $I_2$ ↔ B$I_2$-C | $K_{4b} = f_b \cdot K_{2b}$ | $K_{4b} = f_b \cdot K_{db}^{mB}$ |
| 5a | B-C + $I_1$ ↔ B-C$I_1$ | $K_{5a} = g_{1a} \cdot f_a \cdot K_{3a}$ | $K_{5a} = \frac{K_{da}^{DIC}}{K_{da}^{DIB}} \cdot f_a \cdot {K_{da}}^{mB}$ |
| 5b | B-C + $I_2$ ↔ B-C$I_2$ | $K_{5b} = g_{1b} \cdot f_b \cdot K_{3b}$ | $K_{5b} = \frac{K_{db}^{DIC}}{K_{db}^{DIB}} \cdot f_b \cdot {K_{db}}^{mB}$ |
| 6a | B$I_1$ + C ↔ B$I_1$-C | $K_{6a} = f_a \cdot K_1$ | $K_{6a} = f_a \cdot K_1$ |
| 6b | B$I_2$ + C ↔ B$I_2$-C | $K_{6b} = f_b \cdot K_1$ | $K_{6b} = f_b \cdot K_1$ |
| 7a | B + C$I_1$ ↔ B-C$I_1$ | $K_{7a} = g_{1a} \cdot f_a \cdot K_1$ | $K_{7a} = f_a \cdot \frac{K_{da}^{mB}}{K_{da}^{mC}} \cdot \frac{K_{da}^{DIC}}{K_{da}^{DIB}} \cdot K_1$ |
| 7b | B + C$I_2$ ↔ B-C$I_2$ | $K_{7b} = g_{1b} \cdot f_b \cdot K_1$ | $K_{7b} = f_b \cdot \frac{K_{db}^{mB}}{K_{db}^{mC}} \cdot \frac{K_{db}^{DIC}}{K_{db}^{DIB}} \cdot K_1$ |
| 8a | B$I_1$-C+$I_1$ ↔ B$I_1$-C$I_1$ | $K_{8a} = g_{1a} \cdot g_{2a} \cdot K_{3a}$ | For $I_1^{CO/DI}$: $K_{8a} = K_{da}^{DOC}$<br>For $I_1^{CI/DI}$ & $I_1^{CI/DO}$: $K_{8a} = K_{da}^{DIC}$ |
| 8b | B$I_2$-C+$I_2$ ↔ B$I_2$-C$I_2$ | $K_{8b} = g_{1b} \cdot g_{2b} \cdot K_{3b}$ | For $I_2^{CO/DI}$: $K_{8b} = K_{db}^{DOC}$<br>For $I_2^{CI/DI}$ & $I_2^{CI/DO}$: $K_{8b} = K_{db}^{DIC}$ |
| 9a | B-C$I_1$+$I_1$ ↔ B$I_1$-C$I_1$ | $K_{9a} = g_{2a} \cdot K_{2a}$ | For $I_1^{CO/DI}$: $K_{9a} = K_{da}^{DOB}$<br>For $I_1^{CI/DI}$ & $I_1^{CI/DO}$: $K_{9a} = K_{da}^{DIB}$ |

| | | | |
|---|---|---|---|
| 9b | B-$CI_2$+$I_2$ ↔ $BI_2$-$CI_2$ | $K_{9b} = g_{2b} \cdot K_{2b}$ | For $I_2^{CO/DI}$: $K_{9b} = K_{db}^{DOB}$<br>For $I_2^{CI/DI}$ & $I_2^{CI/DO}$: $K_{9b} = K_{db}^{DIB}$ |
| 10a | $BI_1$+$CI_1$ ↔ $BI_1$-$CI_1$ | $K_{10a} = f_a \cdot g_{1a} \cdot g_{2a} \cdot K_1$ | For $I_1^{CO/DI}$: $K_{10a} = f_a \cdot \frac{K_{da}^{DOC}}{K_{da}^{mC}} \cdot K_1$<br>For $I_1^{CI/DI}$ & $I_1^{CI/DO}$: $K_{10a} = f_a \frac{K_{da}^{DIC}}{K_{da}^{mC}} K_1$ |
| 10b | $BI_2$+$CI_2$ ↔ $BI_2$-$CI_2$ | $K_{10b} = f_b \cdot g_{1b} \cdot g_{2b} \cdot K_1$ | For $I_2^{CO/DI}$: $K_{10b} = f_b \cdot \frac{K_{db}^{DOC}}{K_{db}^{mC}} \cdot K_1$<br>For $I_2^{CI/DI}$ & $I_2^{CI/DO}$: $K_{10b} = f_b \frac{K_{db}^{DIC}}{K_{db}^{mC}} K_1$ |
| 11 | $BI_1$-C+$I_2$ ↔ $BI_1$-$CI_2$ | $K_{11} = g_{1b} g_{3a} \sqrt{f_b/f_a} \cdot K_{3b}$ | $K_{11} = g_{3a} \sqrt{f_b/f_a} \cdot \frac{K_{db}^{DIC}}{K_{db}^{DIB}} \cdot K_{db}^{mB}$ |
| 12 | B-$CI_2$+$I_1$ ↔ $BI_1$-$CI_2$ | $K_{12} = g_{3a} \cdot \sqrt{f_a/f_b} \cdot K_{2a}$ | $K_{12} = g_{3a} \sqrt{f_a/f_b} \cdot K_{da}^{mB}$ |
| 13 | $BI_1$+$CI_2$ ↔ $BI_1$-$CI_2$ | $K_{13} = g_{1b} g_{3a} \sqrt{f_a f_b} \cdot K_1$ | $K_{13} = g_{3a} \frac{K_{db}^{DIC}}{K_{db}^{DIB}} \frac{K_{db}^{mB}}{K_{db}^{mC}} \cdot \sqrt{f_a f_b} \cdot K_1$ |
| 14 | $BI_2$-C+$I_1$ ↔ $BI_2$-$CI_1$ | $K_{14} = g_{1a} g_{3b} \sqrt{f_a/f_b} \cdot K_{3a}$ | $K_{14} = g_{3b} \sqrt{f_a/f_b} \cdot \frac{K_{da}^{DIC}}{K_{da}^{DIB}} \cdot K_{da}^{mB}$ |
| 15 | B-$CI_1$+$I_2$ ↔ $BI_2$-$CI_1$ | $K_{15} = g_{3b} \cdot \sqrt{f_b/f_a} \cdot K_{2b}$ | $K_{15} = g_{3b} \sqrt{f_b/f_a} \cdot K_{db}^{mB}$ |
| 16 | $BI_2$+$CI_1$ ↔ $BI_2$-$CI_1$ | $K_{16} = g_{1a} g_{3b} \cdot \sqrt{f_a f_b} \cdot K_1$ | $K_{16} = g_{3b} \frac{K_{da}^{DIC}}{K_{da}^{DIB}} \frac{K_{da}^{mB}}{K_{da}^{mC}} \cdot \sqrt{f_a f_b} \cdot K_1$ |

Similar reactions of homodimerization of RAF molecules, inhibitor binding and resulting relationships between the equilibrium dissociation constants and the thermodynamic factors describing allosteric effects are presented in the files "Kds.xlsx" and "RAF_MEK_ERK.bngl".

## 4. Total kinase activity of different monomeric and dimeric RAF forms.

The total kinase activity is proportional to the weighted sum of the concentrations of inhibitor-free monomers and dimers and partially inhibited dimers (see List S3.4). Inhibitor bound RAF monomers and RAF dimers that have bound two inhibitor molecules are taken to have no kinase activity.

**List S4.1. Relative activities of different RAF kinase forms.**

| Molecule description | Rule-based representation of the molecule (Chylek et al., 2014) | Kinase activity relative to active BRAF monomer |
|---|---|---|
| **RAF monomers and dimers that are inhibitor-free** | | |
| Active WT BRAF monomer | BRAF(bI) | 1 |
| WT BRAF homodimer | BRAF(Dm!1,bI).<br>BRAF(Dm!1,bI) | 2 |
| CRAF monomer not phosphorylated on S338, regardless of state of S642 | CRAF(S338~0,S642~?,cI) | 0 |
| CRAF monomer phosphorylated on S338 and not phosphorylated on S642 | CRAF(S338~P,S642~0,cI) | 0.2 |
| CRAF monomer phosphorylated on S338 and S642 | CRAF(S338~P,S642~P,cI) | 0 |
| CRAF homodimer, both molecules are not | CRAF(S338~0, S642~?,Dm!1,cI). | 0.01 |

| | | |
|---|---|---|
| phosphorylated on S338, regardless of state of S642 | CRAF(S338~0, S642~?,Dm!1,cI) | |
| CRAF homodimer, both molecules are phosphorylated on S642, regardless of state of S338 | CRAF(S338~?, S642~P,Dm!1,cI).<br>CRAF(S338~?, S642~P,Dm!1,cI) | 0.01 |
| CRAF homodimer with only one protomer phosphorylated S338 and not phosphorylated on S338 | CRAF(S338~P,S642~0,cI).<br>CRAF(S338~0, S642~?,cI) | 0.2 |
| CRAF homodimer, both molecules are phosphorylated on S338 and not phosphorylated on S642 | CRAF(S338~P, S642~0,Dm!1,cI).<br>CRAF(S338~P, S642~0,Dm!1,cI) | 0.4 |
| CRAF homodimer with one protomer phosphorylated S338 and another protomer phosphorylated on S642 | CRAF(S338~P,S642~0,cI).<br>CRAF(S338~?, S642~P,cI) | 0.2 |
| Heterodimer with CRAF not phosphorylated on S338 (regardless of state of S642) and WT BRAF | CRAF(S338~0, S642~?,Dm!1,cI).<br>BRAF(Dm!1,bI) | 15 |
| Heterodimer with CRAF phosphorylated on S642 (regardless of state of S338) and WT BRAF | CRAF(S338~?, S642~P,Dm!1,cI).<br>BRAF(Dm!1,bI) | 15 |
| Heterodimer with CRAF phosphorylated on S338 and not phosphorylated on S642 and WT BRAF | CRAF(S338~P, S642~0,Dm!1,cI).<br>BRAF(Dm!1,bI) | 30 |
| BRAFV600E monomer | BRAFV600E(EI) | 2 |
| BRAFV600E homodimer | BRAFV600E(Dm!1, EI).<br>BRAFV600E(Dm!1, EI) | 4 |
| Heterodimer with BRAFV600E and WT BRAF | BRAF(Dm!1,bI).<br>BRAFV600E(Dm!1, EI) | 3 |
| Heterodimer with BRAFV600E and CRAF not phosphorylated on S338 (regardless of state of S642) | CRAF(S338~0, S642~?,Dm!1,cI).<br>BRAFV600E(Dm!1,EI) | 15 |
| Heterodimer with BRAFV600E and CRAF phosphorylated on S642 (regardless of state of S338) | CRAF(S338~?, S642~P,Dm!1,cI).<br>BRAFV600E(Dm!1,EI) | 15 |
| Heterodimer with BRAFV600E and CRAF phosphorylated on S338 and not phosphorylated on S642 | CRAF(S338~P, S642~0,Dm!1,cI).<br>BRAFV600E(Dm!1,EI) | 30 |
| **RAF dimers bound to one inhibitor molecule** | | |
| CRAF homodimer with one inhibitor bound, protomer free from inhibitor is phosphorylated on S338 and not phosphorylated on S642 | CRAF(S338~P,S642~0,Dm!1,cI).<br>CRAF(S338~?, S642~?,Dm!1,cI!2).<br>Inh(RAFI!2) | 0.2 |
| CRAF homodimer with one inhibitor bound, protomer free from inhibitor is dephosphorylated on S338 regardless of state of S642 | CRAF(S338~0,S642~?,Dm!1,cI).<br>CRAF(S338~?,S642~?,Dm!1,cI!2).<br>Inh(RAFI!2) | 0 |
| CRAF homodimer with one inhibitor bound, protomer free from inhibitor is phosphorylated on S642 regardless of state of S338 | CRAF(S338~?,S642~P,Dm!1,cI).<br>CRAF(S338~?,S642~?,Dm!1,cI!2).<br>Inh(RAFI!2) | 0 |

| | | |
|---|---|---|
| WT BRAF homodimer with one inhibitor molecule bound it | BRAF(Dm!1,bI).<br>BRAF(Dm!1,bI!2).<br>Inh(RAFI!2) | 1 |
| Heterodimer with CRAF not phosphorylated on S338 (regardless of state of S642) and WT BRAF, inhibitor molecule is bound to CRAF | BRAF(Dm!1,bI).<br>CRAF(S338~0,S642~?,Dm!1,cI!2).<br>Inh(RAFI!2) | 8 |
| Heterodimer with CRAF not phosphorylated on S338 (regardless of state of S642) and WT BRAF, inhibitor molecule is bound to BRAF | CRAF(S338~0,S642~?,Dm!1,cI).<br>BRAF(Dm!1,bI!2).<br>Inh(RAFI!2) | 8 |
| Heterodimer with CRAF phosphorylated on S642 (regardless of state of S338) and WT BRAF, inhibitor molecule is bound to CRAF | BRAF(Dm!1,bI).<br>CRAF(S338~?,S642~P,Dm!1,cI!2).<br>Inh(RAFI!2) | 8 |
| Heterodimer with CRAF phosphorylated on S642 (regardless of state of S338) and WT BRAF, inhibitor molecule is bound to BRAF | CRAF(S338~?,S642~P,Dm!1,cI).<br>BRAF(Dm!1,bI!2).<br>Inh(RAFI!2) | 8 |
| Heterodimer with CRAF phosphorylated on S338 and dephosphorylated on S642 and WT BRAF, inhibitor molecule is bound to CRAF | BRAF(Dm!1,bI).<br>CRAF(S338~P,S642~0,Dm!1,cI!2).<br>Inh(RAFI!2) | 15 |
| Heterodimer with CRAF phosphorylated on S338 and dephosphorylated on S642 and WT BRAF, inhibitor molecule is bound to BRAF | CRAF(S338~P, S642~0,Dm!1,cI).<br>BRAF(Dm!1,bI!2).<br>Inh(RAFI!2) | 15 |
| Heterodimer with CRAF not phosphorylated on S338 (regardless of state of S642) and WT BRAFV600E, inhibitor molecule is bound to CRAF | BRAFV600E(Dm!1,bI).<br>CRAF(S338~0,S642~?,Dm!1,cI!2).<br>Inh(RAFI!2) | 8 |
| Heterodimer with CRAF not phosphorylated on S338 (regardless of state of S642) and WT BRAFV600E, inhibitor molecule is bound to BRAFV600E | CRAF(S338~0,S642~?,Dm!1,cI).<br>BRAFV600E(Dm!1,bI!2).<br>Inh(RAFI!2) | 8 |
| Heterodimer with CRAF phosphorylated on S642 (regardless of state of S338) and WT BRAFV600E, inhibitor molecule is bound to CRAF | BRAFV600E(Dm!1,bI).<br>CRAF(S338~?,S642~P,Dm!1,cI!2).<br>Inh(RAFI!2) | 8 |
| Heterodimer with CRAF phosphorylated on S642 (regardless of state of S338) and WT BRAFV600E, inhibitor molecule is bound to BRAFV600E | CRAF(S338~?,S642~P,Dm!1,cI).<br>BRAFV600E(Dm!1,bI!2).<br>Inh(RAFI!2) | 8 |
| Heterodimer with CRAF phosphorylated on S338 and dephosphorylated on S642 and WT BRAFV600E, inhibitor molecule is bound to CRAF | BRAFV600E(Dm!1,bI).<br>CRAF(S338~P,S642~0,Dm!1,cI!2).<br>Inh(RAFI!2) | 15 |
| Heterodimer with CRAF phosphorylated on S338 and dephosphorylated on S642 and WT BRAFV600E, inhibitor molecule is bound to BRAFV600E | CRAF(S338~P, S642~0,Dm!1,cI).<br>BRAFV600E(Dm!1,bI!2).<br>Inh(RAFI!2) | 15 |
| Dimer of WT BRAF and BRAFV600E with one inhibitor molecule bound to WT BRAF | BRAF(Dm!1,bI).<br>BRAFV600E(Dm!1,bI!2).<br>Inh(RAFI!2) | 1 |
| Dimer of WT BRAF and BRAFV600E with one inhibitor molecule bound to BRAFV600E | BRAFV600E(Dm!1,bI).<br>BRAF (Dm!1,bI!2). | 2 |

| | | |
|---|---|---|
| | Inh(RAFI!2) | |

## 5. Parameters of the model

### List S5.1. Model parameters

| Parameter | Value | Description |
|---|---|---|
| MEK_level | 1600 nM | Total concentration of MEK |
| ERK_level | 3000 nM | Total concentration of ERK |
| BRAF_level* | 50 nM | Total concentration of WT BRAF |
| CRAF_level* | 50 nM | Total concentration of CRAF |
| BE_level* | 25 nM | Total concentration of BRAFV600E |
| RasT* | 25 nM | Concentration of active RAS |
| Ph1_tot | 100 nM | Total concentration of MEK phosphatase |
| MKP3_tot | 100 nM | Total concentration of ERK phosphatase |
| p1 | 7 | Effect of ERK feedback phosphorylation on RAF binding to RAS-GTP |
| p2 | 16 | Effect of PM localization of chemicals on reaction Kd |
| p3 | 7 | Effect of ERK feedback phosphorylation on RAF dimerization |
| k_on_typ | 0.001 $(nM \cdot s)^{-1}$ | Scale of forward reaction rate of protein binding |
| k_on_typ_a | 0.1 $(nM \cdot s)^{-1}$<br>$10^{-4}$ $(nM \cdot s)^{-1}$ | Forward reaction rate of inhibitor 1 binding to RAF for the cases of high (highest value) and low (lowest value) $k_{off}$ |
| k_on_typ_b | 0.1 $(nM \cdot s)^{-1}$<br>$10^{-4}$ $(nM \cdot s)^{-1}$ | Forward reaction rate of inhibitor 2 binding to RAF for the cases of high (highest value) and low (lowest value) $k_{off}$ |
| kC1 | k_on_typ $(nM \cdot s)^{-1}$ | Forward rate constant of CRAF binding to RAS-GTP |
| KC1 | 400 nM | Kd of CRAF binding to RAS-GTP |
| kC_1 | KC1·kC1 $s^{-1}$ | Backward rate constant of CRAF binding to RAS-GTP (Kd = 400 nM) |
| kB1 | k_on_typ $(nM \cdot s)^{-1}$ | Forward rate constant of BRAF binding to RAS-GTP |
| KB1 | 80 nM | Kd of BRAF binding to RAS-GTP |
| kB_1 | KB1·kC1 $s^{-1}$ | Backward rate constant of BRAF binding to RAS-GTP (Kd = 80 nM) |
| kCCd1 | k_on_typ $(nM \cdot s)^{-1}$ | Forward rate constant of CRAF homodimerization |
| KCCd1 | 4000 nM | Kd of CRAF homodimerization |
| kCCd_1 | KCCd1·kCCd1 $s^{-1}$ | Backward rate constant of CRAF homodimerization (Kd = 4000 nM) |
| kBBd1 | k_on_typ $(nM \cdot s)^{-1}$ | Forward rate constant of BRAF homodimerization |
| KBB1 | 4000 nM | Kd of BRAF homodimerization |
| kBBd_1 | KBBd1·kBBd1 $s^{-1}$ | Backward rate constant of BRAF homodimerization (Kd = 2000 nM) |
| kCBd1 | k_on_typ $(nM \cdot s)^{-1}$ | Forward rate constant of BRAF-CRAF heterodimerization |
| KCBd1 | 4000 nM | Kd of BRAF-CRAF heterodimerization |
| kCBd_1 | KCBd1·kCCd1 $s^{-1}$ | Backward rate constant of B/CRAF heterodimerization (Kd = 4000 nM) |
| kdERC1 | k_on_typ $(nM \cdot s)^{-1}$ | Forward rate of ERK feedback phosphorylation of CRAF on S642 |
| KdERC1 | 50 nM | Kd of ERK binding to CRAF |
| kdERC_1 | KdERC1·kdERC1 $s^{-}$ | Backward rate CRAF phosphorylation by ERK (Kd = 50 |

| | | |
|---|---|---|
| | $^{1}$ | nM) |
| kcatER | 0.5 $s^{-1}$ | Catalytic rate constant of ERK feedback phosphorylation of CRAF |
| pEC | 5 | Ratio between ERK affinities to S642 and pS642 CRAF |
| VmaxS642 | 0.1 $s^{-1}$ | The CRAF S642 dephosphorylation rate |
| kdERB1 | k_on_typ $(nM \cdot s)^{-1}$ | Forward rate of ERK feedback phosphorylation of BRAF on T753 |
| KdEERB1 | 50 nM | Kd of ERK binding to BRAF |
| kdERB_1 | KdERB1·kdERB1 $s^{-1}$ | Backward rate of ERK phosphorylation of BRAF (Kd = 50 nM) |
| pEB | 5 | Ratio between ERK affinities to T753 and pT753 BRAF |
| VmaxERKT753 | 0.1 $s^{-1}$ | The BRAF T753 dephosphorylation rate |
| kdERBE1 | k_on_typ $(nM \cdot s)^{-1}$ | Forward rate constant of ERK phosphorylation of $BRAF^{V600E}$ on T753 |
| KdERBE1 | 50 nM | Kd of ERK binding to $BRAF^{V600E}$ |
| kdERBE_1 | KdERBE1·kdERB1 $s^{-1}$ | Backward rate constant $BRAF^{V600E}$ phosphorylation by ERK (Kd = 50 nM) |
| pEBE | 5 | Ratio between ERK affinities to T753 and pT753 $BRAF^{V600E}$ |
| VmaxERKT753BE | 0.1 $s^{-1}$ | The $BRAF^{V600E}$ T753 dephosphorylation rate |
| kpS338 | 0.03 $s^{-1}$ | Phosphorylation rate of CRAF on S338 on PM |
| kS338 | 0.03 $s^{-1}$ | Dephosphorylation rate of CRAF on S338 |
| kS259 | 0.015 $s^{-1}$ | Rate of CRAF phosphorylation on S259 in cytoplasm |
| pM259 | 25 | Decrease of rate of CRAF phosphorylation on S259 on PM |
| kS_259 | 0.0003 $s^{-1}$ | Rate of CRAF dephosphorylation on S259 in cytoplasm |
| pMd259 | 100 | Increase of rate of CRAF dephosphorylation on S259 on PM |
| kS365 | 0.015 $s^{-1}$ | Rate of BRAF phosphorylation on S365 in cytoplasm |
| pM365 | 25 | Decrease of rate of BRAF phosphorylation on S365 on PM |
| kS_365 | 0.0003 $s^{-1}$ | Rate of BRAF dephosphorylation on S365 in cytoplasm |
| pMd365 | 100 | Increase of rate of BRAF dephosphorylation on S365 on PM |
| kBE1 | kB1 $(nM \cdot s)^{-1}$ | Forward rate constant of $BRAF^{V600E}$ binding to RAS-GTP |
| kBE_1 | kB_1 $s^{-1}$ | Backward rate constant of $BRAF^{V600E}$ binding to RAS-GTP |
| fa** | 0.01 | Facilitation of RAF dimerization by inhibitor a |
| fb** | 0.01 | Facilitation of RAF dimerization by inhibitor b |
| g3a** | 1 | Thermodynamic factor g3 for inhibitor a |
| g3b** | 1 | Thermodynamic factor g3 for inhibitor b |
| alphaa_11** | 1 | Thermodynamic factor $a_{11}$ for inhibitor a (see section S3.3) |
| alphaa_12** | 1 | Thermodynamic factor $a_{12}$ for inhibitor a (see section S3.3) |
| alphaa_21** | 1 | Thermodynamic factor $a_{21}$ for inhibitor a (see section S3.3) |
| alphaa_22** | 1 | Thermodynamic factor $a_{22}$ for inhibitor a (see section S3.3) |
| alphab_11** | 1 | Thermodynamic factor $a_{11}$ for inhibitor b (see section S3.3) |
| alphab_12** | 1 | Thermodynamic factor $a_{12}$ for inhibitor b (see section S3.3) |
| alphab_21** | 1 | Thermodynamic factor $a_{21}$ for inhibitor b (see section S3.3) |
| alphab_22** | 1 | Thermodynamic factor $a_{22}$ for inhibitor b (see section S3.3) |
| b_C_pS259_m** | 0.01 | Equilibrium constant for DFG-motif transitions in pS259 CRAF monomer |
| c_C_pS259_m** | 0.01 | Equilibrium constant for αC-helix transitions in pS259 CRAF monomer |
| g_C_pS259_m** | 2 | Constant of cooperativity between IN/OUT transitions of DFG-motif and αC-helix for pS259 CRAF monomers |

| | | |
|---|---|---|
| b_C_S259_S338_m** | 0.1 | Equilibrium constant for DFG-motif transitions in S259, S338 CRAF monomer |
| c_C_S259_S338_m** | 0.1 | Equilibrium constant for αC-helix transitions in S259, S338 CRAF monomer |
| g_C_S259_S338_m** | 2 | Constant of cooperativity between IN/OUT transitions of DFG-motif and αC-helix for S259, S338 CRAF monomers |
| b_C_S259_pS338_m** | 1 | Equilibrium constant for DFG-motif transitions in S259, pS338 CRAF monomer |
| c_C_S259_pS338_m** | 1 | Equilibrium constant for αC-helix transitions in S259, pS338 CRAF monomer |
| g_C_S259_pS338_m** | 2 | Constant of cooperativity between IN/OUT transitions of DFG-motif and αC-helix for S259, pS338 CRAF monomers |
| b_C_S259_S338_dimIN** | 0.1 | Equilibrium constant for DFG-motif transitions in S259, S338 CRAF protomer in dimer, the other protomer is in αC-IN |
| c_C_S259_S338_dimIN** | 1 | Equilibrium constant for αC-helix transitions in S259, S338 CRAF protomer in dimer, the other protomer is in αC-IN |
| g_C_S259_S338_dimIN** | 2 | Constant of cooperativity between transitions of DFG and αC-helix for S259, S338 CRAF protomer in dimer, the other protomer is in αC-IN |
| b_C_S259_pS338_dimIN** | 10 | Equilibrium constant for DFG transitions in S259, pS338 CRAF protomer in dimer, the other protomer is in αC-IN |
| c_C_S259_pS338_dimIN** | 10 | Equilibrium constant for αC-helix transitions in S259, pS338 CRAF protomer in dimer, the other protomer is in αC-IN |
| g_C_S259_pS338_dimIN** | 2 | Constant of cooperativity between transitions of DFG-motif and αC-helix for S259, pS338 CRAF protomer in dimer, the other protomer is in αC-IN |
| b_B_pS365_m** | 0.01 | Equilibrium constant for DFG-motif transitions in pS365 BRAF monomer |
| c_B_pS365_m** | 0.01 | Equilibrium constant for αC-helix transitions in pS365 BRAF monomer |
| g_B_pS365_m** | 2 | Constant of cooperativity between IN/OUT transitions of DFG-motif and αC-helix for pS365 BRAF monomers |
| b_B_S365_m** | 1 | Equilibrium constant for DFG-motif transitions in S365 BRAF monomer |
| c_B_S365_m** | 1 | Equilibrium constant for αC-helix transitions in S365 BRAF monomer |
| g_B_S365_m** | 2 | Constant of cooperativity between IN/OUT transitions of DFG-motif and αC-helix for S365 BRAF monomers |
| b_B_S365_dimIN** | 10 | Equilibrium constant for DFG-motif transitions in S365 BRAF protomer in dimer, the other protomer is in αC-IN |
| c_B_S365_dimIN** | 10 | Equilibrium constant for αC-helix transitions in S365 BRAF protomer in dimer, the other protomer is in αC-IN |
| g_B_S365_dimIN** | 2 | Constant of cooperativity between transitions of DFG and αC-helix for S365 BRAF protomer in dimer, the other protomer is in αC-IN |
| b_B_S365_dimOUT** | 10 | Equilibrium constant for DFG-motif transitions in S365 BRAF protomer in dimer, the other protomer is in αC-OUT |
| c_B_S365_dimOUT** | 500 | Equilibrium constant for αC-helix transitions in S365 BRAF protomer in dimer, the other protomer is in αC-OUT |
| g_B_S365_dimOUT** | 2 | Constant of cooperativity between transitions of DFG and αC-helix for S365 BRAF protomer in dimer, the other protomer is in αC-OUT |

| | | |
|---|---|---|
| b_BE_m** | 1 | Equilibrium constant for DFG-motif transitions in BRAFV600E monomer |
| c_BE_m** | 1 | Equilibrium constant for αC-helix transitions in BRAFV600E monomer |
| g_BE_m** | 2 | Constant of cooperativity between IN/OUT transitions of DFG-motif and αC-helix for BRAFV600E monomers |
| b_BE_dimIN** | 10 | Equilibrium constant for DFG transitions in BRAFV600E protomer in dimer, the other protomer is in αC-IN |
| c_BE_dimIN** | 10 | Equilibrium constant for αC-helix transitions in BRAF-V600E protomer in dimer, the other protomer is in αC-IN |
| g_BE_dimIN** | 2 | Constant of cooperativity between transitions of DFG and αC-helix for BRAFV600E protomer in dimer, the other protomer is in αC-IN |
| b_BE_dimOUT** | 10 | Equilibrium constant for DFG transitions in BRAFV600E protomer in dimer, the other protomer is in αC-OUT |
| c_BE_dimOUT** | 500 | Equilibrium constant for αC-helix transitions in BRAF-V600E protomer in dimer, the other protomer is in αC-OUT |
| g_BE_dimOUT** | 2 | Constant of cooperativity between transitions of DFG and αC-helix for BRAFV600E protomer in dimer, the other protomer is in αC-OUT |
| Kda | 10 | Dissociation constant for inhibitor a |
| Kdb | 10 | Dissociation constant for inhibitor b |
| pBE1*** | 2 | Effect of ERK phosphorylation on $BRAF^{V600E}$ binding to RAS-GTP |
| kBEBEd1 | k_on_typ $(nM \cdot s)^{-1}$ | Forward rate constant of $BRAF^{V600E}$ homodimerization |
| KBEBEd1 | 200 nM | Kd of $BRAF^{V600E}$ homodimerization |
| kBEBEd_1 | KBEBEd1· kBEBEd1 $s^{-1}$ | Backward rate constant of $BRAF^{V600E}$ homodimerization (Kd = 200 nM) |
| pBE3*** | 1.7 | Effect of ERK feedback phosphorylation on $BRAF^{V600E}$ dimerization |
| kBEBd1 | kBEBEd1 $(nM \cdot s)^{-1}$ | Forward rate constant of WT BRAF and $BRAF^{V600E}$ dimerization |
| kBEBd_1 | kBEBEd_1 $s^{-1}$ | Backward rate constant of WT BRAF and $BRAF^{V600E}$ dimerization |
| pBEB3*** | 1.7 | Effect of phosphorylation of $BRAF^{V600E}$ by ERK on dimerization with BRAF |
| p3BEpB*** | 1.7 | Effect of phosphorylation of BRAF by ERK on dimerization with $BRAF^{V600E}$ |
| kBECd1 | kBEBEd1 $(nM \cdot s)^{-1}$ | Forward rate constant of CRAF and $BRAF^{V600E}$ dimerization |
| kBECd_1 | kBEBEd_1 $s^{-1}$ | Backward rate constant of CRAF and $BRAF^{V600E}$ dimerization |
| pBEC3*** | 1.7 | Effect of phosphorylation of $BRAF^{V600E}$ by ERK on dimerization with CRAF |
| p3BEpC*** | 1.7 | Effect of phosphorylation of CRAF by ERK on dimerization with $BRAF^{V600E}$ |
| k2a_pS365 | k_on_typ_a $(nM \cdot s)^{-1}$ | Forward rate constant of inhibitor 1 binding to pS365 BRAF |
| k2b_pS365 | k_on_typ_b $(nM \cdot s)^{-1}$ | Forward rate constant of inhibitor 2 binding to pS365 BRAF |
| k_2a_pS365 | K2a_pS365· k2a_pS365 $s^{-1}$ | Backward rate constant of inhibitor 1 binding to pS365 BRAF<br>(value of Kd= K2a_pS365 is calculated in xls file) |
| k_2b_pS365 | K2b_pS365· | Backward rate constant of inhibitor 2 binding to pS365 BRAF |

| | | |
|---|---|---|
| | k2b_pS365 $s^{-1}$ | (value of Kd= K2b_pS365 is calculated in xls file) |
| k2a_S365 | k_on_typ_a $(nM \cdot s)^{-1}$ | Forward rate constant of inhibitor 1 binding to S365 BRAF |
| k2b_S365 | k_on_typ_b $(nM \cdot s)^{-1}$ | Forward rate constant of inhibitor 2 binding to S365 BRAF |
| k_2a_S365 | K2a_S365· k2a_S365 $s^{-1}$ | Backward rate constant of inhibitor 1 binding to S365 BRAF (value of Kd= K2a_S365 is calculated in xls file) |
| k_2b_S365 | K2b_S365· k2b_S365 $s^{-1}$ | Backward rate constant of inhibitor 2 binding to S365 BRAF (value of Kd= K2b_S365 is calculated in xls file) |
| k2Ea | k_on_typ_a $(nM \cdot s)^{-1}$ | Forward rate constant of inhibitor 1 binding to $BRAF^{V600E}$ |
| k2Eb | k_on_typ_b $(nM \cdot s)^{-1}$ | Forward rate constant of inhibitor 2 binding to $BRAF^{V600E}$ |
| k_2Ea | K2Ea·k2Ea $s^{-1}$ | Backward rate constant of inhibitor 1 binding to $BRAF^{V600E}$ (value of Kd= K2Ea is calculated in xls file) |
| k_2Eb | K2Eb·k2Eb $s^{-1}$ | Backward rate constant of inhibitor 2 binding to $BRAF^{V600E}$ (value of Kd= K2Ea is calculated in xls file) |
| k3a_pS259_S338 | k_on_typ_a $(nM \cdot s)^{-1}$ | Forward rate constant of inhibitor 1 binding to pS259/S338 CRAF |
| k3b_pS259_S338 | k_on_typ_b $(nM \cdot s)^{-1}$ | Forward rate constant of inhibitor 2 binding to pS259/S338 CRAF |
| k_3a_pS259_S338 | K3a_pS259_S338· k3a_pS259_S338 $s^{-1}$ | Backward rate constant of inhibitor 1 binding to pS259/S338 CRAF (value of Kd= K3a_pS259_S338 is calculated in xls file) |
| k_3b_pS259_S338 | K3b_pS259_S338· k3b_pS259_S338 $s^{-1}$ | Backward rate constant of inhibitor 2 binding to pS259/S338 CRAF (value of Kd= K3a_pS259_S338 is calculated in xls file) |
| k3a_S259_S338 | k_on_typ_a $(nM \cdot s)^{-1}$ | Forward rate constant of inhibitor 1 binding to S259/S338 CRAF |
| k3b_S259_S338 | k_on_typ_b $(nM \cdot s)^{-1}$ | Forward rate constant of inhibitor 2 binding to S259/S338 CRAF |
| k_3a_S259_S338 | K3a_S259_S338· k3a_S259_S338 $s^{-1}$ | Backward rate constant of inhibitor 1 binding to S259/S338 CRAF (value of Kd= K3a_S259_S338 is calculated in xls file) |
| k_3b_S259_S338 | K3b_S259_S338· k3b_S259_S338 $s^{-1}$ | Backward rate constant of inhibitor 2 binding to S259/S338 CRAF (value of Kd= K3a_S259_S338 is calculated in xls file) |
| k3a_S259_pS338 | k_on_typ_a $(nM \cdot s)^{-1}$ | Forward rate constant of inhibitor 1 binding to S259/pS338 CRAF |
| k3b_S259_pS338 | k_on_typ_b $(nM \cdot s)^{-1}$ | Forward rate constant of inhibitor 2 binding to S259/pS338 CRAF |
| k_3a_S259_pS338 | K3a_S259_pS338· k3a_S259_pS338 $s^{-1}$ | Backward rate constant of inhibitor 1 binding to S259/pS338 CRAF (value of Kd= K3a_S259_pS338 is calculated in xls file) |
| k_3b_S259_pS338 | K3b_S259_pS338· k3b_S259_pS338 $s^{-1}$ | Backward rate constant of inhibitor 2 binding to S259/pS338 CRAF (value of Kd= K3a_S259_pS338 is calculated in xls file) |
| kRAFMEK1 | k_on_typ $(nM \cdot s)^{-1}$ | Forward rate constant of first MEK phosphorylation by RAF |
| KRAFMEK1 | 1500 nM | Kd of RAF binding to MEK |
| kRAFMEK_1 | KRAFMEK1· kRAFMEK1 $s^{-1}$ | Backward rate constant of 1st MEK phosphorylation by RAF (Kd=1500 nM) |
| kRAFMEK2 | k_on_typ $(nM \cdot s)^{-1}$ | Forward rate constant of second MEK phosphorylation by RAF |
| KRAFMEK2 | 1000 nM | Kd of RAF binding to MEK |

| | | |
|---|---|---|
| kRAFMEK_2 | KRAFMEK2· kRAFMEK1 $s^{-1}$ | Backward rate constant of 2nd MEK phosphorylation by RAF (Kd=1000 nM) |
| kcatRAFMEK1 | 0.5 $s^{-1}$ | Catalytic rate constant of first MEK phosphorylation by RAF |
| kcatRAFMEK2 | 0.5 $s^{-1}$ | Catalytic rate constant of second MEK phosphorylation by RAF |
| kPPMEK1 | k_on_typ $(nM \cdot s)^{-1}$ | Forward rate constant of ppMEK dephosphorylation |
| KPPMEK1 | 2000 nM | Kd of phosphatase binding to MEK |
| kPPMEK_1 | KPPMEK1· kPPMEK1 $s^{-1}$ | Backward rate constant of ppMEK dephosphorylation (Kd = 2000 nM) |
| kcatPPMEK | 0.1 $s^{-1}$ | Catalytic rate constant of pMEK dephosphorylation |
| kPMEK1 | k_on_typ | Forward rate constant of pMEK dephosphorylation |
| KPMEK1 | 2000 nM | Kd of phosphatase binding to MEK |
| kPMEK_1 | KPMEK1· kPMEK1 | Backward rate constant of pMEK dephosphorylation (Kd=2000 nM) |
| kcatPMEK | 0.5 $s^{-1}$ | Catalytic rate constant of pMEK dephosphorylation |
| kMERKT1 | k_on_typ | Forward rate constant of ERK phosphorylation on T |
| KMERKT1 | 2000 nM | Kd of MEK binding to ERK |
| kMERKT_1 | KMERKT1· kMERKT1 | Backward rate constant of ERK phosphorylation on T (Kd = 2000 nM) |
| kcatMERKT1 | 0.001 $s^{-1}$ | Catalytic rate constant of ERK phosphorylation on T |
| kMERKY1 | k_on_typ | Forward rate constant of ERK phosphorylation on Y |
| KMERKY1 | 2000 nM | Kd of MEK binding to ERK |
| kMERKY_1 | KMERKY1· kMERKY1 | Backward rate constant of ERK phosphorylation on Y (Kd = 2000 nM) |
| kcatMERKY1 | 0.1 $s^{-1}$ | Catalytic rate constant of ERK phosphorylation on Y |
| kMERKT2 | k_on_typ | Forward rate constant of pERK phosphorylation on T |
| KMERKT2 | 1000 nM | Kd of MEK binding to ERK |
| kMERKT_2 | KMERKT2· kMERKT2 | Backward rate constant of pERK phosphorylation on T (Kd = 1000 nM) |
| kcatMERKT2 | 0.2 $s^{-1}$ | Catalytic rate constant of pERK phosphorylation on T |
| kMERKY2 | k_on_typ | Forward rate constant of pERK phosphorylation on Y |
| KMERKY2 | 1000 nM | Kd of MEK binding to ERK |
| kMERKY_2 | KMERKY2· kMERKY2 | Backward rate constant of pERK phosphorylation on Y (Kd = 1000 nM) |
| kcatMERKY2 | 0.2 $s^{-1}$ | Catalytic rate constant of pERK phosphorylation on Y |
| kPERKT1 | k_on_typ | Forward rate constant of pERK dephosphorylation on T |
| KPERKT1 | 2000 nM | Kd of phosphatase binding to ERK |
| kPERKT_1 | KPERKT1· kPERKT1 | Backward rate constant of pERK dephosphorylation on T (Kd = 2000 nM) |
| kcatPERKT1 | 1 $s^{-1}$ | Catalytic rate constant of pERK dephosphorylation on T |
| kPERKT2 | k_on_typ | Forward rate constant of ERK phosphatase association with its product |
| KPERKT2 | 10000 nM | Kd of phosphatase binding to ERK |
| kPERKT_2 | KPERKT2· kPERKT2 | Backward rate constant of ERK phosphatase association with its product |
| kPERKY1 | k_on_typ | Forward rate constant of pERK dephosphorylation on Y |
| KPERKY1 | 2000 nM | Kd of phosphatase binding to ERK |
| kPERKY_1 | KPERKY1· | Backward rate constant of pERK dephosphorylation on T |

| | | |
|---|---|---|
| | kPERKY1 | (Kd = 2000 nM) |
| kcatPERKY1 | 1 $s^{-1}$ | Catalytic rate constant of pERK dephosphorylation on Y |
| kPERKY2 | k_on_typ | Forward rate constant of ERK phosphatase association with its product |
| KPERKY2 | 10000 nM | Kd of phosphatase binding to ERK |
| kPERKY_2 | KPERKY2· kPERKY2 | Backward rate constant of ERK phosphatase association with its product |
| kPPERK1 | k_on_typ | Forward rate constant of ppERK dephosphorylation |
| KPPERK1 | 2000 nM | Kd of phosphatase binding to ERK |
| kPPERK_1 | KPPERK1· kPPERK1 | Backward rate constant of ppERK dephosphorylation (Kd=2000 nM) |
| kcatPPERK1 | 0.5 $s^{-1}$ | Catalytic rate constant of ppERK dephosphorylation |
| kPPERK2 | k_on_typ | Forward rate constant of ERK phosphatase association with its product |
| KPPERK2 | 10000 nM | Kd of phosphatase binding to ERK |
| kPPERK_2 | KPPEERK2· kPPERK2 | Backward rate constant of ERK phosphatase association with its product |
| KA_actBRAFmon$^{+}$ | 1 | Relative kinase activity of active BRAF monomer |
| KA_actBRAFhom$^{+}$ | 2 | Relative kinase activity of active BRAF homodimer |
| KA_nactCRAFhom$^{+}$ | 0.01 | Relative kinase activity of non-active CRAF homodimer |
| KA_actCRAFm$^{+}$ | 0.2 | Relative kinase activity of active CRAF monomer |
| KA_hactCRAFhom$^{+}$ | 0.2 | Relative kinase activity of half-active CRAF homodimer |
| KA_CCI$^{+}$ | 0.2 | Relative kinase activity of half-inhibited CRAF homodimer |
| KA_actCRAFhom$^{+}$ | 0.4 | Relative kinase activity of active CRAF homodimer |
| KA_nactRAFhet$^{+}$ | 15 | Relative kinase activity of non-active RAF heterodimer |
| KA_act_RAF_het$^{+}$ | 30 | Relative kinase activity of active RAF heterodimer |
| KA_CnBI$^{+}$ | 8 | Relative kinase activity of half-inhibited RAF heterodimer |
| KA_CnIB$^{+}$ | 8 | Relative kinase activity of half-inhibited RAF heterodimer |
| KA_CaBI$^{+}$ | 15 | Relative kinase activity of half-inhibited RAF heterodimer |
| KA_CaIB$^{+}$ | 15 | Relative kinase activity of half-inhibited RAF heterodimer |
| KA_BEm$^{+}$ | 2 | Relative kinase activity of BRAFV600E monomer |
| KA_BEhom$^{+}$ | 4 | Relative kinase activity of BRAFV600E homodimer |
| KA_BEBa$^{+}$ | 3 | Relative kinase activity of BRAFV600E-BRAF dimer |
| KA_BEBn$^{+}$ | 2 | Relative kinase activity of BRAFV600E-BRAF dimer |
| KA_BECa$^{+}$ | 30 | Relative kinase activity of BRAFV600E-CRAF dimer |
| KA_BECn$^{+}$ | 15 | Relative kinase activity of BRAFV600E-CRAF dimer |
| KA_BEBaI$^{+}$ | 2 | Relative kinase activity of half-inhibited BRAFV600E-BRAF dimer |
| KA_BEIBa$^{+}$ | 2 | Relative kinase activity of half-inhibited BRAFV600E-BRAF dimer |
| KA_BEBnI$^{+}$ | 2 | Relative kinase activity of half-inhibited BRAFV600E-BRAF dimer |
| KA_BEIBn$^{+}$ | 2 | Relative kinase activity of half-inhibited BRAFV600E-BRAF dimer |
| KA_BECaI$^{+}$ | 15 | Relative kinase activity of half-inhibited BRAFV600E-CRAF dimer |
| KA_BEICa$^{+}$ | 15 | Relative kinase activity of half-inhibited BRAFV600E-CRAF dimer |
| KA_BECnI$^{+}$ | 8 | Relative kinase activity of half-inhibited BRAFV600E- |

| | | |
|---|---|---|
| | | CRAF dimer |
| KA_BEICn$^{+}$ | 8 | Relative kinase activity of half-inhibited BRAFV600E-CRAF dimer |
| KA_BEBEI$^{+}$ | 2 | Relative kinase activity of half-inhibited BRAFV600E homodimer |

* – if not specified otherwise in the figure legends

** – if not specified otherwise in Excel spreadsheet "Kds.xlsx"

*** – for the sensitivity analysis, the total control exerted by BRAFV600E feedback phosphorylation was calculated as the sum of the response coefficients to equal factional changes in the indicated parameters (for detail see, (Kholodenko et al., 1997; Kholodenko et al., 1998; Kholodenko and Westerhoff, 1995). For illustration purposes, this is depicted as the change in the parameter pBE3 in Fig. 7 and S7.

$^{+}$ – see List S4.1

## 6. Assessment of drug synergy effects

### 6.1 Conditions for drug additivity, synergy and antagonism.

***Loewe isoboles are straight lines for non-interacting drugs.*** Drug interactions are commonly described in terms of the Bliss independence or the Loewe additivity, synergy and antagonism (Yeh et al., 2009). Although the Bliss independence is an intuitively clear concept, it does not account for nonlinearity of dose-response curves, formally resulting in interactions of a drug with itself, when the drug dose increases (Greco et al., 1995; Keith et al., 2005). Therefore, we use Loewe isoboles that are lines of constant inhibition across a two-dimensional plane of two drug concentrations.

Let $ICZ_1$ and $ICZ_2$ be the concentrations of inhibitors $I_1$ and $I_2$ that produce the same effect $Z$ when given separately. $Z$ indicates an arbitrary inhibition level, which can be, for example, 10, 20, 30, 50, 70 or 90%. We create a response surface by plotting lines of constant $Z$ values on the ($Y$, $X$) plane where $Y = [I_1]/ICZ_1$ and $X = [I_2]/ICZ_2$. If inhibitors, $I_1$ and $I_2$, do not interact with each other, the same effect Z is achieved not only by doses $I_1 = ICZ_1$, $I_2 = ICZ_2$, but also by any dose combination that satisfy the following equation,

$$I_1/ICZ_1 + I_2/ICZ_2 = 1 \qquad \text{(S6.1)}$$

Eq. S6.1 determines a straight line in the ($Y$, $X$) plane. Loewe isoboles that are straight lines indicate the absence of drug interactions, which is termed Loewe additivity (see scheme S6.1). If a combination of two drugs is more efficient than either of the two drugs on their own, i.e., they demonstrate synergy, the left part of Eq. S6.1 is less than 1, and the Loewe isoboles are concave. Conversely, if drugs antagonize each other the Loewe isoboles are convex (see scheme S6.1).

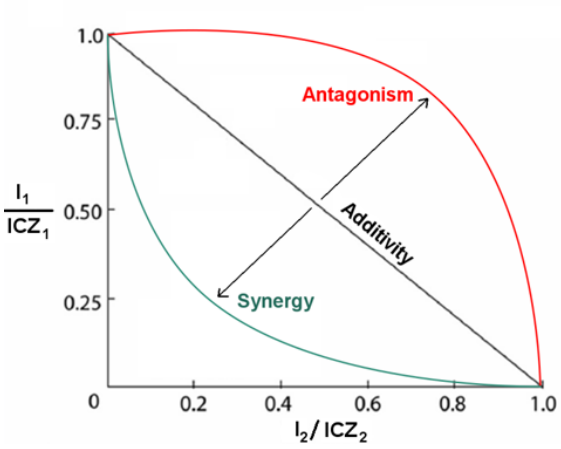


Scheme S6.1

Importantly, to assess synergy effects by Loewe isoboles we can use either absolute inhibitor doses or doses normalized by $ICZ_1$ and $ICZ_2$. Normalization of drug doses results only in the linear stretching or compression of the Loewe isoboles along the vertical and horizontal axes (see Scheme S6.1). In the case of the Loewe additivity each straight line given by Eq. S6.1 will still be the straight line, even if $I_1$ and $I_2$ are not normalized by $ICZ_1$ and $ICZ_2$. In case of drug synergy or antagonism, each concave or convex line will remain concave or convex, respectively.

When the number of data points across the two-dimensional plane of inhibitor doses is insufficient to reconstruct the Loewe isoboles, the Talalay-Chou combination index (CI) can be used (Chou, 2006). For any particular drug combination and a dose ratio, the CI allows detecting whether the Loewe isoboles are under a straight line of non-interacting drugs, i.e., isoboles are concave, or they are above this line, i.e, convex.

$$CI = \frac{I_1}{ICZ_1} + \frac{I_2}{ICZ_2} \qquad \text{(S6.2)}$$

Therefore, circumventing the need to search the entire response surface of drug mixtures, the CI indicates synergy when CI < 1 and antagonism when CI > 1 (Chou, 2006). The definition of the Talalay-Chou combination index CI (see Eq. S6.2) can be extended to analyze not only the levels of signal inhibition ICZ, but also the levels of signal activation above the basal level. For levels of the signal above the basal level there can be two concentration points that result in the same signal level (see Figs 3-5). In such cases the concentration value on the descending part of the dose-response curve is chosen. For example, for dose-response curves in Figs 3-5, the higher concentration values should be chosen during analysis of synergy effects between RAF inhibitors for the cases of activation of the ERK pathway by RAF inhibitors. For example, in Figure 5B the doses of inhibitors were normalized on the doses that result in 250% of ppERK activation to interpret experimental data. It can be clearly seen that the dose-response curves for a combination of B0R and sorafenib is essentially lower than dose-response curves for either inhibitor applied separately (Fig. 5B).

### 6.2. Measures of drug effects in the case of paradoxical pathway activation by a drug

Both Loewe isoboles and the Talalay-Chou combination index have been methods that are developed to assess effects of drugs which can only inhibit a target process and not activate it. RAF inhibitors are known to activate ERK signaling at low doses and inhibit signaling at high doses. Thus, these methods are not directly applicable for low doses of RAF inhibitors. To assess the efficiency of a drug combination for both low and high drug doses we have also calculated area under normalized dose-response curves in present paper (Kholodenko, 2015; Pozdeyev et al., 2016; Yadav et al., 2014).

### 6.3. Optimal stoichiometry of drug combinations

For a combination of two independent drugs ($I_1$ and $I_2$), the total dose is the same for each point on the straight line of drug additivity (Scheme 6.1). However, if two drugs exhibit synergy, their total dose changes for different points on the Loewe isobole. Note that the drug doses can be normalized by the corresponding IC levels or given in absolute, molar concentrations. For each inhibition effect Z, the optimal drug doses ($I_1^*$ and $I_2^*$) correspond to the point on the ICZ isobole that yields the minimal total dose (T). The minimum of the absolute molar doses and the minimum of the normalized doses are obtained by solving the conditional extremum problem, Eq. S6.3a and Eq. S6.3b, respectively

$$I_1^* + I_2^* = \min(I_1 + I_2)|_{I_1, I_2 \in ICZ} = T \tag{S6.3a}$$

$$\frac{I_1^*}{ICZ_1} + \frac{I_2^*}{ICZ_2} = \min\left(\frac{I_1}{ICZ_1} + \frac{I_2}{ICZ_2}\right)\Big|_{I_1, I_2 \in ICZ} = T_{norm} \tag{S6.3b}$$

Finding of the conditional minimums in Eqs. 6.3 is illustrated in Scheme S6.2. Here, lines $I_1 + I_2 = T$ and $\frac{I_1^*}{ICZ_1} + \frac{I_2^*}{ICZ_2} = T_{norm}$ are the tangent lines that touch the ICZ isobole at the point where the sum of molar or normalized drug doses is minimal.

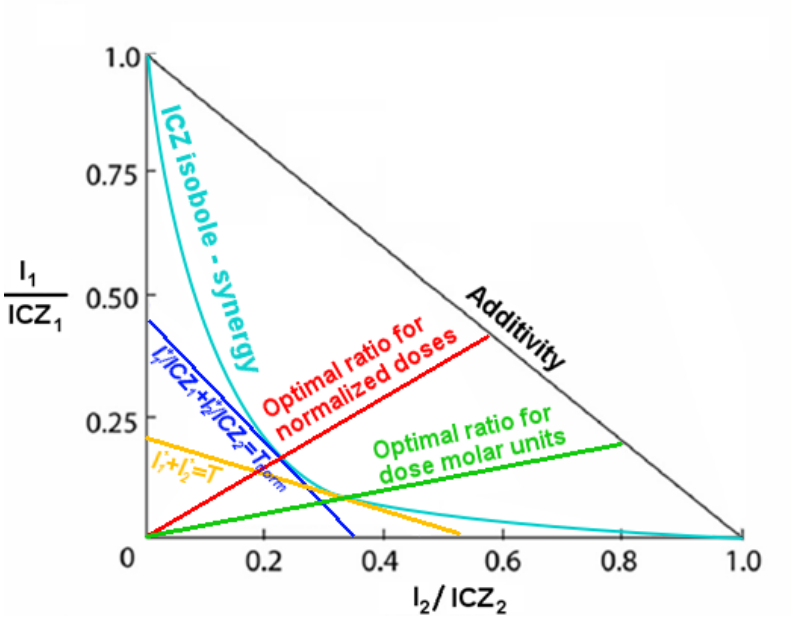


Scheme S6.2

Importantly, the distinctive features of Loewe isoboles that separate synergy, additivity and antagonism do not depend on the normalization method, or even absolute, non-normalized inhibitor doses can be plotted (Kholodenko, 2015). Thus, if two drugs show synergy at a certain ICZ level, both molar (see Eqn. S6.3a) and normalized (see Eqn. S6.3b) total doses for a drug combination will be lesser than the dose of each drug on its own that causes the same inhibition level (see Scheme S6.2). The converse statement is also true, i.e. if the same inhibition effect (ICZ) can be achieved by combining these two drugs at the lower molar or normalized sum of their doses compared to the dose of each drug on its own.

## 7. Induction of RAF dimerization increases the concentration of RAS-RAF complexes and RAF priming

RAF inhibitors inhibit RAF kinase activity, lock RAF molecules in specific conformations, and induce dimerization of RAF molecules (Hatzivassiliou et al., 2010; Karoulia et al., 2016; Kholodenko, 2015; Poulikakos et al., 2010). It was experimentally observed that RAF inhibitors increase the concentrations of RAS-RAF complexes (Hatzivassiliou et al., 2010; Karoulia et al., 2016). These data were interpreted as proof that RAF inhibitors can directly promote RAS-RAF interaction (Karoulia et al., 2016), although a structural mechanism explaining this effect is unknown. Here we show that induction of RAF dimerization is sufficient to explain the increase in the RAS-RAF complex concentration caused by RAF inhibitors.

As an illustration, first we consider a simplified, toy model of RAF recruitment by active RAS to the plasma membrane and subsequent RAF dimerization. A complete list of reactions for the simplified model is presented in List S7.1.

**List S7.1. Reactions and relationships between equilibrium dissociation constants for a toy model of RAF recruitment of plasma membrane and dimerization**

| Reaction number | Reactions | Equilibrium Dissociation Constants |
|---|---|---|
| 1 | RAS + RAF ↔ RAS-RAF | $K_1 = K_{RAS}$ |
| 2 | RAF + RAF ↔ RAF-RAF | $K_2 = K_{dim}$ |
| 3 | RAS-RAF + RAS-RAF ↔ RAS-RAF-RAF-RAS | $K_3 = K_{dim}/p_2^2$ |
| 4 | RAS-RAF-RAF + RAS ↔ RAS-RAF-RAF-RAS | $K_4 = 2K_{RAS}/p_2^2$ |
| 5 | RAS-RAF + RAF ↔ RAS-RAF-RAF | $K_5 = K_{dim}$ |
| 6 | RAF-RAF + RAS ↔ RAS-RAF-RAF | $K_6 = K_{RAS}/2$ |

In List S7.1 factor $p_2$ accounts for effects of spatial localization of RAF molecules in the near-membrane space, which results in an increase of their local concentration with respect to the cytoplasmic volume (Kholodenko et al., 2000).

The simplified model allows one to obtain an analytical expression for the total concentration of RAS-RAF complexes ($[RAS-RAF]_T$) at steady states (see Eq. S7.1).

$$[RAS-RAF]_T = [RAS-RAF] + 2[RAS-RAF-RAF-RAS] + [RAS-RAF-RAF] = \\ = \frac{[RAS]\cdot[RAF]}{K_{RAS}} \cdot \left(1 + \frac{2\cdot[RAF]}{K_{dim}} + \frac{2\cdot p_2^2 \cdot [RAS]\cdot[RAF]}{K_{RAS}\cdot K_{dim}}\right) \quad \text{(S7.1)}$$

Equation S7.1 shows that a decrease in the dissociation constant for RAF dimerization, $K_{dim}$, leads to an increase of the total concentration of RAS-RAF complexes. In other words, an increase in the affinity of RAF dimerization accounts for an increase in the concentration of RAS-RAF complexes.

The simplified model illustrates that if a RAF inhibitor increases the RAF dimerization affinity, it inevitably promotes RAS-RAF interaction. We have used our full model to check whether the induction of RAF dimerization by RAF inhibitors can account for the known effect of promotion of RAS-RAF interaction and RAF priming. Fig. S6E shows that an increase in inhibitor concentration results in an

increase of CRAF and BRAF bound to RAS-GTP. The highest amount of RAS-RAF complexes corresponds to inhibitors that induce the highest levels of RAF dimerization and paradoxical activation.

## 8. **Alternative mechanisms of RAF inhibitor resistance**

Not only RAS oncogenic mutations (or overexpression of receptor tyrosine kinases resulting in high RAS-GTP levels) confer resistance to RAF inhibitors (Nazarian et al., 2010; Straussman et al., 2012), but also other mechanisms, such as BRAFV600E splice variants (Poulikakos et al., 2011) and CRAF overexpression (Lito et al., 2013; Montagut et al., 2008). In this section we will consider the efficiency of inhibitor combinations in cells that exhibit these resistance mechanisms. We do not analyze the cases when resistance to RAF inhibitors is explained by bypassing of signaling through MEK, e.g. COT overexpression (Lito et al., 2013).

To describe RAS-to-ERK signaling in the case when p61 BRAFV600E splice variants are expressed, the corresponding additional p61 BRAFV600E molecule was added to our rule-based model. The modified file ("RAF_MEK_ERK_SV.bngl") is provided in Supplemental files. p61 splice variant of mutant BRAFV600E lacks RBD domain (Poulikakos et al., 2011). In the model, this splice variant is assumed to have 10-fold higher affinity for dimerization. The simulation results show that a combination of CO/DI and CI/DO inhibitors demonstrates synergy and effectively inhibit ERK signaling in cells expressing splice variants of mutant BRAF (Fig. S6F). Model also suggests if RAF inhibitor resistance is caused by CRAF overexpression, both a combination of CI/DI and CI/DO inhibitors, and a combination of CO/DI and CI/DO inhibitors demonstrate strong synergistic effects in inhibition of ERK signaling (Figs. S6G and S6H).

## Supplemental references


Aksamitiene, E., Hoek, J.B., Kholodenko, B., and Kiyatkin, A. (2007). Multistrip Western blotting to increase quantitative data output. Electrophoresis *28*, 3163-3173.

Arora, K., and Brooks, C.L., 3rd (2007). Large-scale allosteric conformational transitions of adenylate kinase appear to involve a population-shift mechanism. Proc Natl Acad Sci U S A *104*, 18496-18501.

Chiloeches, A., Mason, C.S., and Marais, R. (2001). S338 phosphorylation of Raf-1 is independent of phosphatidylinositol 3-kinase and Pak3. Mol Cell Biol *21*, 2423-2434.

Chou, T.C. (2006). Theoretical basis, experimental design, and computerized simulation of synergism and antagonism in drug combination studies. Pharmacol Rev *58*, 621-681.

Chylek, L.A., Harris, L.A., Tung, C.-S., Faeder, J.R., Lopez, C.F., and Hlavacek, W.S. (2014). Rule-based modeling: a computational approach for studying biomolecular site dynamics in cell signaling systems. Wiley Interdisciplinary Reviews: Systems Biology and Medicine *6*, 13-36.

Daily, M.D., Phillips, G.N., Jr., and Cui, Q. (2010). Many local motions cooperate to produce the adenylate kinase conformational transition. J Mol Biol *400*, 618-631.

Dhillon, A.S., and Kolch, W. (2002). Untying the regulation of the Raf-1 kinase. Arch Biochem Biophys *404*, 3-9.

Dhillon, A.S., Meikle, S., Yazici, Z., Eulitz, M., and Kolch, W. (2002). Regulation of Raf-1 activation and signalling by dephosphorylation. EMBO J *21*, 64-71.

Dougherty, M.K., Muller, J., Ritt, D.A., Zhou, M., Zhou, X.Z., Copeland, T.D., Conrads, T.P., Veenstra, T.D., Lu, K.P., and Morrison, D.K. (2005). Regulation of Raf-1 by direct feedback phosphorylation. Mol Cell *17*, 215-224.

Ehrenberger, T., Cantley, L.C., and Yaffe, M.B. (2015). Computational prediction of protein-protein interactions. Methods Mol Biol *1278*, 57-75.

Fischer, A., Hekman, M., Kuhlmann, J., Rubio, I., Wiese, S., and Rapp, U.R. (2007). B- and C-RAF display essential differences in their binding to Ras: the isotype-specific N terminus of B-RAF facilitates Ras binding. J Biol Chem *282*, 26503-26516.

Freeman, A.K., Ritt, D.A., and Morrison, D.K. (2013). Effects of Raf dimerization and its inhibition on normal and disease-associated Raf signaling. Mol Cell *49*, 751-758.

Garnett, M.J., Rana, S., Paterson, H., Barford, D., and Marais, R. (2005). Wild-type and mutant B-RAF activate C-RAF through distinct mechanisms involving heterodimerization. Mol Cell *20*, 963-969.

Greco, W.R., Bravo, G., and Parsons, J.C. (1995). The search for synergy: a critical review from a response surface perspective. Pharmacol Rev *47*, 331-385.

Hakulinen, R., and Puranen, S. (2016). Probabilistic model to treat flexibility in molecular contacts. Molecular Physics, 1-20.

Hatzivassiliou, G., Song, K., Yen, I., Brandhuber, B.J., Anderson, D.J., Alvarado, R., Ludlam, M.J., Stokoe, D., Gloor, S.L., Vigers, G., *et al.* (2010). RAF inhibitors prime wild-type RAF to activate the MAPK pathway and enhance growth. Nature *464*, 431-435.

Jaumot, M., and Hancock, J.F. (2001). Protein phosphatases 1 and 2A promote Raf-1 activation by regulating 14-3-3 interactions. Oncogene *20*, 3949-3958.

Karoulia, Z., Wu, Y., Ahmed, T.A., Xin, Q., Bollard, J., Krepler, C., Wu, X., Zhang, C., Bollag, G., Herlyn, M., *et al.* (2016). An Integrated Model of RAF Inhibitor Action Predicts Inhibitor Activity against Oncogenic BRAF Signaling. Cancer Cell *30*, 485-498.

Keith, C.T., Borisy, A.A., and Stockwell, B.R. (2005). Multicomponent therapeutics for networked systems. Nat Rev Drug Discov *4*, 71-78.

Kholodenko, B.N. (2006). Cell-signalling dynamics in time and space. Nat Rev Mol Cell Biol *7*, 165-176.

Kholodenko, B.N. (2015). Drug resistance resulting from kinase dimerization is rationalized by thermodynamic factors describing allosteric inhibitor effects. Cell Rep *12*, 1939-1949.

Kholodenko, B.N., Demin, O.V., Moehren, G., and Hoek, J.B. (1999). Quantification of short term signaling by the epidermal growth factor receptor. J Biol Chem *274*, 30169-30181.

Kholodenko, B.N., Demin, O.V., and Westerhoff, H.V. (1997). Control Analysis of Periodic Phenomena in Biological Systems. The Journal of Physical Chemistry B *101*, 2070-2081.

Kholodenko, B.N., Hoek, J.B., and Westerhoff, H.V. (2000). Why cytoplasmic signalling proteins should be recruited to cell membranes. Trends Cell Biol *10*, 173-178.

Kholodenko, B.N., Schuster, S., Garcia, J., Westerhoff, H.V., and Cascante, M. (1998). Control analysis of metabolic systems involving quasi-equilibrium reactions. Biochim Biophys Acta *1379*, 337-352.

Kholodenko, B.N., and Westerhoff, H.V. (1995). The macroworld versus the microworld of biochemical regulation and control. Trends in Biochemical Sciences *20*, 52-54.

Lamson, R.E., Takahashi, S., Winters, M.J., and Pryciak, P.M. (2006). Dual role for membrane localization in yeast MAP kinase cascade activation and its contribution to signaling fidelity. Curr Biol *16*, 618-623.

Lavoie, H., and Therrien, M. (2015). Regulation of RAF protein kinases in ERK signalling. Nat Rev Mol Cell Biol *16*, 281-298.

Leicht, D.T., Balan, V., Kaplun, A., Singh-Gupta, V., Kaplun, L., Dobson, M., and Tzivion, G. (2007). Raf kinases: function, regulation and role in human cancer. Biochim Biophys Acta *1773*, 1196-1212.

Lito, P., Rosen, N., and Solit, D.B. (2013). Tumor adaptation and resistance to RAF inhibitors. Nat Med *19*, 1401-1409.

Markevich, N.I., Moehren, G., Demin, O., Kiyatkin, A., Hoek, J.B., and Kholodenko, B.N. (2004). Signal processing at the Ras circuit: What shapes Ras activation patterns? IEE Systems Biology *1*, 104-113.

Matallanas, D., Birtwistle, M., Romano, D., Zebisch, A., Rauch, J., von Kriegsheim, A., and Kolch, W. (2011). Raf family kinases: old dogs have learned new tricks. Genes Cancer *2*, 232-260.

Montagut, C., Sharma, S.V., Shioda, T., McDermott, U., Ulman, M., Ulkus, L.E., Dias-Santagata, D., Stubbs, H., Lee, D.Y., Singh, A., *et al.* (2008). Elevated CRAF as a potential mechanism of acquired resistance to BRAF inhibition in melanoma. Cancer Research *68*, 4853-4861.

Nazarian, R., Shi, H., Wang, Q., Kong, X., Koya, R.C., Lee, H., Chen, Z., Lee, M.K., Attar, N., Sazegar, H., *et al.* (2010). Melanomas acquire resistance to B-RAF(V600E) inhibition by RTK or N-RAS upregulation. Nature *468*, 973-977.

Obenauer, J.C., Cantley, L.C., and Yaffe, M.B. (2003). Scansite 2.0: Proteome-wide prediction of cell signaling interactions using short sequence motifs. Nucleic Acids Res *31*, 3635-3641.

Park, Jin H., Liu, Y., Lemmon, Mark A., and Radhakrishnan, R. (2012). Erlotinib binds both inactive and active conformations of the EGFR tyrosine kinase domain. Biochemical Journal *448*, 417.

Poulikakos, P.I., Persaud, Y., Janakiraman, M., Kong, X., Ng, C., Moriceau, G., Shi, H., Atefi, M., Titz, B., Gabay, M.T., *et al.* (2011). RAF inhibitor resistance is mediated by dimerization of aberrantly spliced BRAF(V600E). Nature *480*, 387-390.

Poulikakos, P.I., Zhang, C., Bollag, G., Shokat, K.M., and Rosen, N. (2010). RAF inhibitors transactivate RAF dimers and ERK signalling in cells with wild-type BRAF. Nature *464*, 427-430.

Pozdeyev, N., Yoo, M., Mackie, R., Schweppe, R.E., Tan, A.C., and Haugen, B.R. (2016). Integrating heterogeneous drug sensitivity data from cancer pharmacogenomic studies. Oncotarget *7*, 51619-51625.

Rajakulendran, T., Sahmi, M., Lefrancois, M., Sicheri, F., and Therrien, M. (2009). A dimerization-dependent mechanism drives RAF catalytic activation. Nature *461*, 542-545.

Ritt, D.A., Monson, D.M., Specht, S.I., and Morrison, D.K. (2010). Impact of feedback phosphorylation and Raf heterodimerization on normal and mutant B-Raf signaling. Mol Cell Biol *30*, 806-819.

Roskoski, R., Jr. (2010). RAF protein-serine/threonine kinases: structure and regulation. Biochem Biophys Res Commun *399*, 313-317.

Rushworth, L.K., Hindley, A.D., O'Neill, E., and Kolch, W. (2006). Regulation and role of Raf-1/B-Raf heterodimerization. Mol Cell Biol *26*, 2262-2272.

Shao, Q., Xu, Z., Wang, J., Shi, J., and Zhu, W. (2017). Energetics and structural characterization of the "DFG-flip" conformational transition of B-RAF kinase: a SITS molecular dynamics study. Phys Chem Chem Phys *19*, 1257-1267.

Straussman, R., Morikawa, T., Shee, K., Barzily-Rokni, M., Qian, Z.R., Du, J., Davis, A., Mongare, M.M., Gould, J., Frederick, D.T., *et al.* (2012). Tumour micro-environment elicits innate resistance to RAF inhibitors through HGF secretion. Nature *487*, 500-504.

Yadav, B., Pemovska, T., Szwajda, A., Kulesskiy, E., Kontro, M., Karjalainen, R., Majumder, M.M., Malani, D., Murumagi, A., Knowles, J., *et al.* (2014). Quantitative scoring of differential drug sensitivity for individually optimized anticancer therapies. Sci Rep *4*, 5193.

Yeh, P.J., Hegreness, M.J., Aiden, A.P., and Kishony, R. (2009). Drug interactions and the evolution of antibiotic resistance. Nat Rev Microbiol *7*, 460-466.

Supplemental Figure 1

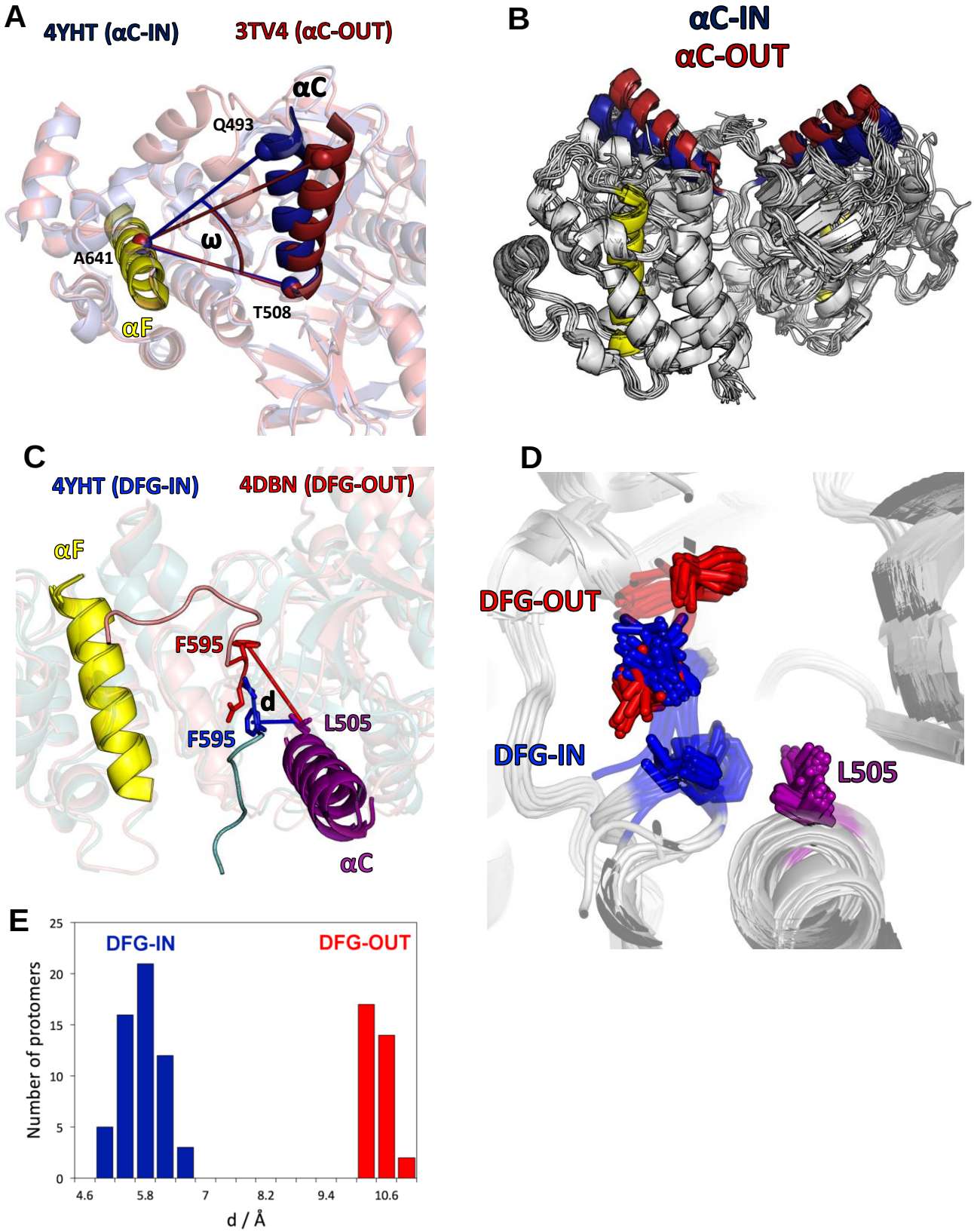


**Figure S1 related to Figure 1.** (**A**) Overlay of two structures, one of which is αC-helix-IN (4YHT, blue color), and the other is αC-helix-OUT (3TV4, red color). The αC-helix angle ω, which defines IN (ω > 54º) or OUT (ω < 52º) positions is highlighted in blue and red. (**B**) Overlay of the 46 BRAF dimer structures analysed showing the αC-helix IN and OUT in blue and red respectively. (**C**) Overlay of two structures one of which is DFG-IN (4YHT, blue color) and the other is DFG-OUT (4DBN, red color). The L505-F595 distance, which defines IN (d < 7 Å) and OUT (d > 9.5 Å) conformations, is depicted in blue and red lines, respectively. (**D**) Overlay of the 45 BRAF dimer structures analysed showing the DFG IN (blue) and OUT (red) (3C4C was not included because it has a different DFG conformation). (**E**) Distribution of the DFG conformations in 90 BRAF kinase domain protomers based on the analysis of 45 BRAF dimer structures deposited in PDB.

Supplemental Figure 2

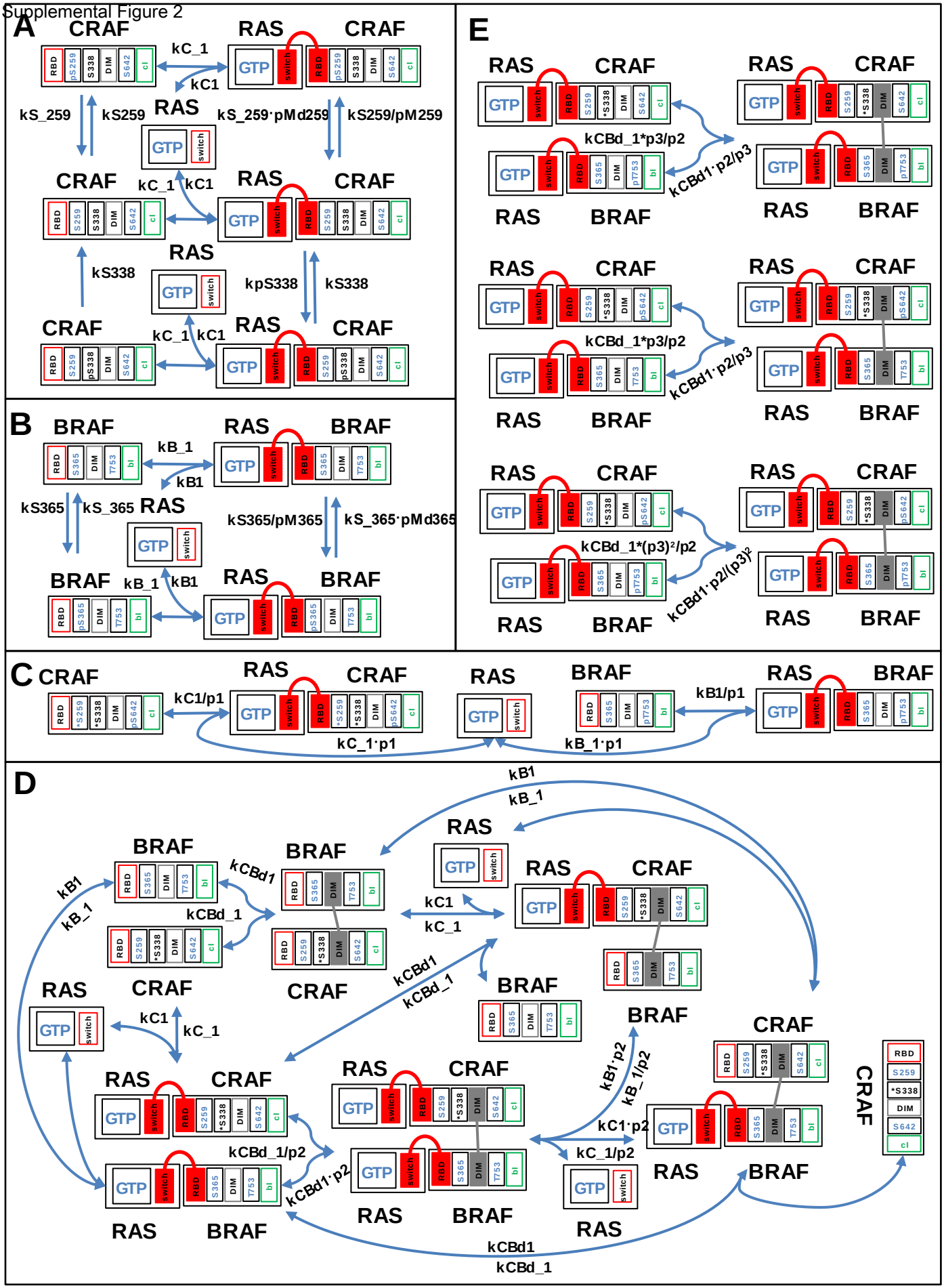

**Figure S2 related to Figure 2.** Kinetic schemes of the rules governing: (**A**) CRAF binding to RAS and CRAF activation cycle; (**B**) BRAF binding to RAS and BRAF activation cycle; (**C**) Influence of ERK feedback phosphorylation on binding of RAF kinases to RAS; (**D**) RAF hetero-dimerization cycle; (**E**) Influence of ERK feedback phosphorylation on CRAF-BRAF hetero-dimerization. Protein domain designations are the same as in Fig. 2. Parameter notations on the arrows are explained in the SI, sections 1 and 2, see also List S5.1.

Supplemental Figure 3

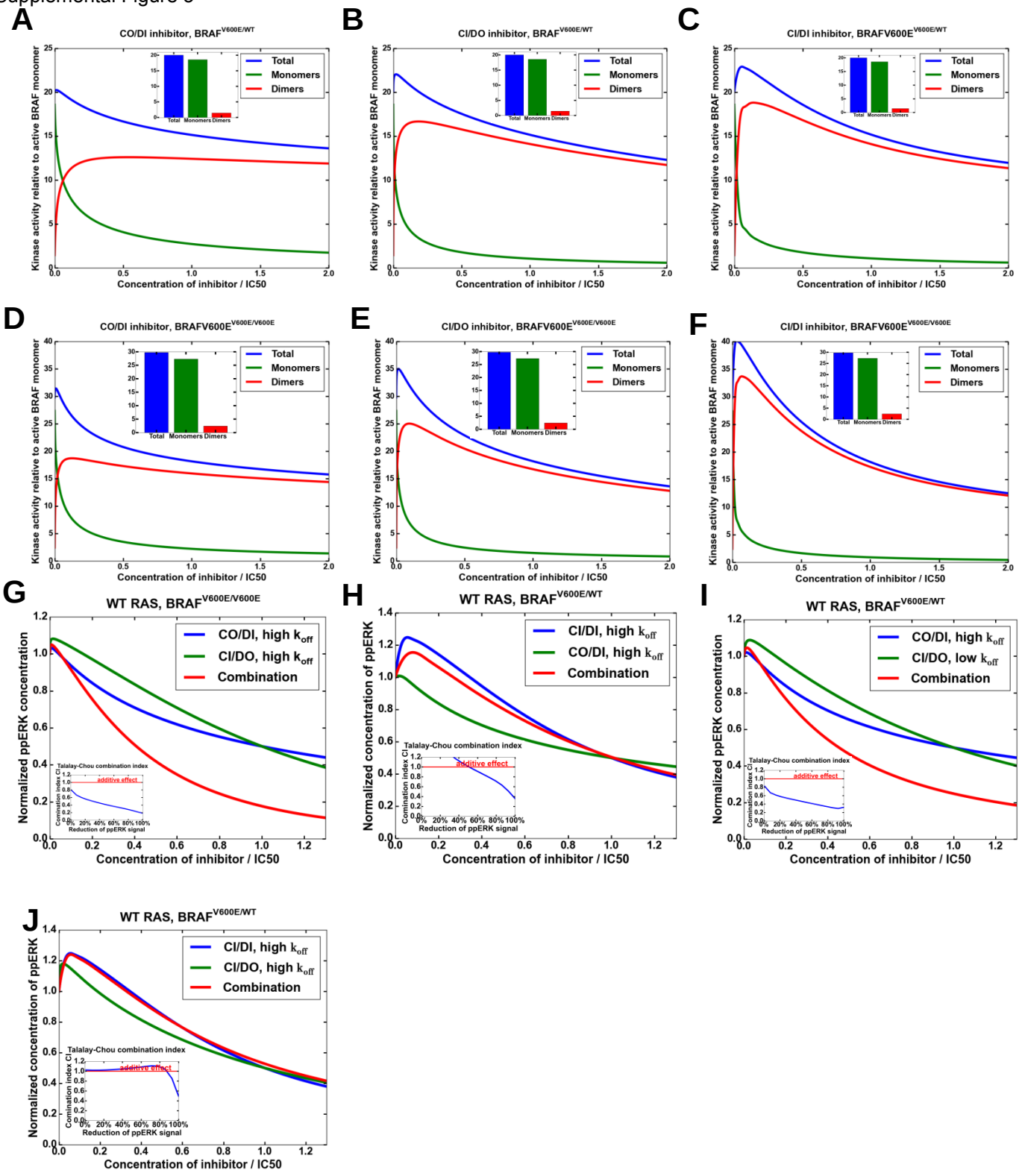

**Figure S3 related to Figure 3.** (**A-F**) Model-predicted relative contribution of kinase activity of RAF monomers and dimers into the total RAF kinase activity during treatment with CO/DI (**A, D**), CI/DO (**B, E**) and CI/DI (**C, F**) inhibitors and in the absence of inhibitors (inserts) for cells with heterozygous (**A-C**) and homozygous (**D-F**) BRAFV600E mutation and WT RAS. **(G-J**) Model-predicted response of MEK and ERK signaling to: CO/DI and CI/DO inhibitors and their combination (**G, I**), CI/DI and CO/DI inhibitors and their combination (**H**), and CI/DI and CI/DO inhibitors and their combination (**J**) in cells with homozygous (**G**) and heterozygous (**H-J**) BRAFV600E mutation. Inhibitor doses are normalized by IC50. The residence time $1/k_{off}$ of CO/DI and CI/DI inhibitors is 1 s. The residence times $1/k_{off}$ of CI/DO inhibitor are 1 s (**B, E, G, J**) and $10^4$ s (**I**). In each combination, the ratio of CO/DI and CI/DO inhibitor doses is 1.2:1, the ratio of CI/DI and CO/DI inhibitor doses is 1.2:1, and the ratio of CI/DI and CI/DO inhibitor doses is 1.2:1. Parameters for (**A-C**) and (**H-J**) are: [RAS-GTP]=25 nM, [$BRAF^{V600E}$]=25 nM, [$BRAF^{WT}$]=25 nM. Parameters for (**D-F**) and (**G**) are: [RAS-GTP]=25 nM, [$BRAF^{V600E}$]=50 nM, [$BRAF^{WT}$]=0 nM. The remaining parameters are given in Lists S4.1 and S5.1 in SI. In panels (**G-J**), the inserts assess synergy, additivity or antagonism, using the Talalay-Chou combination index (CI).

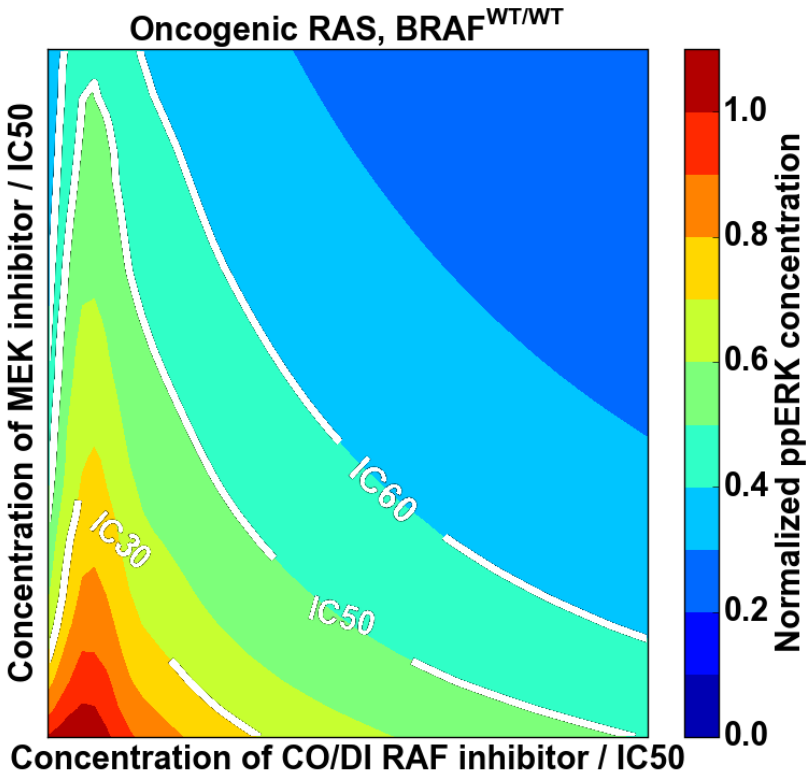


**Figure S4 related to Figure 4.** Predictive simulations of Loewe isoboles demonstrate antagonism rather than synergy of inhibiting ERK signaling by combinations of CO/DI RAF inhibitor and MEK inhibitor in cells bearing oncogenic RAS and WT BRAF (cf. Figs. S5 and 5). [RAS-GTP]=250 nM, [$BRAF^{V600E}$]=0, [$BRAF^{WT}$]=50 nM, basal ppERK level is 480 nM.

Supplemental Figure 5

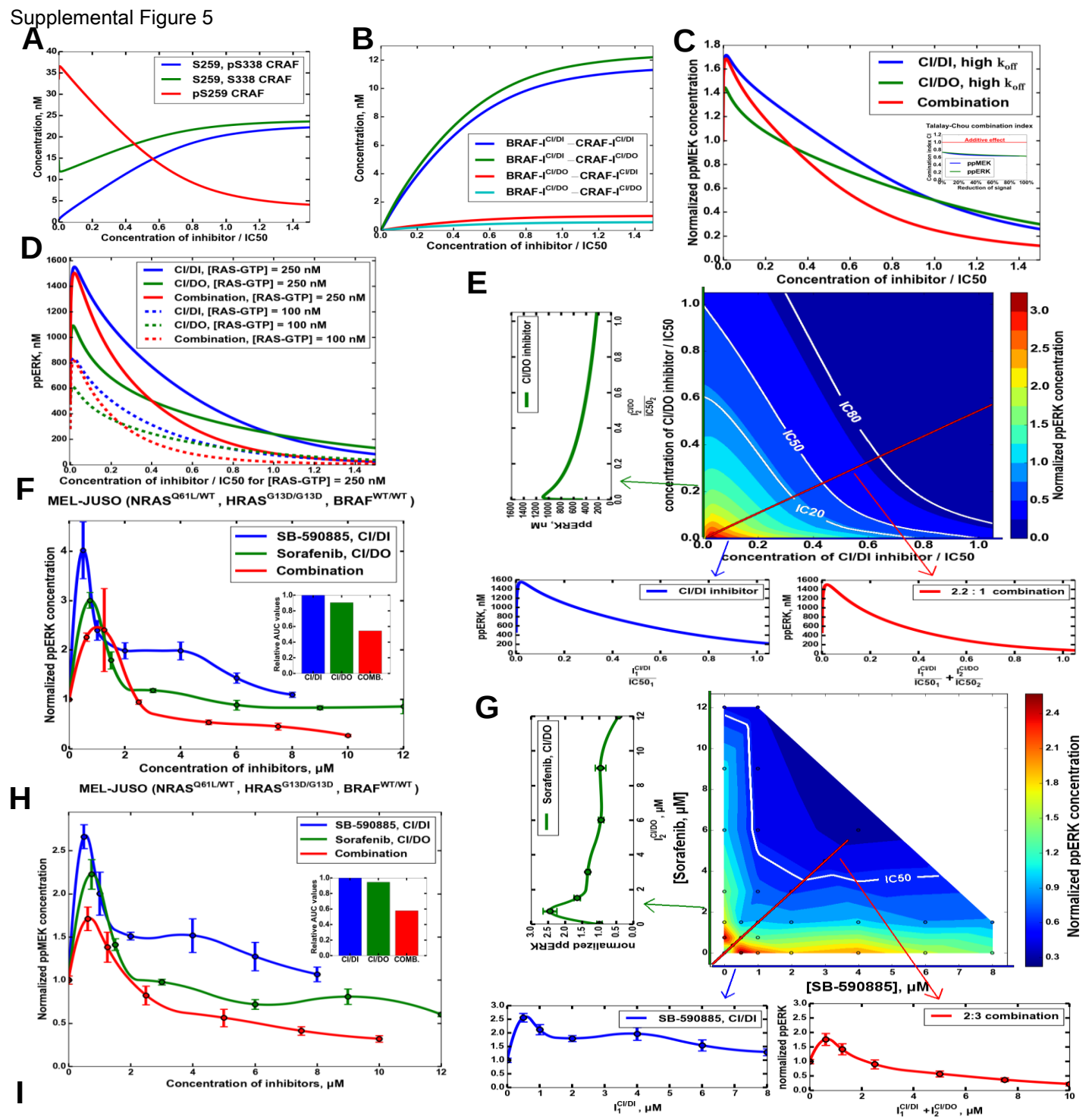

**Figure S5 related to Figure 5. (A-E**) Model predicted stationary responses to CI/DI and CI/DO inhibitors and their combination of: **(A)** CRAF phosphorylation on S259 and S338; **(B)** RAF heterodimers bound with two molecules of RAF inhibitor; **(C)** MEK signaling; **(D-E)** ERK signaling. (**C**) Talalay-Chou index for MEK and ERK inhibition is presented on the insert. [RAS-GTP]=250 nM (**A-E**), [RAS-GTP]=100 nM (**D**), $[BRAF^{V600E}]$=0, $[BRAF^{WT}]$=50 nM, basal ppERK levels are 480 nM (**A-E**) and 279 nM (**D**), the ratio of CI/DI and CI/DO inhibitor doses applied in combination is 2.2:1 (**A-E**). (**F-I**). ERK (**F-G, I**) and MEK (**H**) signaling responses in growing MEL-JUSO ($NRAS^{Q61L/WT}$, $HRAS^{G13D/G13D}$, $BRAF^{WT/WT}$) cells to SB-590885 (CI/DI), sorafenib (CI/DO) and their combination, which are measured using MESOSCALE (**F**) and LUMINEX (**G-H**) systems, and Western Blot (**I**), 24 hr. The Western Blots (**I**) are taken from a single membrane which was obtained using multistrip western blotting (Aksamitiene et al., 2007). For inhibitor combinations, the ratio of SB590885 to sorafenib is 1:1.5. The ppERK responses are plotted vs the absolute concentrations of inhibitors applied separately and vs the sum of the absolute concentrations for their combination.

Supplemental Figure 6

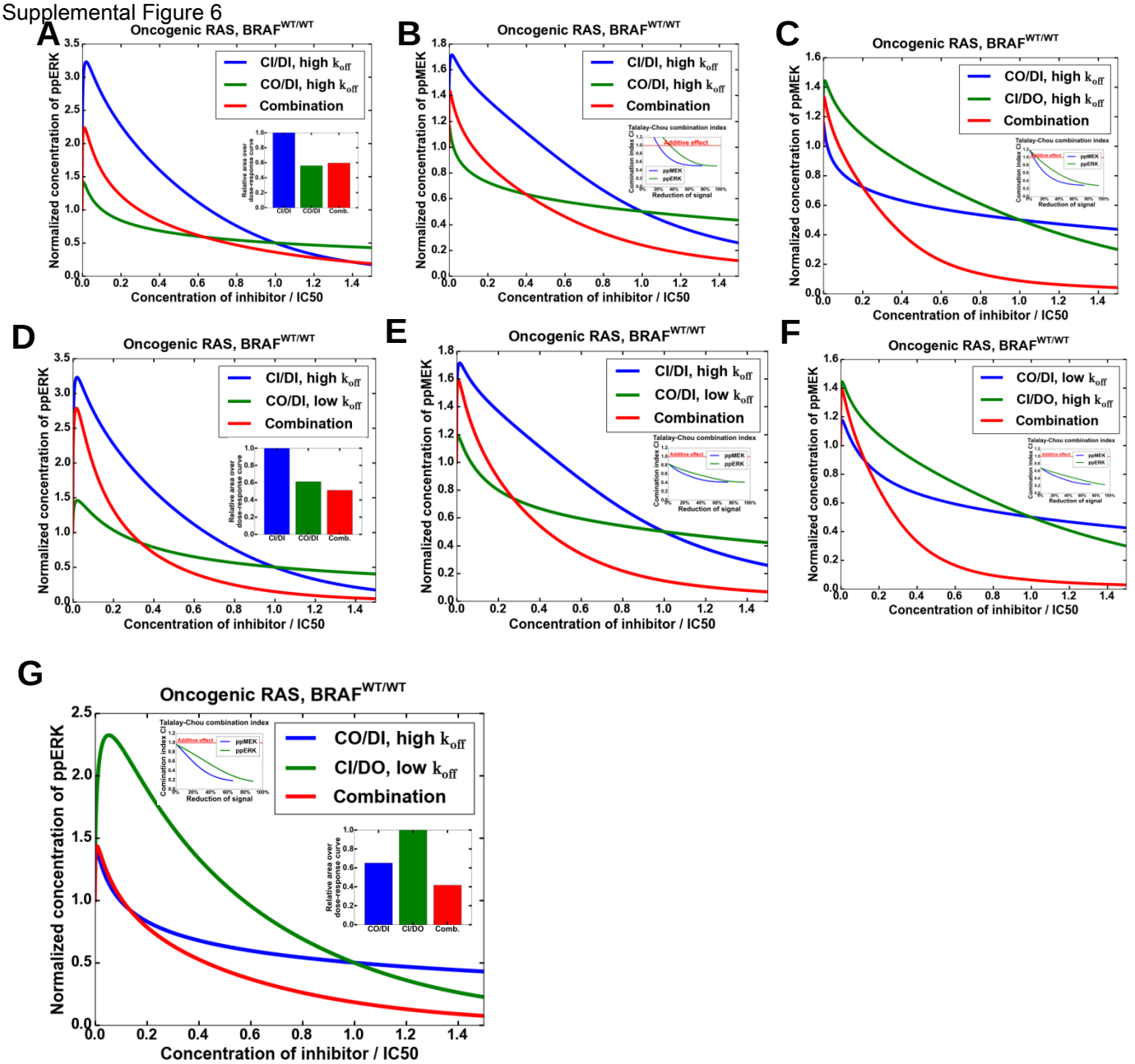


**Figure S6 related to Figure 6.** Model-predicted responses of MEK (**B-C**, **E-F**) and ERK (**A**, **D**, **G**) signaling to CI/DI, CO/DI inhibitors and their combination (**A-B**, **D-E**) and to CO/DI, CI/DO inhibitors and their combination (**C**, **F**, **G**). The residence times $t_{off} \sim 1/k_{off}$ of CO/DI inhibitor are 1 s (**A-C, G**) and $10^4$ s (**D-F**). Inserts assess synergy, additivity or antagonism, using the AUC (**A, D, G**) and CI (**B, C, E-G**).The residence times of CI/DO inhibitor are 1 s (**C, F**) and $10^4$ s (**G**). Inhibitor doses are normalized by IC50, the total doses shown for the combination correspond to the optimal ratios of inhibitor doses. [RAS-GTP]=250 nM, [$BRAF^{V600E}$]=0, [$BRAF^{WT}$]=50 nM, basal ppERK level is 484 nM. The ratios of CI/DI and CO/DI inhibitor doses applied in combination are 3:5 (**A-B**) and 1:1 (**D-E**). The ratios of CO/DI and CI/DO inhibitor doses applied in combination are 1:1 (**C, F, G**).

Supplemental Figure 7

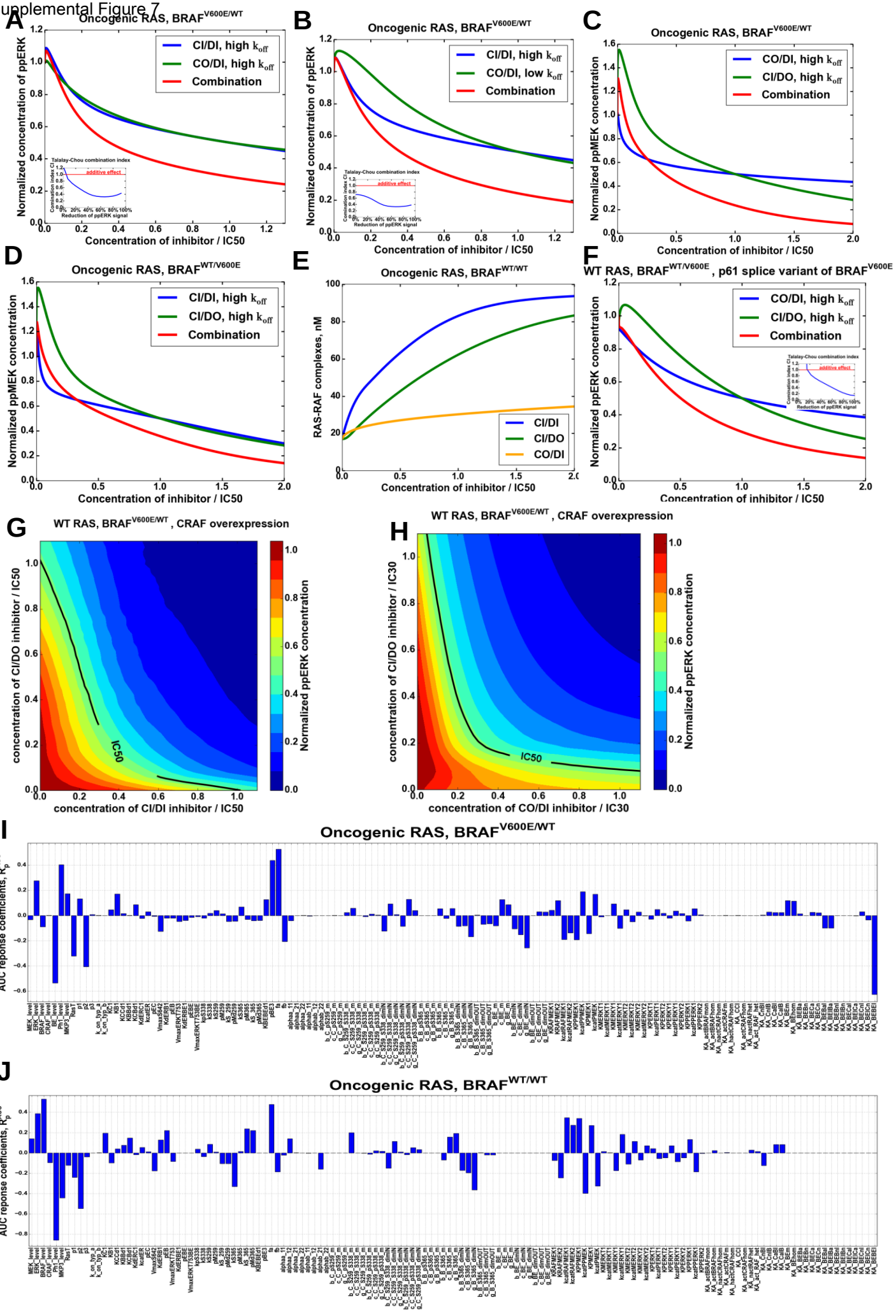

**Figure S7 related to Figure 7.** (**A-D**) Model-predicted stationary responses of ERK (**A-B**) and MEK (**C-D**) signaling in cells with oncogenic RAS mutation and heterozygous BRAFV600E mutation to: CI/DI and CO/DI inhibitors and their combination (**A-B**), CO/DI and CI/DO inhibitors and their combination (**C**), and CI/DI and CI/DO inhibitors and their combination (**D**). The residence time $t_{off} \sim 1/k_{off}$ of all inhibitors is 1 s. Inhibitor doses are normalized by IC50. In combinations, the ratio of CI/DI and CO/DI inhibitor doses are 1:1 (**A**) and 2.2:1 (**B**), the ratio of CO/DI and CI/DO inhibitor doses is 1:1 (**C**), and the ratio of CI/DI and CI/DO inhibitor doses is 6:1 (**D**). [RAS-GTP]=250 nM, [$BRAF^{V600E}$]=25 nM, [$BRAF^{WT}$]=25 nM, basal ppERK level is 2151 nM. (**E**) Model-predicted response of RAS-RAF complexes concentration to different RAF inhibitors in cells with WT BRAF and oncogenic RAS. [RAS-GTP]=250 nM, [$BRAF^{V600E}$]=0, [$BRAF^{WT}$]=50 nM, basal ppERK level is 480 nM. (**F**) Model-predicted stationary response of ERK signaling to CO/DI, CI/DO inhibitors and their combination in cells with WT RAS and p61 splice variant of heterozygous BRAFV600E. [RAS-GTP]=25 nM, [$BRAF^{V600E}$]=0, [$p61BRAF^{V600E}$]=25 nM, [$BRAF^{WT}$]=25 nM, basal ppERK level is 1627 nM. Inhibitor doses are normalized by IC50. In combination, the ratio of CO/DI and CI/DO inhibitor doses is 7:1. (**A**, **B**, **F**) Inserts assess drug synergy using the Talalay-Chou combination index (CI). **G-H**. Model-predicted stationary responses of ERK signaling in cells with WT RAS, heterozygous BRAFV600E mutation and CRAF overexpression to: CI/DI, CI/DO inhibitors and their combination, and to CO/DI, CI/DO inhibitors and their combination. Inhibitor doses are normalized by IC50 (**G**) and IC30 (**H**). [RAS-GTP]=25 nM, [$BRAF^{V600E}$]=25 nM, [$BRAF^{WT}$]=25 nM, [CRAF]=250 nM, basal ppERK level is 2603 nM. (**I–J**) Sensitivities of the areas under dose-response curves (AUC) to parameter changes for a combination of CO/DI (inhibitor a) and CI/DO (inhibitor b) RAF inhibitors in cells bearing both oncogenic RAS and BRAFV600E mutations (**I**) or only oncogenic RAS and WT BRAF (**J**).

Table for calculation of apparent Kd

Raw Luminex and Mesoscale data

Click here to access/download

**Supplemental Movies and Spreadsheets**

Luminex_MESOSCALE_raw_data.xlsx

File of rule-based model

Click here to access/download
**ZIP File**
RAF_MEK_ERK.bngl.zip

BNGL file of the model with focus on BRAF splice variants

Click here to access/download
**ZIP File**
RAF_MEK_ERK_SV.bngl.zip